Strong Photon-Photon Interactions at the Single-Photon Level

by

Wenlan Chen

Submitted to the Department of Physics
in partial fulfillment of the requirements for the degree of

Doctor of Philosophy in the Department of Physics

at the

MASSACHUSETTS INSTITUTE OF TECHNOLOGY

February 2015

© Massachusetts Institute of Technology 2015. All rights reserved.

Author .....
Department of Physics
Jan. 8, 2015

Certified by .....
Vladan Vuletić
Lester Wolfe Professor of Physics
Thesis Supervisor

Accepted by .....
Krishna Rajagopal
Associate Department Head for Education

Strong Photon-Photon Interactions at the Single-Photon Level

by

Wenlan Chen

Submitted to the Department of Physics
on Jan. 8, 2015, in partial fulfillment of the
requirements for the degree of
Doctor of Philosophy in the Department of Physics

Abstract

Engineering light at the single photon level is a long-standing goal in physics. In this thesis, we investigate optical nonlinearities at the single photon level orchestrated by an optical cavity.

We demonstrate an all-optical transistor where one stored 'gate' photon controls the propagation of a 'source' light beam. The system is based on EIT and a high-cooperativity cavity. Each 'gate' photon is converted to an EIT polariton and strongly suppresses the cavity transmission of subsequently applied source photons. One stored gate photon can be retrieved from the atomic ensemble after switching off more than one source photon. Without retrieval, one stored gate photon can switch up to several hundreds source photons.

Next, instead of storing the photon, we let it propagate slowly and operate the system in the continuous mode. We observe an anti-cross-correlation between free-space and cavity beams. The cross-correlation function at zero time is $g_2 = 0.89$ which means a photon in one beam extinguishes one photon in the other beam with a probability of 11%. It is a deterministic photon-photon interaction at the single photon level.

Using similar skills, we propose a new method to measure zero or one photon fock states, without destroying the photons. We are improving the setup which is approaching the non-destructive measurement of photons. Potentially, this method will enable new applications in quantum information and computation. It will also enable the observation of different internal degrees of the photons, such as polarization or photon number, at the same time without losing the photons.

By reducing the power to zero, we investigate the nonlinearity of the vacuum field in the optical cavity. By replacing the control beam in EIT by the vacuum field, we observe vacuum induced transparency (VIT). This effect indicates that vacuum field strongly distorts the dispersion of atoms in a way that cannot be explained by classical electromagnetism.

In order to reach even stronger single-photon interaction regime, we need to enhance the cavity cooperativity to even higher parameters. At the end of this thesis,

I describe our progress towards the micro cavity system. By using a micro cavity, we enhance the cooperativity by a factor of 20. This improvement will suppress decoherence and move forward research into single photon nonlinearities.

Thesis Supervisor: Vladan Vuletić
Title: Lester Wolfe Professor of Physics

Acknowledgments

As a member of the Vuletić group I have worked with and around many brilliant and kind scientists, who have made works in this thesis possible and taught me physics and beyond. Among them, Prof. Vladan Vuletić, Haruka Tanji and Kristin Beck deserve my foremost thanks. Vladan is the best mentor I can ever hope for. He is a fount of smart ideas, an enthusiastic and talented scientist and a willing and gifted teacher. He is a role model for me, both as a scientist and as a teacher. I appreciate his incisive understanding and intuitive explanation of physics, his company in the lab debugging electronics or pulling out signal from vague, his support and tolerate when I was expecting and caring for a baby, and his encouragement and advice that keeps me going.

Haruka Tanji was my tutor both in and out of lab from day one. She was incredibly patient in teaching me the basics in the lab. She is particularly considerate as a friend, helping me through transition to the new environment. Together we achieved the fantastic VIT experiment, and made the apparatus work stably which enabled wonderful results long after her graduation. Haruka taught me how to care and influence others and the value of leadership. It was an excellent learning experience to work with her.

Kristin Beck is exceptional friend and colleague. Her solid technical skills, her persistence, and her organization helped tremendously in achieving exciting experimental results. I really enjoyed the insightful and profound scientific discussions with her. She was also my English teacher and my resource on American culture, who has helped me tremendously in polishing the language of our papers and this thesis. Now she is leading the experiment with Mahdi Hosseini, who has brilliant ideas and is also a great scientist. I have no doubt that Kristi and Mahdi will produce exciting physics results in no time.

I would like to thank all of my colleagues in Vladan's group for the nourishing environment and exciting discussions. I appreciate Jonathan Simon for his deep understanding of physics and sharing of creative ideas. I appreciate Fedja Orucevic

for his kind mentoring in micro mirror fabrication in my early days. I appreciate Renate Landig for her precision of work and joyful chat. I appreciate the late-night chats with Marko Cetina about research and life, and caring both in lab and in life from Monika Schleier-Smith. The trip heading to DAMOP was much fun with Alexei Bylinskii, Dorian Gangloff and Molu Shi. Thibault Peyronel, Qiyu Liang, Boris Braverman and Akio Kawasaki were one floor away, but we probably had the most frequent exchange of equipment with them. It was always fun to hop into their lab to discuss physics among other things.

We have some great visitors and undergraduates working in our lab, including Qian Lin, Xudong Yu, Mallika Randeria, Chao Zheng and Senka Ćuk, who all made great contributions to the on-going experiments. Particularly, Qian updated the laser locking system and collected the preliminary cross modulation data with me. Xudong diligently worked on measuring micro mirror and micro cavities.

The CUA is the most friendly and inspiring environment in which to carry on AMO research. I would like to thank everyone down the hallway, for exciting discussions in and beyond physics, and for sharing knowledge and equipment, particularly Wujie Huang and Junru Li.

I cannot possibly name all the wonderful people who supported me outside the lab. I would like to thank Martin Zwierlein, who has been an excellent academic advisor. He was always happy to talk with me to make sure that things were going well, despite his tight schedule, and gave me critical advice when I need it. I would like to thank Catherine Modica, who coordinated the financial support for my last semester. Giving birth and taking care of a baby while writing my thesis would not have been so smooth without her help and truly care. I would like to thank Bea Kleppner for her advice and caring in my first few years at MIT, which enlightened my route through confusion and upset.

For turning the stress into pleasure and for enriching me in all ways, I would like to thank my friends. I appreciate the times we've shared, whether we have been traveling, rock climbing, hiking, boating, or running together; whether you've cooked for me, sharing your insight with me, or supplied me with listening ears. Jiexi Zhang,

Ning Hua, Yufei Ge, Wei Wang and Yannan Zheng, special thanks to your caring and sharing.

Lastly, I would like to thank my families. I appreciate my parents Dengming Chen, Xiaolan Zhong and my sister Wenjia Zhong for their unconditionally love and support. I appreciate my husband Jiazhong Hu for sharing the curiosity towards the beautiful world, for the accompany through difficulties, and for being brave and sharing wisdom that brought me to a larger and richer world. I appreciate my son Baldo, without whom I would have graduated half year earlier; with whom, I am stepping out of my comfort zone, experiencing wonderful things and become a better person.

Contents

List of Figures

List of Tables

Chapter 1

Introduction

In 1704, Isaac Newton published *Opticks*, in which he presented that light was made up of extremely subtle corpuscles (particles) [1]: two intersecting rays travel in straight lines without changing each other. At the same time, physicists found light behaved as wave [2]: two waves propagate in their original directions in vacuum and pass through each other. Then, in 1905, Albert Einstein used the idea of light quanta to explain the photoelectric effect, finding that light is particle-like with quantized energy [3]. Today, the modern theory of optics pictures light as both a particle and a wave, with particle-like energy quantization and a wave-like probability density distribution. We call each energy quantum a photon.

With the development of modern optics, engineering light and interactions between beams of light remains one of the hottest topics in physics [4–20]. Researchers have already made significant advances in engineering light consisting of many photons [15–20]. Some of the results even have been applied to our daily life, such as fiber transmission and LED displays. With the establishment of quantum mechanics and quantum electrodynamics, scientists have been interested in exploring photon-photon interactions at the quantum level [4–14]. In this regime, the energy of light becomes much weaker and the quantum properties become dominant.

Today, nonclassical states of light such as photon Fock states [21–27], squeezed states [28, 29] and photon-pair-bound states [30] have already been demonstrated, which illustrate quantum properties completely different from the predictions of clas-

sical physics. Most of these experiments were realized in beams in the same propagation mode. For two or more crossed beams with different propagation modes, exciting experiments [31–37] have been demonstrated at the femtojoule level. In these systems, correlation, entanglement and strong interactions between photons have been observed.

Among these results, electromagnetically induced transparency (EIT) has been one of the most elegant phenomena and powerful tools. By showing that two perpendicular beams could strongly affect each other at quantum level [37], EIT provided a new approach to make photon-photon interactions in extreme situations. Even when one beam is weaker than the other beam, this beam's presence could drastically slow down the stronger beam. The light's group velocity can be slowed down from 3×10^8 m/s by seven orders of magnitude to a few meters per second [38, 39], and even fully stopped [40]. By using the slowing light mechanism of EIT, we could store light in a "portable hard drive" and apply such storage to both classical and quantum information carried by photons. This technique could solve problems, for example, dealing with the communication fidelity decrease in long distance quantum key distribution by using the DLCZ scheme [41]. Some of these ideas and results are now being converted to commercial products. EIT established a practical platform to control and manipulate light with light.

In recent years, the quest for even stronger interactions between photons has been a very popular research topic [4–14], driven by extensive applications of optical communication and the development of the field of quantum information. Using high-finesse cavities, which suppress dissipation and enhance the coherent coupling strength between matter and light, researchers have demonstrated single-photon nonlinearities and photon-photon interactions at the level of tens of photons [4,6–9,13,14]. Additionally, an all-optical switch [8, 13, 14] and cross-phase modulator [12, 42] were demonstrated by using EIT schemes. The mutual interaction between atoms and light in optical cavities also allows for coherent control and engineering of atomic systems. Strong entanglement between atoms has been demonstrated in an optical cavity by using the collective interaction in atoms and light [28].

Reaching single-photon interactions by these different techniques could help us to develop and improve future technology and human lives. I could imagine people using light at the single photon level to control and operate appliances in the future, which will potentially reduce energy costs, increase efficiency and enable "green" devices. I also could imagine people using entanglement via photons and atoms to communicate with each other, replacing the regular cell phone network with an all optical network or quantum-secure network.

This thesis studies strong photon-photon interaction at the single photon level, which constitutes the main body of this thesis. We utilized two different mechanisms to confine two photons traveling in perpendicular beams locally in the atomic ensemble and to overlap them with each other in both time and space, so they can interact strongly in the nonlinear atomic medium. One of the photons (free-space photon) travels through the atomic ensemble as a dark-state polariton, which is a superposition of a photon and a collective atomic excitation to the state coupling to the cavity transition, introduced by the mechanism of EIT; the other photon (cavity photon) is trapped by a high-cooperativity cavity and interacts strongly with the atomic excitation component of the first photon, in the N-type level structure of the atomic medium.

In Chapter 2, I quantitatively describe EIT and cavity-atom interactions and establish a theoretical model of our experimental system, which I will use to predict results of the different experiments described in the following chapters.

Then, I proceed to present the experimental apparatus in Chapter 3. The three crucial elements to realize strong photon-photon interactions are a high-cooperativity cavity, an atomic ensemble prepared with the specific transition structure and correct initial state, and a free-space mode that couples strongly with the atoms addressed by the cavity mode.

In Chapters 4-6, I illustrate three experiments utilizing this strong photon-photon interaction. Chapter 4 uses a single photon to control the state of a whole optical system. A single photon and no photon (the vacuum) in the free-space channel switch the system between two completely different states, turning on or off the transmission

of the laser beam through the cavity mode. In this experiment, we realize an optical switch and transistor controlled by a single photon. When I was young, I learned that one photon carries a tiny amount of energy and our eyes receive trillions of photons every day. At that time, it was hard to image that a single photon could change anything on its own. However, this experiment convincingly shows that one photon is strong. This photon is like a hero who can stop hundreds of photons which are much stronger than him. In Chapter 4, I will tell this story of the power of one photon.

The second experiment I present demonstrates an interaction between two continuous beams (Chap. 5). After the progress we made with single photon pulse manipulation, we wanted to generalize the techniques to weak continuous beams. In this case, the existence of one beam modulates another beam at the single photon level. It is a deterministic effect which makes two originally uncorrelated beams anti-bunched. The correlation function of the beams leaving the system is measured to be $g^{(2)} = 0.89(1)$. This means that one photon extinguishes a photon in the other beam with a probability of 11%. This technology could be applied to non-destructive measurement. For instance, one could measure the photon number without destroying the photons using this method. This could be useful, for example, in enhancing the security of optical quantum key distribution.

Using the same apparatus and strong interactions, we are working on a third experiment towards real-time nondestructive detection of a traveling photon. Unlike photodiode that detects a photon by converting it to an electronic excitation that destroys this photon, this special detector could tell when a photon travels by without changing this photon's original mode. As a result, the quantum information carried by this photon, if any, such as its polarization, will be untouched while we obtain information about the arrival of this photon. Theoretical predictions and preliminary experimental results will be presented in Chapter 6.

The last experiment I will present is vacuum induced transparency (VIT). We have known that the vacuum is not empty since quantum electrodynamics was established. Even when there are no photons excited in the cavity mode, there are always vacuum

fluctuations which connect the vacuum to higher excited states. The most famous examples of the measurable vacuum fluctuation are the van der Waals force and Casimir force. In our experiment, we replace the coupling beam in EIT by vacuum. This experiment shows that vacuum behaves as a laser field, coupling two atomic levels and generating a transmission window for a laser beam through an otherwise opaque medium. It also clarifies that "empty" is not empty. In order to observe this effect, we use an optical cavity to quantize the light field and enhance the interaction strength between the atoms and the vacuum. In Chapter 7, I will discuss how to control and realize this vacuum effect.

The vacuum in the last experiment and a single photon in the first experiment both tell us a "weak" single photon (or vacuum) is not weak; instead, it can be very useful. It becomes powerful with the help of high-cooperativity cavity. We are working with a cavity of geometric cooperativity of $\eta = 8.6$, which already brings us the interesting results mentioned above. A cavity with even higher cooperativity and lower loss would enable even stronger photon-photon interactions and thus more exciting explorations. In Chap. 8, a step toward a higher cooperativity cavity, namely the fabrication of micro mirrors and the measurement of a micro cavity, is documented.

Chapter 2

Photon-Photon Interactions

In order to set up strong interactions between two photons in different beam paths, we utilized two different mechanisms to confine each photon locally in the atomic ensemble, and to overlap them with each other in both the temporal and spatial domains. Then they can interact quite strongly in the nonlinear atomic medium, which enables interesting phenomena and useful devices. One of the photons (free-space photon) travels through the atomic ensemble as a dark-state polariton, which is a superposition of a photon and a collective atomic excitation to the state coupling to the cavity transition, introduced by the mechanism of electromagnetically induced transparency. The other photon (cavity photon) is trapped by a high-cooperativity cavity and interacts strongly with the atomic excitation component caused by the first photon, through the N-type level structure of the atomic medium (fig. 2-1).

In this chapter, I first introduce the four-level atomic structure and the Hamiltonian of this system (Sec. 2.1). Then, Sec. 2.2 gives an example, utilizing the Hamiltonian to predict the cross modulation of two light beams in the weak-field limit of this system when each of the beams and the cavity are resonant with their atomic transitions. In Sections 2.3 and 2.4, two different mechanisms that confine photons are described separately, both in intuitive pictures and quantitative expressions. Sec. 2.3 illustrates electromagnetically induced transparency, used to trap free-space photons as dark-state polaritons. Sec. 2.4 describes atom-cavity interactions, where the cavity cooperativity is derived, and the transmission, reflection and free-space scattering of

an incident cavity photon are quantified using this cooperativity parameter. Lastly, Sec. 2.5 shows how the free-space photons, in the form of dark-state polaritons, interact strongly with the cavity photons, even at single-photon level. The intuitive understanding of such strong photon-photon interactions and principles to predict interaction performance in different conditions are presented.

2.1 System Hamiltonian

The essential features of the photon-photon interaction in our system are captured by a simplified model in terms of four-level atoms uniformly coupled to an optical cavity as well as a focused free-space beam. I will discuss how our real system maps onto this model in Sec. 2.2-2.5 below. For now, let us assume that each atom has a four-state N-type level structure $|f\rangle \leftrightarrow |d\rangle \leftrightarrow |c\rangle \leftrightarrow |e\rangle$ with two stable ground states $|f\rangle$, $|c\rangle$, and two electronic excited states $|d\rangle$, $|e\rangle$, as shown in figure 2-1. For atoms prepared in state $|f\rangle$, this atomic structure mediates an effective interaction between free-space photons (photons near resonant with the $|f\rangle \rightarrow |d\rangle$ transition coupled to the free-space mode) and cavity photons (photons near resonant with the $|c\rangle \rightarrow |e\rangle$ transition coupled to the optical cavity mode). These two transitions are connected via a coupling laser that addresses the $|d\rangle \rightarrow |c\rangle$ transition. This coupling laser induces electromagnetically induced transparency (EIT) for the free-space photons and converts free-space photons into collective atomic excitations in state $|c\rangle$ that interact strongly with cavity photons. On the other hand, cavity photons introduce energy shift or decoherence for the collective atomic excitation components in state $|c\rangle$, which in turn introduces absorption or phase shift for free-space photons.

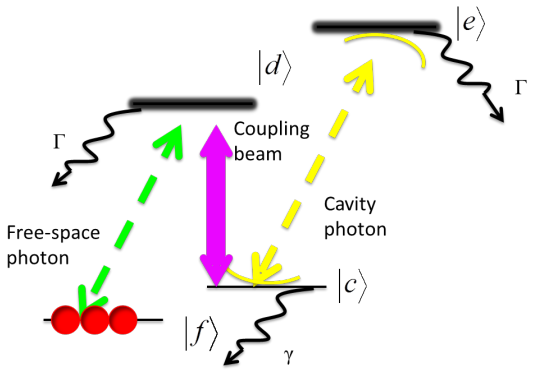

Figure 2-1: Atomic level structure scheme of the strong photon-photon interaction system.

The Hamiltonian for this system, including the decay, can be written as [43]

$$\begin{aligned} H_{eff}/\hbar = & \sum_k c\,|k|\, a_k^\dagger a_k + (\omega_c - \mathrm{i}\kappa/2) b^\dagger b + \mathrm{i}\mathcal{E}(b^\dagger - b) \\ & + (\omega_{fd} - \mathrm{i}\Gamma/2) \sum_j |d\rangle_j \langle d| + (\omega_{ce} - \mathrm{i}\Gamma/2) \sum_j |e\rangle_j \langle e| + (\omega_{fc} - \mathrm{i}\gamma/2) \sum_j |c\rangle_j \langle c| \\ & + \sum_x \left(\Omega/2\, e^{\mathrm{i}\omega_{dc}t} |c\rangle_x \langle d| + g_f a^\dagger(x)\ |f\rangle_x \langle d| + g_c\, b^\dagger |c\rangle_x \langle e| + h.c. \right) \end{aligned} \tag{2.1}$$

Here, c denotes the speed of light, k is the wavenumber of the free-space field, ω_c is the cavity frequency and κ is the decay rate of the cavity. The electric field operators for the free-space and cavity fields can be written as $\hat{\mathcal{E}}_f(x) = \sqrt{\frac{\hbar c k_0}{\epsilon_0 V}} a(x)$ and $\hat{\mathcal{E}}_c = \sqrt{\frac{\hbar\omega_c}{\epsilon_0 V}} b$, where $a(x) = N^{-1/2} \sum_k e^{\mathrm{i}kx} a_k$ and b are bosonic annihilation operators, ck_0 is the center frequency of the free-space field, and V is the quantization volume. Additionally, $\mathcal{E}$ is the amplitude of the cavity input field, $\omega_{\mu\nu}$ is the atomic transition energy between states μ and ν, Ω is the classical Rabi frequency for the coupling field, Γ is the spontaneous emission rate out of the excited states $|d\rangle$ and $|e\rangle$, γ is decoherence rate of two stable ground states $|f\rangle$ and $|c\rangle$, and g_f, g_c are the bare couplings of the atomic transition to the two fields.

2.2 Cross Modulation

We will first look at the simplest case, where the free-space and cavity fields are resonant with the atoms so that $ck_0 = \omega_{fd}$ and $\omega_c = \omega_{ce}$. We are interested in the interactions of free-space photons and cavity photons at the single photon level (quantum limit). Such interactions can be measured by sending coherent fields into the system. As the characteristic time that free-space photons and cavity photons live in the system are Γ/Ω^2 and $1/\kappa$ respectively, when the input fields are weak enough so that average input photon numbers in each of these characteristic times is much less than one, the projected input photon number Fock state is either $|0\rangle$ or $|1\rangle$ (the probability of $|2\rangle$ is negligible). Then the output fields of the system describe the interaction of free-space and cavity photons in their single photon level. Now we will analyze the situation that describes the steady state for the case of input fields in the weak coherent states $g_f \langle a\rangle \ll \Omega^2/\Gamma$ and $g_c \langle b\rangle \ll \kappa$. In this limit, we can calculate the two-time correlation function between the free-space and cavity transmission fields, which is expressed as

$$g^{(2)}(x,\tau) = \frac{\langle b^\dagger(t)a^\dagger(x,t+\tau)a(x,t+\tau)b(t)\rangle}{\langle a^\dagger(x,t)a(x,t)\rangle\langle b^\dagger(t)b(t)\rangle}. \tag{2.2}$$

This function describes the dependencies of the free-space and cavity beams after transmission through this system as a function of separation time. It can be used to assess the interaction of the two beams in the system, by detecting and measuring the output beams' correlation, when the original input beams are independent and uncorrelated with $g^{(2)}(\tau) = 1$. This function quantifies the cross modulation efficiency of one photon by the other (free-space photon or cavity photon) in continuous operation, as shown later in this subsection.

By working in the weak field limit to express the steady state of the Hamiltonian, and taking the picture where the detection of a photon corresponds to a quantum jump from the steady state $|\chi_{ss}\rangle$ into the state $a(x,t)|\chi_{ss}\rangle$ for $\tau < 0$ and $b(t)|\chi_{ss}\rangle$ for $\tau > 0$, we calculate the two-time correlation function to be (see details in ref. [43])

$$g^{(2)}(\tau) = \left[1 - \left(1 - e^{-\frac{\mathcal{N}}{2\zeta}}\right)\frac{\eta}{1+\eta}e^{-\kappa_{\gtrless}|\tau|/2}\right]^2 \tag{2.3}$$

For $\tau < 0$, $\kappa_< = \kappa$ is the cavity linewidth; for $\tau > 0$, $\kappa_> = \Omega^2/\Gamma + \gamma$ is the EIT linewidth including decoherence γ [37]. η is the cavity cooperativity, which is a crucial parameter for the cavity and will be described in detail in Sec. 2.4. $\mathcal{N}$ is the optical depth of the free-space path, while $\zeta = \frac{\kappa_>}{\kappa_> - \gamma}\left(1 + \frac{\kappa_>}{\kappa_<(1+\eta)}\right) > 1$ is a correction factor. In this correction factor ζ, the first multiplicative factor arises from imperfect EIT, which reduces the cross modulation efficiency by introducing decoherence and decreasing the probability that the polarization survives. The second multiplicative factor accounts for the difference in the full (broadened) cavity lifetime and the polariton lifetime: when the polariton lifetime is comparable with or shorter than the cavity lifetime, the interaction time (and thus the cross modulation) is reduced.

At time $\tau = 0$, the correlation function $g^{(2)}(\tau = 0) < 1$. We can quantify the cross modulation efficiency with $1 - g^{(2)}(\tau = 0)$. It shows that a free-space photon and a cavity photon would modulate, or partially block each other, when they come into the system at the same time. The correlation function $g^{(2)}(\tau)$ shows the mutual blocking is asymmetric in time, one side ($\tau < 0$) being determined by the lifetime of cavity photon living in the cavity, the other side ($\tau > 0$) being determined by the EIT polariton lifetime. The modulation efficiency is determined by the combination of cavity cooperativity η, the optical depth of the free-space path $\mathcal{N}$ and the correction factor ζ. In the extreme case that $\mathcal{N} \gg \zeta$ and $\eta \gg 1$, $g^{(2)}(\tau = 0)$ will tend to zero, which shows a complete blocking of the two beams by each other.

This cross modulation behavior of the system, using transmission probability of free-space and cavity photons, will be understood intuitively and described experimentally in Chapter 5, after acquiring intuitive knowledge and quantified expression of EIT and atom-cavity interaction in Sec. 2.3 and 2.4.

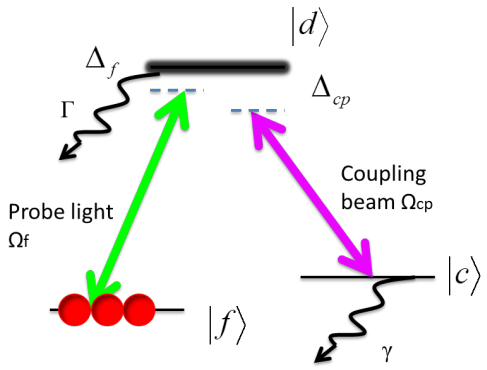

Figure 2-2: 3-level Λ type scheme for EIT and dark-state polariton. $|f\rangle$ and $|c\rangle$ are (meta-)stable ground states and $|d\rangle$ is electronic excited states. The $|f\rangle \rightarrow |d\rangle$ and the $|c\rangle \rightarrow |d\rangle$ transitions are coupled with probe field Ω_f and coupling field with Rabi frequency Ω_{cp}, respectively.

2.3 Electromagnetically Induced Transparency and the Dark-state Polariton

The idea of electromagnetically induced transparency (EIT) has been around for almost three decades now, and it has developed into a powerful tool to suppress dissipation and control the dispersive properties of a material for transmitted photons, using another light field [37, 44, 45]. Using this effect, a photon's absorption by an atomic ensemble is suppressed via quantum interference, and the photon's group velocity in this ensemble is slowed down due to the sharp dispersion slope. EIT is helpful because the suppression of absorption removes dissipation from the system, as dissipation is harmful for any quantum coherent processes; at the same time, EIT enables strong nonlinear optical interactions [46, 47].

Our interest lies in EIT in the atomic system of Λ type structure $|f\rangle \leftrightarrow |d\rangle \leftrightarrow |c\rangle$, as shown in Fig. 2-2. Here, the states $|f\rangle$ and $|c\rangle$ are (meta-)stable ground states, while $|d\rangle$ is the electronic excited state. The states pairs, $|f\rangle$ and $|d\rangle$, $|c\rangle$ and $|d\rangle$ are coupled via a electric dipole transition, while the transition between states $|f\rangle$ and $|c\rangle$ is dipole-forbidden. When a probe field Ω_f resonant with the $|f\rangle \leftrightarrow |d\rangle$ transition is incident onto the atoms alone, the photons will be absorbed and rescattered into free space as happens in a two-level atomic system. However, when there is an additional

field, the coupling field Ω_{cp} (usually much stronger than probe field) on the $|c\rangle \leftrightarrow |d\rangle$ transition, the absorption of the probe field is suppressed. This is achieved through destructive interference between the two transition couplings, which, combined with atomic coherence, cancels the atomic excited-state population, and prevents the probe photons from being scattered into free space.

From the viewpoint of electric-field interference, the coupling field Ω_{cp} builds up an indirect pathway to excite the atomic component to state $|d\rangle$, via the $|f\rangle \leftrightarrow |d\rangle \leftrightarrow |c\rangle \leftrightarrow |d\rangle$ path. This indirect pathway has a excitation probability of equal magnitude and opposite sign to the excitation probability of the direct pathway, via the $|f\rangle \leftrightarrow |d\rangle$ path. Thus the population amplitude for $|d\rangle$, which is the only decaying state and thus the only way to provide absorption and dissipation in the system (assume γ is zero for now), is cancelled. As a result, the coupling field engineers the atomic medium, canceling the linear susceptibility at resonance through destructive interference and removing the dissipation of the system. At the same time, the coupling field also enhances the nonlinear susceptibility through constructive interference [37].

The same physics underlying the cancellation of absorption of the probe field in EIT is observed in the phenomena of the dark-state and coherent population trapping in the atomic ensemble. When both the probe field and coupling field are applied to a the Λ-type three-level atom, the light-atom system in Fig. 2-2 result in the Hamiltonian $H = H_0 + H_{int}$, where H_0 is the Hamiltonian of the bare atom and H_{int} is that of the interaction with the fields. Introducing the rotating wave approximation, where Ω_f, Ω_{cp} are the Rabi frequencies of the atom-field interaction for probe field and coupling field respectively, the Hamiltonians are written as

$$H_0 = -\frac{\hbar}{2}\begin{bmatrix} 0 & 0 & 0 \\ 0 & i\Gamma & 0 \\ 0 & 0 & i\gamma \end{bmatrix}. \tag{2.4}$$

$$H_{int} = -\frac{\hbar}{2}\begin{bmatrix} 0 & \Omega_f & 0 \\ \Omega_f & -2\Delta_f & \Omega_{cp} \\ 0 & \Omega_{cp} & -2(\Delta_f - \Delta_{cp}) \end{bmatrix}. \tag{2.5}$$

Here $\Delta_f = \omega_{df} - \omega_f$ and $\Delta_{cp} = \omega_{dc} - \omega_{cp}$ are the detunings of the probe and coupling field frequencies from the corresponding atomic transitions, Γ is decay rate of the excited state $|d\rangle$, and γ is the dephasing rate of the dipole-forbidden transition $|c\rangle \leftrightarrow |f\rangle$.

One of the eigenstates of the interaction Hamiltonian is

$$|D\rangle = \frac{\Omega_{cp}|f\rangle - \Omega_f|c\rangle}{\Omega_f^2 + \Omega_{cp}^2}, \tag{2.6}$$

This state contains no amplitude of the excited state $|d\rangle$ and has ground state amplitudes proportional to the fields. This so called "dark state" is effectively decoupled from the light fields. Thus in the time-scale that γ is ignorable, this state is a non-dissipative state of the light-atom system and maintains maximal coherence.

When the light field interacts with an atomic ensemble instead of one atom, one needs to use master equation to work out the optical properties of the atomic ensemble for the probe field [37]. It turns out that the amplitude transfer function of the atomic ensemble t can be expressed in terms of the linear susceptibility $\chi^{(1)}$,

$$t = \exp\left(i\frac{1}{2}kL\chi^{(1)}\right), \tag{2.7}$$

where

$$\chi^{(1)} = i\frac{\mathcal{N}}{kL}\Gamma\left[\frac{4\delta\left(\Omega_{cp}^2 - 4\delta\Delta\right) - 4\Delta\gamma^2}{\left(\Omega_{cp}^2 + (\Gamma + i2\Delta)(\gamma + i2\delta)\right)^2} + i\frac{8\delta^2\Gamma + 2\gamma\left(\Omega_{cp}^2 + \Gamma\gamma\right)}{\left(\Omega_{cp}^2 + (\Gamma + i2\Delta)(\gamma + i2\delta)\right)^2}\right]. \tag{2.8}$$

Here, we define the single-photon detuning as $\Delta = \Delta_f$, two-photon detuning as $\delta = \Delta_f - \Delta_{cp}$, resonant optical depth of the atomic ensemble with length L as $\mathcal{N}$, and wave number of the probe field as k.

The transmission probability T and group velocity v_{gr} of probe field transmitting through the atomic ensemble, when both probe and coupling fields are on atomic

resonance, turn out to be

$$\begin{aligned} T = |t|^2 &= \exp\left(ikL\chi^{(1)}\right) \\ &= \exp\left(-\frac{\mathcal{N}}{\frac{\Omega_{cp}^2}{\Gamma\gamma_d}+1}\right), \end{aligned} \tag{2.9}$$

and

$$\begin{aligned} v_{gr} &= \frac{c}{n+\omega_f\frac{dn}{d\omega_f}} \\ &= \frac{c}{1+\mathcal{N}\frac{c}{L}\frac{1}{\gamma}\frac{1}{\frac{\Omega_{cp}^2}{\Gamma\gamma_d}+1}} \end{aligned} \tag{2.10}$$

as $n = \sqrt{1+\Re[\chi^{(1)}]}$.

Thus, for a fixed coupling field Rabi frequency Ω_{cp}, the reduced group velocity v_{gr} of the probe field gives rise to a group delay τ_d in the atomic ensemble,

$$\tau_d = L\left(\frac{1}{v_{gr}}-\frac{1}{c}\right) = \frac{Ln_{gr}}{c} = \frac{\mathcal{N}}{\frac{\Omega_{cp}^2}{\Gamma}+\gamma}. \tag{2.11}$$

In the cold atomic ensemble we are working with, $\mathcal{N} \approx 1$ and $\gamma \ll \Gamma$. One can choose a fixed coupling field Rabi frequency letting $\frac{\Omega_{cp}^2}{\Gamma} \gg \gamma$, so that $T \to 1$ and $v_{gr} \ll c$. So the probe field gets fully transmitted and is significantly delayed by a time of τ_d. We can consider it as if the probe field gets stored in the atomic ensemble for an average time of τ_d.

When the probe field is a quantum field instead of a classical field, to describe the propagation properties of such field in EIT media, Fleischhauer and Lukin introduced the concept of "dark-state polaritons", which is a formstable quantum excitations associated with the propagation of quantum fields in EIT media [36].

When the Rabi-frequency of the probe quantum field Ω_f is initially much smaller than the Rabi-frequency of the coupling field $\Omega_{cp}(t)$, the number of photons in the probe pulse is much less than the number of atoms in the ensemble addressed by the probe field, and the change of coupling field Rabi-frequency $\Omega_{cp}(t)$ is sufficiently slow,

the propagation of the probe pulse $\mathbf{E}(z,t)$ is governed by the equation

$$\left(\frac{\partial}{\partial t}+c\frac{\partial}{\partial z}\right)\mathbf{E}(z,t)=-\frac{g^2N}{\Omega_{cp}(t)}\frac{\partial}{\partial t}\frac{\mathbf{E}(\mathbf{z},\mathbf{t})}{\Omega_{cp}(t)}. \tag{2.12}$$

The collective, slowly varying atomic operators $\sigma_{fc}(z,t)$ are governed by the equation

$$\sigma_{fc}(z,t)=-g\frac{\mathbf{E}(z,t)}{\Omega_{cp}(t)} \tag{2.13}$$

where $\sigma_{fc}(z,t)$ is appropriately averaged over small but macroscopic volumes containing $N_z \gg 1$ particles at position z,

$$\sigma_{fc}(z,t)=\frac{1}{N_z}\sum_{j=1}^{N_z}|f\rangle\langle c|\,e^{-i\omega_{fc}t}. \tag{2.14}$$

Defining a quantum field operator as

$$\begin{gathered}\mathbf{\Psi}(z,t)=\cos\theta(t)\,\mathbf{E}(z,t)-\sin\theta(t)\sqrt{N}\sigma_{fc}(z,t),\\ \cos\theta(t)=\frac{\Omega_{cp}(t)}{\sqrt{\Omega_{cp}^2(t)+g^2N}},\sin\theta(t)=\frac{g\sqrt{N}}{\sqrt{\Omega_{cp}^2(t)+g^2N}},\end{gathered} \tag{2.15}$$

it can be shown that this operator $\mathbf{\Psi}(z,t)$ possesses bosonic commutation relations, and creates dark-states in the ground state where the electromagnetic field is in the vacuum state and atoms are all in state $|f\rangle$ [36]. So the quasi-particles created by this operator are called "dark-state polaritons", which are exactly the eigenstates of this system.

The dark-state polaritons propagate with velocity $v_{gr}(t)=c\cos\theta(t)$. This velocity is directly related to the ratio of the collective Rabi-frequency of the two atomic couplings, which can be externally controlled by adiabatically changing the coupling field as the pulse propagates. In particular, dark-state polaritons can be stopped and reaccelerated in such a way that their temporal shape and quantum state are preserved, as used in Chap. 4. By adiabatically decreasing $\theta(t)$ from 0 to $\pi/2$, the original polaritons with full photonic component gradually turn into polaritons

with full atomic excitation component, mapping the initial light pulse onto collective, metastable states of the atomic ensemble. In this process, the quantum state of light is ideally transferred to collective atomic excitations. Likewise, the collective atomic excitation can be re-accelerated back to a light pulse, with both the temporal shape and quantum state of the original light pulse.

For a fixed Rabi-frequency of the coupling field, as used in the experiments described in Chapters 5 and 6, the polaritons are composed partially of photonic components and partially of collective atomic excitation components. The details associated with each experiment will be discussed further in these chapters, as the collective atomic excitation components will change the transmission, reflection and emission of the cavity photons.

As shown above, EIT can store and retrieve, or slow the light pulse by mapping it onto the collective atomic excitation. This achieves the dissipation-free trapping of traveling photons that is required to realize strong dissipation-free photon-photon interactions. However, EIT alone does not provide such interactions between two single-photon pulses due to the mismatched group velocities of the two interacting pulses. So we used another mechanism, namely a high-cooperativity cavity that traps the other photon in both temporal and spatial domains that overlap with the first photon. The properties of strong photon-atom interactions in a high-cooperativity cavity are illustrated below.

2.4 Atom-Cavity Interactions

The essential features of the atom-cavity interactions in our system can be quantitatively described using a classical picture, in terms of two-level atoms coupled to an high-finesse optical cavity [48]. I will first use the key parameter, the cavity cooperativity parameter, to predict the interaction between atoms and a cavity in the ideal case of uniformly coupled atoms and non-loss cavity. Then I will show how to adapt the ideal system to our real system.

For now, let us assume that each atom has two states, the ground state $|c\rangle$, and

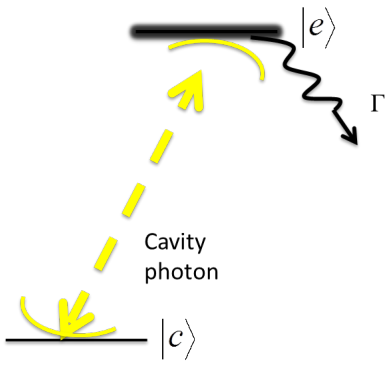

Figure 2-3: Atomic level structure scheme of atom-cavity interaction when the atom has a two level structure. Here, $\Delta_c = \omega - \omega_{ec}$ is the detuning between the incident light and the atomic resonance, and $\delta_c = \omega - \omega_c$ is the detuning between the incident light and the cavity resonance detuning.

the excited state $|e\rangle$ with linewidth Γ at energy $\hbar\omega_{ec}$ (see Fig. 2-3). All the atoms couple uniformly to a high-finesse standing-wave optical cavity of Gaussian TEM_{00} mode with a waist w and cavity length L. In the ideal case, we assume this cavity to have two identical, lossless, partially transmitting mirrors of amplitude transmission coefficient $q \ll 1$, with all the atoms located on the cavity mode axis near the waist at an antinode.

For the ideal cavity without atoms inside, the resonance frequencies of the cavity are integer multiples of the free spectral range ν_{FSR}, given by

$$\nu_{\mathrm{FSR}} = \frac{c}{2L}, \tag{2.16}$$

which is the inverse of the time that a photon makes one round trip inside this cavity. The quality of the cavity is characterized by the finesse $\mathcal{F}$, given by

$$\mathcal{F} = \frac{\pi}{q^2}. \tag{2.17}$$

It turns out that the number of average round trips $\langle N \rangle$ a photon can make before

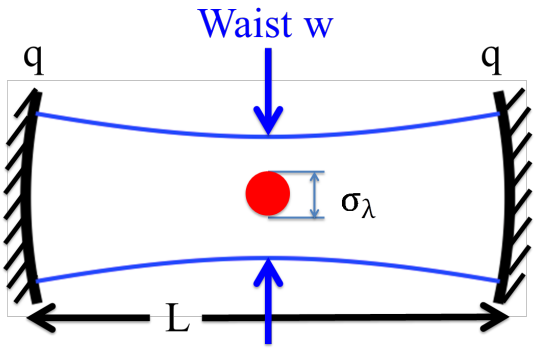

Figure 2-4: Schematic of an atom with cross section σ_λ in an optical cavity.

leaving the cavity by transmitting through the mirrors is

$$\begin{aligned}\langle N\rangle &= \sum_{N=1}^{\infty} N\left(1-2q^2\right)^{N-1} 2q^2 \\ &= \frac{1}{2q^2} = \frac{\mathcal{F}}{2\pi}\end{aligned} \tag{2.18}$$

As shown in Fig. 2-4, the resonant atomic absorption cross section for each of the atoms (for a traveling light field) is

$$\sigma_{res} = \frac{6\pi}{k^2}, \tag{2.19}$$

where $k = \omega_{ec}/c$ is the amplitude of the wave vector on atomic resonance. Then, for a resonant photon pulse propagating along the cavity Gaussian TEM_{00} mode with waist w and thus spatial cross section

$$A = \frac{\pi}{2}w^2, \tag{2.20}$$

the absorption probability is

$$P_{abs} = \frac{\sigma_{res}}{A} = \frac{12}{k^2 w^2} \tag{2.21}$$

for a single trip.

Now we can define the antinode cavity cooperativity parameter η as

$$\eta = P_{abs} \times 4 \times \langle N \rangle = \frac{24\mathcal{F}}{\pi k^2 w^2}, \tag{2.22}$$

where the additional factor of four accounts for the four times larger intensity at an antinode of a standing wave compared to a traveling wave. The cavity cooperativity η is dimensionless and can be understood as the absorption probability of a resonant photon by an atom inside a cavity in the weak-coupling limit $\eta \ll 1$. In the strong-coupling limit $\eta > 1$, the atomic dipole is driven strongly enough by the cavity field that the back action of the field generated by the atomic dipole has to be taken into account. In both weak and strong coupling cases, the cooperativity can always be understood as the ratio of the reemission probability into the cavity mode to the emission probability into the free-space mode when there is one atom inside the cavity.

The cavity cooperativity can also be understood as the ratio between coherent processes and dissipative processes in a cavity system with a single atom inside, as

$$\eta = \frac{4g^2}{\Gamma\kappa}. \tag{2.23}$$

Here Γ is the decay rate of atomic excited state $|e\rangle$, which quantifies the dissipation process of the atom scattering a photon into the free-space mode; $\kappa = \nu_{\text{FSR}}/\langle N \rangle$ is the cavity linewidth, which quantifies the dissipation rate of a photon leaking out of the cavity; $2g$ is the single-photon Rabi frequency at the antinode, which quantifies the coherent interactions between a single photon and a single atom inside of the cavity.

The cavity cooperativity parameter η plays a central role in describing the interactions between atoms and cavity photons. η predicts the transmission, reflection and emission for photons incident onto the cavity with atoms inside, and also predicts the back action on the atoms. We consider a cavity with N_c atoms sitting at antinode on the cavity axis, and the light incident onto the cavity with light field E_{in} and power P_{in}. Following the classical analysis described in reference [48], the field E^i_{tr} transmitted through the cavity, the field E^i_{ref} reflected by the cavity, and the power $P^i_{4\pi}$ emitted by the atoms into free space are determined by the cooperativity parameter

η, given the excited state $|e\rangle$ decay rate Γ, cavity linewidth κ, and the detunings Δ_c and δ_c:

$$\begin{aligned}
E_{tr}^{i} &= \frac{1}{1-2i\frac{\delta_c}{\kappa}-iN_c\eta\left[\mathcal{L}_d\left(\Delta_c\right)+i\mathcal{L}_a\left(\Delta_c\right)\right]}E_{in},\\
E_{r}^{i} &= 1-\frac{1}{1-2i\frac{\delta_c}{\kappa}-iN_c\eta\left[\mathcal{L}_d\left(\Delta_c\right)+i\mathcal{L}_a\left(\Delta_c\right)\right]}E_{in},\\
P_{4\pi}^{i} &= N_c\eta\frac{2\mathcal{L}_a\left(\Delta_c\right)}{\left[1+N_c\eta\mathcal{L}_a\left(\Delta_c\right)\right]^2+\left[2\frac{\delta_c}{\kappa}+N_c\eta\mathcal{L}_d\left(\Delta_c\right)\right]^2}P_{in},
\end{aligned} \tag{2.24}$$

where $\mathcal{L}_d\left(\Delta_c\right)=-\frac{2\Delta_c\Gamma}{\Gamma^2+4\Delta_c^2}$ and $\mathcal{L}_a\left(\Delta_c\right)=\frac{\Gamma^2}{\Gamma^2+4\Delta_c^2}$. Here, $\Delta_c\equiv\omega-\omega_{ec}$ is the detuning between the incident light and the atomic resonance, and $\delta_c\equiv\omega-\omega_c\ll\nu_{\mathrm{FSR}}$ is the detuning between the incident light and the cavity resonance detuning. δ_c much smaller than the cavity free spectral range, as we care about the near detuned situation. For a single photon incident onto the cavity with N_c atoms, the transmission probability $\left|\frac{E_{tr}^{i}}{E_{in}}\right|^2$, transmission phase shift $\mathrm{Arg}\left(\frac{E_{tr}^{i}}{E_{in}}\right)$, reflection probability $\left|\frac{E_{r}^{i}}{E_{in}}\right|^2$, reflection phase shift $\mathrm{Arg}\left(\frac{E_{r}^{i}}{E_{in}}\right)$, and free-space emission probability $\frac{P_{4\pi}^{i}}{P_{in}}$, with or without atoms, can then be determined. I have shown those curves with respect to the photon detunings $\Delta_c=\delta_c$ (assuming cavity is on the atomic resonance $\omega_{ec}=\omega_c$) in Fig. 2-5.

In the real cavity system, the scattering losses from mirror high-reflection coatings are usually not ignorable. We consider cavity with two identical mirrors of amplitude transmission q, reflection r, and loss coefficients l, where $r^2+q^2+l^2=1$, $l\ll1$ and $q\ll1$. In the cavity with mirror loss, the cavity transmitted field E_{tr}^{l}, cavity reflected field E_{ref}^{l} and the power scattered into free-space $P_{4\pi}^{l}$ turn out to be

$$\begin{aligned}
E_{tr}^{l} &= \frac{q^2}{q^2+l^2}\frac{1}{1-2i\frac{\delta_c}{\kappa}-iN_c\eta\left[\mathcal{L}_d\left(\Delta_c\right)+i\mathcal{L}_a\left(\Delta_c\right)\right]}E_{in},\\
E_{r}^{l} &= 1-\frac{q^2}{q^2+l^2}\frac{1}{1-2i\frac{\delta_c}{\kappa}-iN_c\eta\left[\mathcal{L}_d\left(\Delta_c\right)+i\mathcal{L}_a\left(\Delta_c\right)\right]}E_{in},\\
P_{4\pi}^{l} &= N_c\eta\frac{q^2}{q^2+l^2}\frac{2\mathcal{L}_a\left(\Delta_c\right)}{\left[1+N_c\eta\mathcal{L}_a\left(\Delta_c\right)\right]^2+\left[2\frac{\delta_c}{\kappa}+N_c\eta\mathcal{L}_d\left(\Delta_c\right)\right]^2}P_{in}.
\end{aligned} \tag{2.25}$$

The mirror losses act in the cavity-atoms interactions as if there are two beam splitters

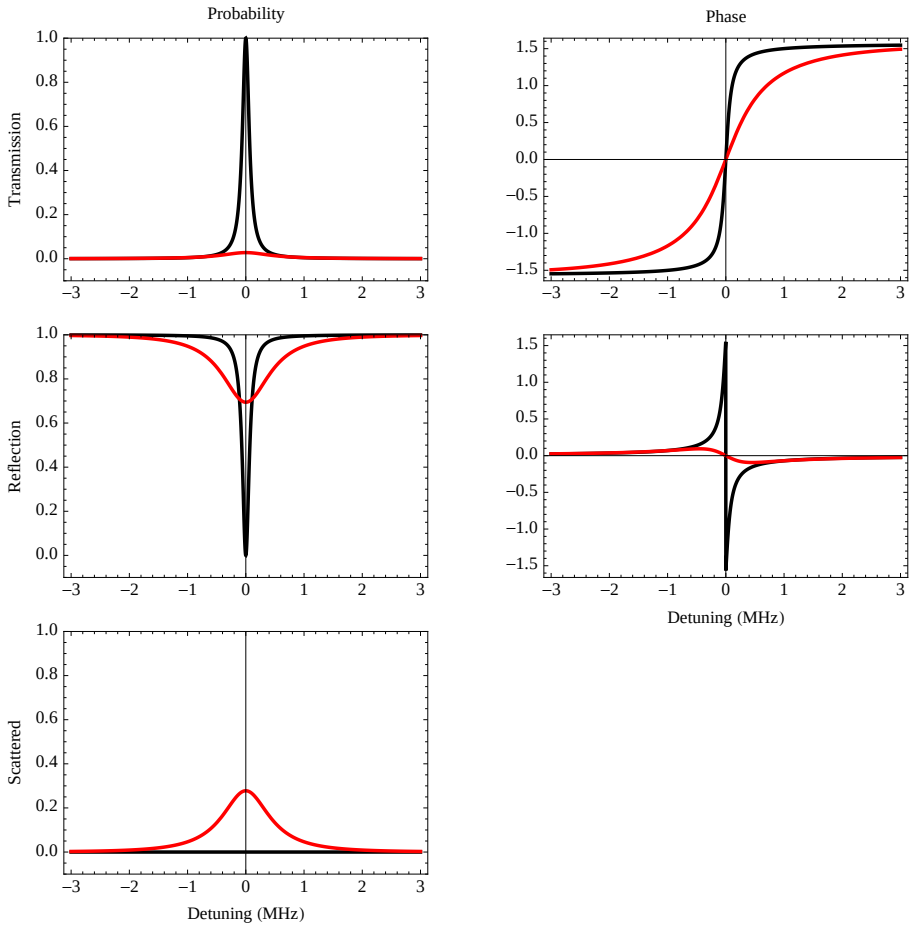

Figure 2-5: Transmission, reflection and free-space emission for a photon incident onto a cavity, with (red curves) and without (black curves) atoms, versus $\Delta_c = \delta_c$ (assuming cavity is on the atomic resonance $\omega_{ec} = \omega_c$). The parameters are chosen as $\Gamma = 2\pi \times 5.2$ MHz, $\kappa = 2\pi \times 0.14$ MHz and $N_c\eta = 5$ in this figure.

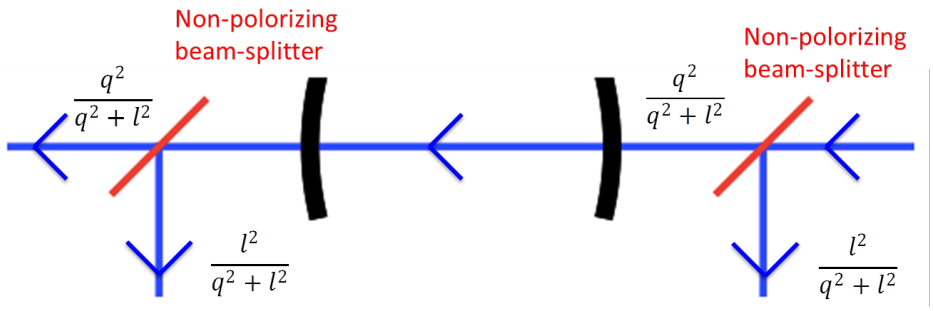

Figure 2-6: Cavity mirrors with scattering and absorption losses act as if there are two beam splitters with transmission ratio of $\frac{q^2}{q^2+l^2}$ positioned before and after the ideal cavity system when we describe the cavity system theoretically.

with transmission ratio of $\frac{q^2}{q^2+l^2}$ positioned on the either side of the ideal cavity system without mirror losses as shown in Fig. 2-6.

In the real cavity-atom system, atoms in the ensemble are located at different positions, not necessarily at the antinode and on the cavity axis. The spatial distribution of the atomic ensemble that photon-photon interactions care about is determined by the details of the atom trap and the volume of atoms that the free-space light addresses. An atom at an antinode experiences a cavity cooperativity η, while an atom at another position experiences equal or lower cavity cooperativity proportional to the cavity coupling field power at that position. To predict the collective performance of the interaction between the cavity and the atomic ensemble, one needs to average expressions (eqn. 2.25) over the cooperativity at different positions, weighted by the atomic distribution. Similarly, to predict the performance of the interaction between the cavity photons and the free-space photons, one needs to average over the cooperativity at different position, weighted by the distribution of the atoms addressed by the free-space photons. Details of the spatial average will be elaborated on in the chapters for each of the experiment.

2.5 Experimental System Model

The experimental system scheme is shown in Fig. 2-7. An ensemble of laser-cooled ^{133}Cs atoms is trapped inside an high-cooperativity cavity. The atomic N-type struc-

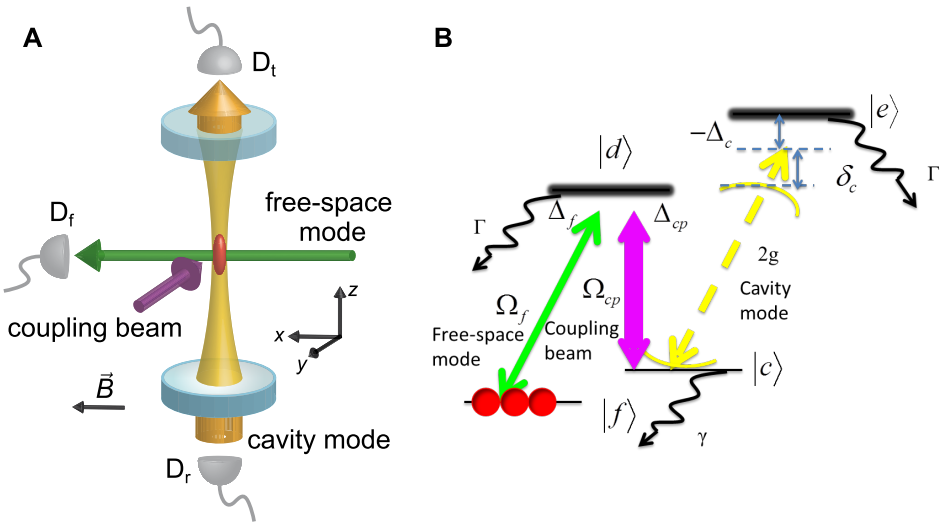

Figure 2-7: Strong photon-photon interaction experimental system scheme. (A) Experimental setup and (B) atomic level scheme. An ensemble of laser-cooled atoms is trapped inside a high-finesse optical resonator and prepared in state $|f\rangle$. The ensemble and the coupling beam mediate interactions between free-space ($|f\rangle \rightarrow |d\rangle$) and cavity photons ($|c\rangle \rightarrow |e\rangle$). Photons are measured with photon counters D_f, D_t and D_r, D_f for free space photon transmitted through atomic ensemble, D_t for cavity photon transmitted through the cavity, and D_r for reflected cavity photons analyzed by some optics (optics not shown in this figure).

ture has four levels chosen as $|f\rangle \equiv \left|6S_{1/2}, F = 3, m_F = 3\right\rangle$, $|d\rangle \equiv \left|6P_{3/2}, 4, 4\right\rangle$, $|c\rangle \equiv \left|6S_{1/2}, 4, 4\right\rangle$ and $|e\rangle \equiv \left|6P_{3/2}, 5, 5\right\rangle$ to provide a good combination of oscillator strengths in both free-space and cavity coupling transitions ($f_{fd} = 0.42, f_{ce} = 0.50$). The choice also has the benefit that the coupling laser efficiently cleans up atoms scattered into state $|c\rangle$. The quantization axis is defined by a uniform magnetic field along the propagation direction ($\vec{x}$) of the free-space beam which is perpendicular to the cavity mode. Two independent weak lasers drive the free-space mode ($|f\rangle \rightarrow |d\rangle$) and the cavity mode ($|c\rangle \rightarrow |e\rangle$). These two transitions are connected by a coupling laser resonant with the $|d\rangle \rightarrow |c\rangle$ transition, mediating an effective interaction between the free-space and cavity modes. All atoms in the ensemble are initially optically pumped to state $|f\rangle$.

In the absence of cavity photons, free-space photons on resonance of transition $|f\rangle \rightarrow |d\rangle$ are transmitted through the ensemble, traveling in the medium as dark-state polaritons as mentioned in Sec. 2.3. The free-space photons travel slowly in

the atomic medium as a superposition of a traveling photon and a collective atomic excitation to the state $|c\rangle$, staying in the ensemble for an average time of $\tau_d = \frac{\mathcal{N}}{\frac{\Omega_{cp}^2}{\Gamma}+\gamma}$, determined by the free-space optical density $\mathcal{N}$, the coupling beam Rabi frequency Ω_{cp}, the excited state $|d\rangle$ decay rate Γ and the dephasing rate γ between states $|f\rangle$ and $|c\rangle$. As one can always make the dephasing rate γ much smaller than Ω_{cp}^2/Γ by increasing Ω_{cp}, the free-space photons can be fully transmitted through the atomic ensemble, since the transmission $T = \exp\left(-\frac{\mathcal{N}}{\frac{\Omega_{cp}^2}{\Gamma\gamma}+1}\right) \to 1$ as $\frac{\Omega_{cp}^2}{\Gamma\gamma} \gg \mathcal{N}$.

In the absence of free-space photons, all atoms remain in state $|f\rangle$, and state $|c\rangle$ is unpopulated. As the transition $|f\rangle \to |d\rangle$ is far detuned from the cavity photon frequency, we can assume that the atoms in state $|f\rangle$ only act to provide a constant refractive index for a cavity photon. Then cavity photons incident onto the "empty" cavity are either reflected or transmitted through the cavity, with amplitude and phase expressed in Eqn. 2.25 for atom number $N_c = 0$, as shown in black curves in Fig. 2-5. There will be no photons rescattered into any free-space mode. Specifically, photons that are resonant with the empty cavity are simply transmitted through the cavity without any reflection or phase shift.

If photons are present in both free-space and cavity modes, they will affect each other's behavior. If a cavity photon comes into the system while a free-space photon is traveling in the atomic ensemble as a dark-state polariton, the cavity photon interacts strongly with the collective atomic excitation component in state $|c\rangle$ of this dark-state polariton. Such interaction changes the probability amplitude of cavity photon transmission and reflection, shifts its phase, and introduces additional cavity loss through photon emission into free space on the $|c\rangle \to |e\rangle$ transition. Such changed propagation of the cavity photon can be predicted by Equation 2.25, using the effective atomic excitation component probability to replace atom number N_c. An example of cavity transmission and reflection spectroscopy is shown in Fig. 2-5. By choosing different detunings and optical analyzers on the cavity mode, we can turn this systems into optical transistor (Sec. 4), optical modulator (Sec. 5), phase shifter and photon detector, all working at single-photon level.

On the other hand, the interaction between cavity photon and dark-state polariton

influences the free-space photon. If the cavity photon is scattered by the collective atomic excitation component in state $|c\rangle$, such scattering carries information about which exact atom scattered this photon and projects the collective atomic excitation into an excitation of this specific atom. Then the dark-state polariton is collapsed into single atom excitation, and loses its ability to retrieve the free-space photon into its original mode. As a result, the free-space photon is absorbed and is not transmitted through the atomic ensemble. If the cavity photon gets reflected or transmitted through the cavity with a phase shift, such phase shift will make a back action on the dark-state polariton as if the state $|c\rangle$ has a shifted energy level, and changes the transmission probability or phase of the retrieved free-space photon. If the cavity photon gets reflected or transmitted through the cavity without any phase shift, the collective excitation will keep the mapped information and the dark-state polariton will be mapped back into a free-space photon in its original mode. The last situation is how a quantum nondemolition detector can be achieved in this system, as the cavity reflection amplitude change is detected while the free-space photon transmitting through the atomic ensemble without loss. Working conditions and experimental details will be illustrated in Sec. 6.

Chapter 3

Experimental Setup

Now I proceed to present the apparatus that realize strong interactions between two photons. The three crucial elements are a high-cooperativity cavity, an atomic ensemble with specific transition structure, and a free-space mode that couples strongly with atoms addressed by the cavity mode. I describe the physical parameters of the high-cooperativity cavity in Sec. 3.1. We cool and optically trap the cesium atoms in a dipole trap overlapped with the cavity mode, select atoms spatially addressed by the side beam to avoid cavity shifts due to atom number fluctuations, and optically pump atoms to the initial state, as explained in Sec. 3.2. Details of the optimization and calibration for the side beam (free-space mode) are provided in Sec. 3.3, while Sec. 3.4 presents the frequency locking and control scheme for the cavity and all the laser beams. To calibrate this complex system, we optimize and measure the atomic optical depth for the free-space mode, calibrate the coupling beam Rabi frequency for EIT spectra, and use cavity transmission to measure atom numbers of a few to calibrate the cavity-atoms interactions, as explained in Sec. 3.5. This experimental setup, with a few changes of the analyzing optics, is used to realize the experiments that described in the following chapters.

The design and assembly of the core structure including cavity and side lenses are elaborated on Jonathan Simon's and Haruka Tanji's theses [49, 50]. As shown in Fig. 3-1, two high-reflection dielectric coated curved mirrors are each mounted to a tube piezo fixed on a Macor plate to form a vertical cavity. On the same Macor plate

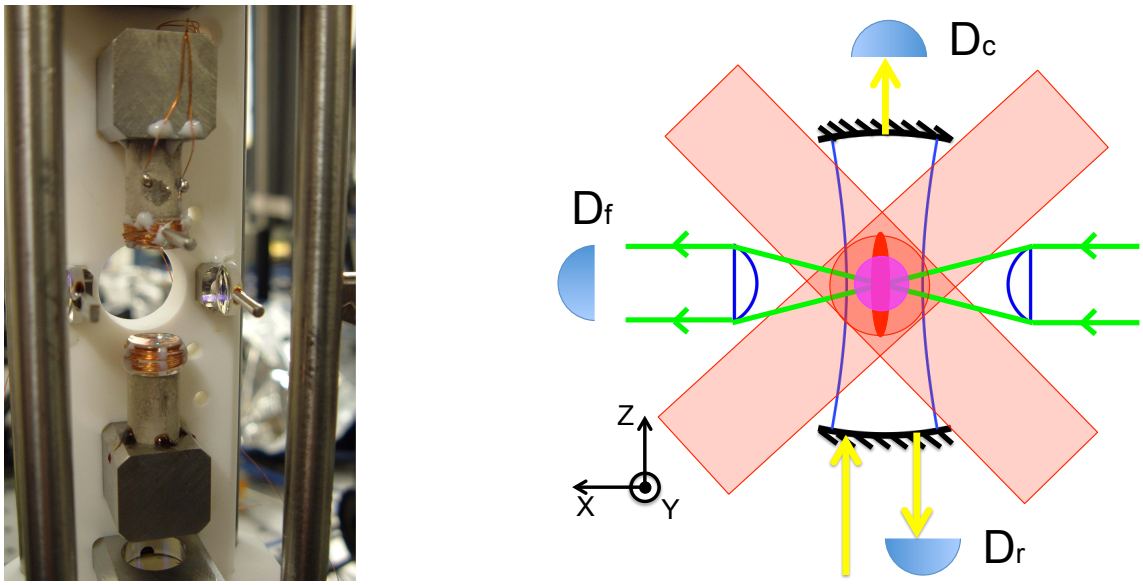

Figure 3-1: The core structure of our apparatus. (Left) A photograph of the assembled structure before placing into chamber. (Right) The schematic of the structure showing how cavity mode, free-space mode and three pairs of MOT beams configure in this core structure.

mounting the cavity, there is a pair of aspheric collimator lenses mounted horizontally to focus the free-space mode to a 2μm waist where it overlaps with the cavity mode. The parameters of the cavity and side lenses are chosen so that both modes have the smallest mode waist possible (to enable stronger interactions) for a stable and high-finesse cavity, and there is sufficient optical access let two of the MOT beams pass diagonally through the mirrors and lenses.

3.1 High-cooperativity Cavity

The optical cavity parameters are listed in Tab. 3.1. The cavity length L is determined by the measured free spectral range ν_{FSR} via the cavity transmission spectrum (see Sec. 2.4). The mirror curvature radius R_M is quoted from the mirror manufacturer datasheet. Cavity linewidth at the wavelength of 852.3 nm is measured to be $\kappa/(2\pi) = (142 \pm 1)$ kHz via the ring-down method when there are no atoms trapped in the cavity (Fig. 3-2). The cavity linewidth is further confirmed by directly observing the cavity transmission spectrum, which fits to a Lorentzian curve with linewidth

of $\kappa/(2\pi) = (158 \pm 7)$ kHz [50], given that our laser-cavity locking system results in a cavity probe laser with linewidth of ~ 20 kHz relative to the cavity (See Sec. 3.4). The cavity finesse is given by $\mathcal{F}_{852} = 2\pi\nu_{\mathrm{FSR}}/\kappa$, infering a total reflection loss for each mirror to be $q^2 + l^2 = \pi/\mathcal{F} = 41\ ppm$. The mirror transmission $q^2 = 27$ ppm and loss $l^2 = 14$ ppm were both measured before being placed them into chamber, and later confirmed as not being contaminated as they agree with the total reflection loss induced from the cavity finesse. The cavity mode waist w_{852} is deduced from the radius of curvature of the cavity mirrors R_M and the cavity length L, since the cavity mode is a Gaussian TEM_{00} mode, where the radius of curvature $R(z)$ of the wavefronts comprising the beam changes as a function of position as $R(z) = z\left[1 + (\frac{z_R}{z})^2\right]$, and the Rayleigh range is $z_R = \frac{\pi w_{852}^2}{\lambda_{852}}$. Similarly, the finesse $\mathcal{F}_{936}$ and mode waist w_{936} for the cavity at our dipole trap wavelength 936 nm, and the finesse $\mathcal{F}_{817}$ for the cavity at the cavity lock laser wavelength 817 nm are all measured as listed in Tab. 3.1.

Optical resonator		$\lambda_{852} = 852.3$ nm
Cavity length	L	13.7 mm [a]
Mirror curvature radius	R_M	(10.0 ± 0.2) mm
Mirror transmission	q^2	27 ppm
Free spectral range	ν_{FSR}	10909 MHz [a]
Linewidth	$\kappa/(2\pi)$	(142 ± 1) kHz
Finesse	$\mathcal{F}_{852}$	$(7.71 \pm 0.05) \times 10^4$
Mode waist	w_{852}	(35.5 ± 0.2) μm
Optical dipole trap		$\lambda_{936} = 936.7$ nm
Mode waist	w_{936}	(37.2 ± 0.2) μm
Finesse	$\mathcal{F}_{936}$	368 ± 20
Trap depth	U_0/h	(6.0 ± 0.3) MHz
Cavity lock mode		$\lambda = 817$ nm
Finesse	$\mathcal{F}_{817}$	$5.0 \pm 0.5 \times 10^4$

Table 3.1: Experimental parameters. The mirror separation and cavity free spectral range (marked [a]) have standard deviations better than the precision we quote.

As a result, for the photons at wavelength of 852.3 nm where we perform all our experiments, the cavity geometric cooperativity parameter $\eta = \frac{24\mathcal{F}_{852}}{\pi k^2 w_{852}^2}$ turns out to be $\eta = 8.6(0.3)$. We thus find our cavity in the single-atom-single-photon strong coupling regime $\eta > 1$, where the coherent processes are stronger than the dissipation

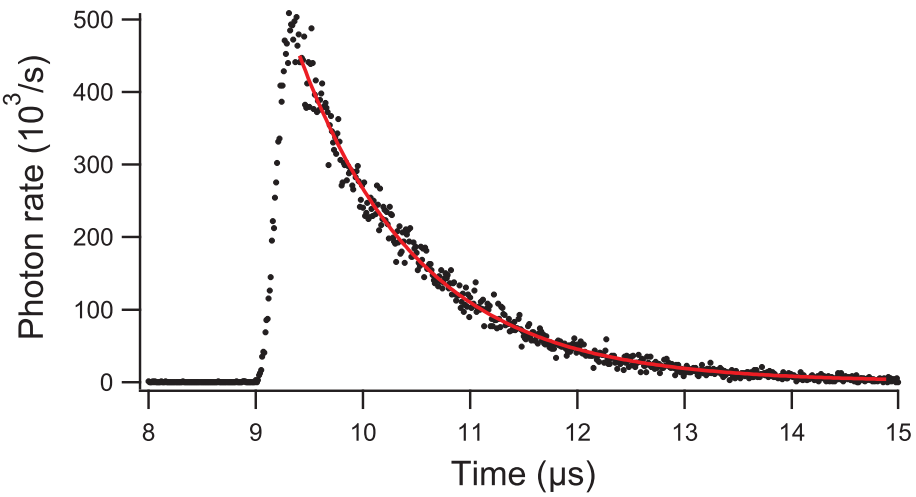

Figure 3-2: Cavity ring-down measurement curve for the empty cavity. We observe a decay of cavity transmission after switching off the frequency component of the cavity incident beam that is on resonant of the empty cavity. This decay is fitted to an exponential formula $y_0 + Ae^{\kappa(t-t_0)}$ to obtain the empty cavity linewidth $\kappa = 0.890 \pm 0.006\mu s^{-1} = 2\pi\,(142 \pm 1)\,\mathrm{kHz}$. When there are atoms stay inside the cavity, those atoms introduce a new decay channel by scattering cavity photons into free space, and increase the decay rate and linewidth of the cavity.

processes, even when the actual cooperativity is reduced by the atomic transition's Clebsch-Gordon coefficients and atomic spatial distribution at locations with field weaker than that at antinode and on cavity axis.

3.2 Preparation of the Atomic Ensemble

The experimental setup and atomic structure scheme are shown in Fig. 3-3 and Fig. 3-4. This atomic N-type structure has four levels chosen as $|f\rangle \equiv \left|6S_{1/2}, F = 3, m_F = 3\right\rangle$, $|d\rangle \equiv \left|6P_{3/2}, 4, 4\right\rangle$, $|c\rangle \equiv \left|6S_{1/2}, 4, 4\right\rangle$ and $|e\rangle \equiv \left|6P_{3/2}, 5, 5\right\rangle$ to provide a good combination of oscillator strengths for both the free-space and cavity coupling transitions ($f_{fd} = 0.42, f_{ce} = 0.50$). The essential requirements to enable strong interactions between photons in our system are that the same ensemble of atoms interacts strongly with both free-space photons and cavity photons. Thus we need to prepare an optically thick (optical density $\mathcal{N} > 1$) sample of atoms that are trapped within the cavity mode for the free-space mode, and cool the atoms down so that the decoherence

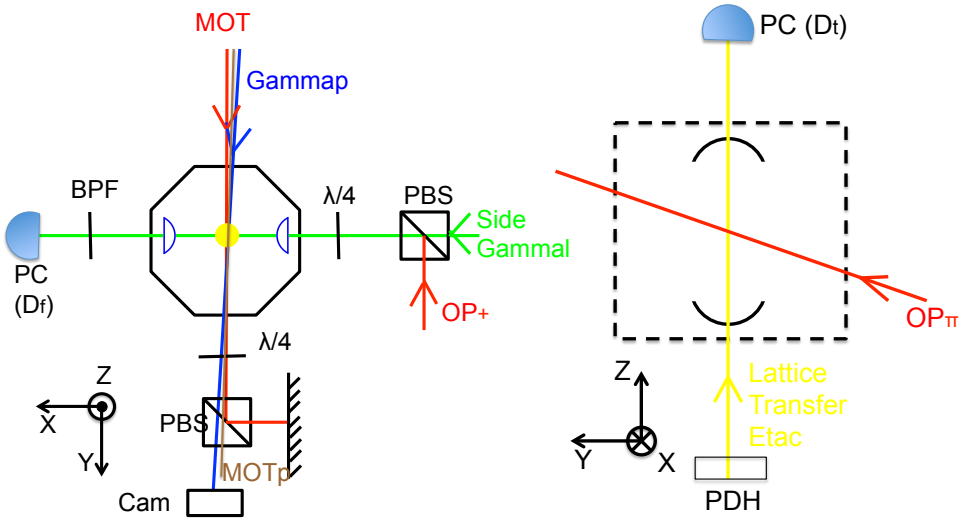

Figure 3-3: (Left) Top view and (Right) side view of experimental setup for atom trapping, cooling, spatial selection and state preparation. PC indicates photon counter. PBS and BS indicate polarizing and non-polarizing beamsplitters. $\lambda/4$ indicates quarter waveplate. PDH indicates Pound-Drever-Hall locking technique optics. Cam indicates camera for absorption imaging. BPF indicates optical bandpass filter transparent at 852 nm. Laser beams are listed in Tab. 3.2.1, along with their coupling atomic transitions, wavelengths, laser sources and purposes.

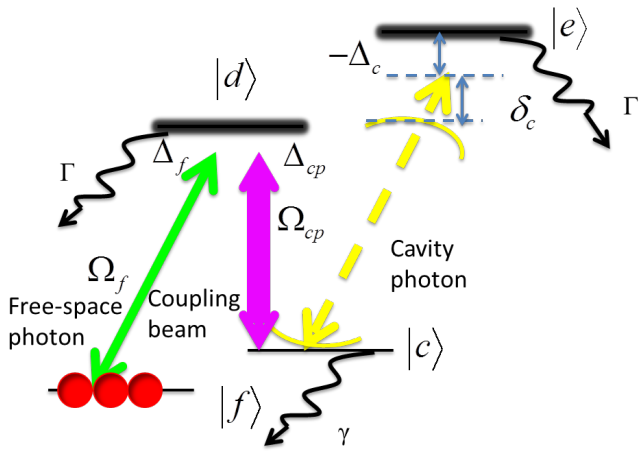

Figure 3-4: The N-type four-level atomic scheme for our experiments.

between the two ground states introduced by Doppler effect is small. An ensemble of cold and dense atoms trapped in the cavity mode is thus preferable, which is achieved by cooling and trapping as described below.

3.2.1 Cooling and Trapping

We first load a magneto-optical trap (MOT) with ^{137}Cs atoms. Then the atomic ensemble is compressed by ramping up the magnetic field gradient to 22 Gauss/cm, and being held at this value for 27 ms. At the beginning of the compression, the MOT beam frequency is detuned further away from resonance and the repump beam power is reduced by a factor of ~ 100. The bias magnetic field is adjusted so that the densest part of the compressed MOT is overlapped with both the optical dipole trap and the focused side beam. The compressed atomic ensemble in the MOT is directly loaded into the optical dipole trap. To observe and optimize the spatial overlap of the compressed MOT and the optical dipole trap, absorption images of atoms were taken, both in the compressed MOT trap and in the optical dipole trap, as shown in Fig. 3-5. Then the compressed MOT trap is turned off and atoms that are not trapped by the optical dipole trap fall down by gravity. By optimizing MOT loading, the spatial overlap and the optical molasses cooling, we achieved a typical atom number of 10^5 trapped in the cavity mode at a temperature of 30 μK. The atom number is precisely measured via the shift of the cavity resonance, which is due to the vacuum Rabi splitting and proportional to the atom number [50, Sec. 2.3.3].

The optical dipole trap we used is a one-dimensional linearly-polarized intra-cavity lattice operated at 936.7 nm, whose optical field intensity and trap depth is amplified by the cavity finesse. The cavity finesse at this wavelength is 368(20), as measured by the trap laser transmission spectral linewidth through the cavity. The trap depth at the antinode is up to 27 MHz, given by the intra-cavity power up to 1.1 W and the cavity mode waist of $w_{936} = 37.2(0.2)$ μm. Typically, we work at a trap depth at the antinode of 6.0(0.3) MHz, and axial and radial trap frequencies of $\omega_{\mathrm{ax}} = 2\pi \times 200$ kHz and $\omega_{\mathrm{rad}} = 2\pi \times 1.1$ kHz, respectively. In fact, we can measure the axial frequency of the trap by modulating trap depth at different frequencies, since atoms are heated

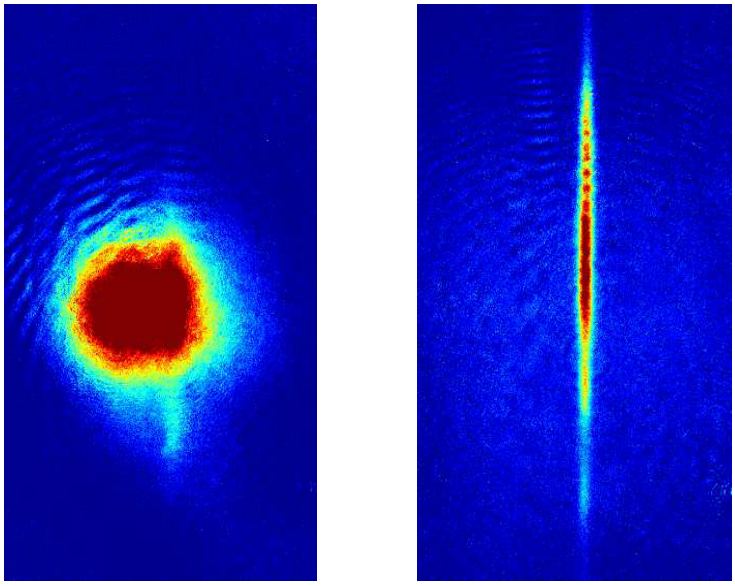

Figure 3-5: Absorption images of the atomic cloud (Left) in compressed MOT and (Right) in the optical dipole trap in cavity mode. We can optimize the spatial overlap of compressed MOT and optical dipole trap by watching their positions in absorption image for two dimensions, and by maximizing the atomic density in the optical dipole trap for a third dimension.

up faster at a frequency that is twice the axial trap frequency. When the trap depth is modulated at different frequencies, the atom numbers left in the trap after a fixed amount of time changes. The frequency at which least atoms are detected is twice the axial frequency. The measured axial trap frequency can be used to confirm the depth of the dipole trap. Fig. 3-6 gives an example of this measurement, showing a axial trap frequency of $2\pi \times 180$ kHz.

The wavelength of the optical trap is chosen to be near the magic wavelength of Cesium atoms for linearly-polarized light, so that the ac Stark shifts for the ground state and excited state of D_2 line remain the same [51]. Therefore the trap depth is state-insensitive; atoms trapped at different trap depth experience the same resonance frequencies for the transitions of interest.

3.2.2 Spatial Selection and Optical Pumping

As mentioned above, we load as many as 10^5 atoms in the optical dipole trap. This helps the interactions in the free-space mode, since a denser atomic sample results in

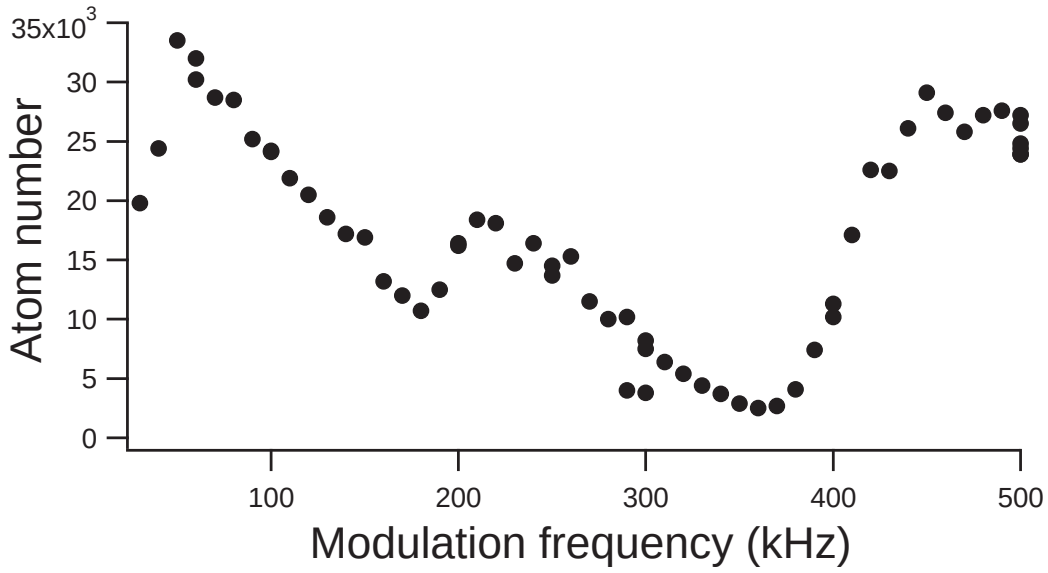

Figure 3-6: Measurement of axial trap frequency of our optical dipole trap. We modulate the trap depth at different modulation frequencies by modulating the frequency of the trap beam via an AOM. The atom numbers are monitored by measuring cavity resonance shift. This plot shows an atom number dip at $2\pi\times180$ kHz and $2\pi\times360$ kHz which gives an axial trap frequency of $2\pi \times 180$ kHz.

higher optical density in the free-space path and stronger interaction between free-space photons and the collective atomic ensemble. However, this large number of atoms in the cavity carries problems for the cavity-atom interaction. First, atoms prepared in state $|f\rangle \equiv \left|6S_{1/2}, F=3, m_F=3\right\rangle$ will be scattered into state $|c\rangle \equiv \left|6S_{1/2}, 4, 4\right\rangle$ by the far detuned optical dipole trap light. This scattering rate is small for each of the atoms, typically at 9/s (App. A.1). However, the rate that one of atoms gets scattered is significantly large at 0.9 $/\mu s$, for a total of 10^5 atoms. When one atom is scattered by the trap light and ends up in $|c\rangle$ state, this atom will spoil the cavity finesse and introduce a dissipation path for cavity photons. This atom is different from the atomic components of the dark-state polaritons traveling in the atomic ensemble, as it will not be retrieved as a free-space photon. Thus, the dissipation of our strong photon-photon interaction system will be increased, and the coherent interaction will be weakened. To prevent this destructive process from happening, we need to limit the total atom number in the cavity. Since the time scale we care about is several microsecond, determined by the coupling beam pumping

Laser beams	atomic transition	Laser source	Used for (as)
Ref beam	$F = 3 \rightarrow F' = 2$	Ref laser	frequency reference
MOT beam	$F = 4 \rightarrow F' = 5$	MOT laser	magneto-optical trap
Repump beam	$F = 3 \rightarrow F' = 4$	Repump laser	magneto-optical trap
Side beam	$F = 3 \rightarrow F' = 4$	Gamma laser	free-space photon
Gammal beam	$F = 4 \rightarrow F' = 4$	Gamma laser	spatial selection
OP_π beam	$F = 3 \rightarrow F' = 2$	Repump laser	optical pumping
OP_+ beam	$F = 3 \rightarrow F' = 2$	Repump laser	optical pumping
Gammap beam	$F = 4 \rightarrow F' = 4$	Gamma laser	coupling, absorption image
MOTp beam	$F = 4 \rightarrow F' = 5$	MOT laser	spatial selection
Etac beam	$F = 4 \rightarrow F' = 5$	Eta laser	cavity photon
Lattice beam	936.7 nm	936 laser	optical dipole trap
Transfer beam	817 nm	817 laser	cavity frequency lock

Table 3.2: List of laser beams used in our system and the atomic transitions that these laser beams address. We can control frequencies of these beams within ~ 1 GHz to meet the experimental requirements.

rate $\frac{\Omega_{cp}^2}{\Gamma}$ that empties out the $|c\rangle$ state, which is fundamentally determined by photon lifetime in the empty cavity, the largest total atom number in the cavity that we can afford to work with is several thousand. Second, since the atom number loaded in the cavity mode on each trial fluctuates, those atoms in $|F = 3, m_F = 3\rangle$ state will introduce a cavity resonance shift and effectively broaden the cavity linewidth and decrease the effective cavity cooperativity. For an atom number loading fluctuation of 10%, 10^5 atoms give a total cavity shift of 3 MHz and a broadening of 0.3 MHz, which is more than the cavity linewidth. This effect limits the total atom number to 4×10^3 which introduce a cavity broadening of 12 kHz, one tenth of the cavity linewidth.

To minimize these fluctuations and absorptions while retaining large optical density for the free-space photon (in "Side beam" mode) investigation, we choose to spatially select the atomic ensemble in the volume addressed by "Side beam", shelve them, and push the rest of the atoms out of the optical dipole trap with a large beam. We first optically pump all the atoms in the optical dipole trap into the state $\left|6S_{1/2}, F = 4\right\rangle$ using a "Repump beam". Then, we protect the atomic ensemble in the volume addressed by the "Side beam" by optically pumping them into $\left|6S_{1/2}, F = 3\right\rangle$

state, using the "Gammal beam" pulse resonant with $\left|6S_{1/2}, F=4\right\rangle \rightarrow \left|6P_{3/2}, F=4\right\rangle$ transition. The "Gammal beam" is aligned with "Side beam" with a larger beam waist at the atoms' position than the waist of "Side beam". We adjust the power and pulse duration of the "Gammal beam" so that atoms in small enough volume are protected to keep the remaining atom number low, and that atoms in a big enough volume are protected to save most of the atoms in the lattice pancakes addressed by "Side beam" (noting that the atomic distributions in each pancake are Guassian with widths of ~ 15 μm, larger than the 2 μm "Side beam" waist). Next, the "MOTp beam" resonant with the closed transition $\left|6S_{1/2}, F=4\right\rangle \rightarrow \left|6P_{3/2}, F'=5\right\rangle$ illuminates on all the atoms, heating all the atoms left in $\left|6S_{1/2}, F=4\right\rangle$ out of the optical dipole trap. As this "MOTp beam" scatters atoms to $\left|6S_{1/2}, F=3\right\rangle$ state (via far-detuned $\left|6S_{1/2}, F=4\right\rangle \rightarrow \left|6P_{3/2}, F'=4\right\rangle$ and $\left|6S_{1/2}, F=4\right\rangle \rightarrow \left|6P_{3/2}, F'=3\right\rangle$ transition) and protects them from being heated out, with a small but not negligible probability, this spatial selection process is repeated for three times. As a result, the total atom number is decreased to 3×10^3 with a sacrifice in the optical density of the side beam that decreases to 90%.

After loading and spatial selection of the atoms, we ramp up magnetic field to 12 Gauss along the x axis (see Fig. 3-3) to define the quantization axis to facilitate optical pumping. Atoms are optically pumped to $|f\rangle \equiv \left|6S_{1/2}, F=3, m_F=3\right\rangle$ state using a π-polarized "OP_π beam" resonant with the $\left|6S_{1/2}, F=3\right\rangle \rightarrow \left|6P_{3/2}, F'=2\right\rangle$ transition and a weak σ_+-polarized "OP_+ beam" on the same transition to break the symmetry. At the same time, the "Gammap beam" on the $|F=4\rangle \rightarrow |F'=4\rangle$ transition pumps atoms back to $F=3$. This optical pumping process pumps more than 90% of the atoms into $|f\rangle$ state. The rest of the atoms can be ignored by the σ_+-polarized free-space photons which are resonant on the $|F=3, m_F=3\rangle \rightarrow |F=4, m_F=4\rangle$ transition, as even the closest and strongest other transition $|F=3, m_F=2\rangle \rightarrow |F=4, m_F=3\rangle$ is 8.6 MHz (more than one linewidth) away and with weaker Clebsch-Gordan coupling coefficient. Now the atomic ensemble is ready to mediate strong interactions between a free-space photon and a cavity photon.

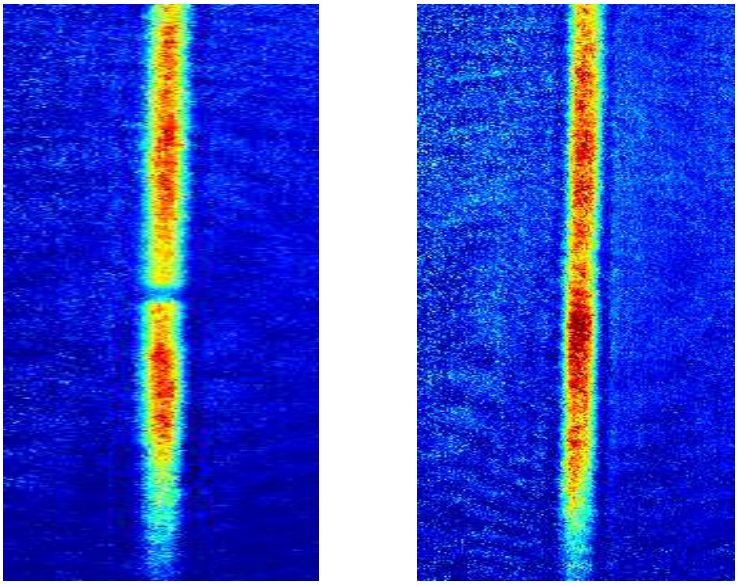

Figure 3-7: Absorption images of the atomic cloud trapped in the optical dipole trap when the side beam is focused onto the densest part of the atomic ensemble. (Left) Atoms addressed by the "Side beam" is heated out of the trap, showing a dark line in the optical dipole trap; (Right) Atoms that are not heated out of the trap by the "Side beam" are shown as a comparison.

3.3 Optimizing the Free-Space Mode

The free-space mode ("Side beam") is focused down to 2 μm in order to probe the densest part of the atomic ensemble in the optical dipole trap, and to guarantee high optical density for the free-space mode. As the optical trap mode overlaps with the cavity mode, probing the densest part automatically guarantees that the atomic ensemble addressed by the side beam couples with cavity photon near the cavity mode axis where the interaction with cavity photons is stronger than off axis. The position of the focus point of the "side beam" inside the chamber can be controlled by optics outside the chamber in all the three dimensions. The design of optics to align the side beam focus with atoms trapped in the cavity mode are described in detail in the thesis of Haruka Tanji-Suzuki [50].

We use absorption imaging (Fig. 3-7) to roughly align the focal point of the "Side beam" to the densest part of atomic ensemble in all three dimensions. The atomic distribution is not sensitive on z axis (within 100 μm range), thus absorption image has good enough resolution to optimize the position in this dimension. For fine align-

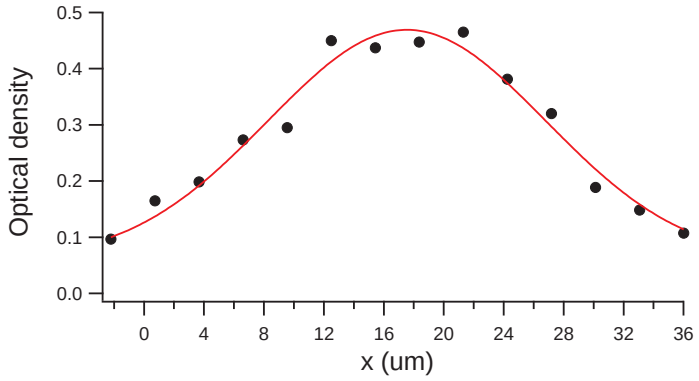

Figure 3-8: The atomic optical density detected by "Side beam" with respect to the beam waist position along the y axis (black dots). Gaussian fitting (red curve) of the data shows the size of the convoluted profile of atomic cloud and the "Side beam" waist to be 13 μm.

ment along the x axis, we use the fact that the focal point of a beam has the highest intensity. Initiating atoms in state $|f\rangle \equiv \left|6S_{1/2}, F = 3, m_F = 3\right\rangle$, we detect the on-resonance optical density of the "Side beam" passing through atomic ensemble with a single-photon counting module (Perkin-Elmer SPCM-AQR), when the π-polarized "Gammap beam" is $\sim$ 5MHz detuned from the $|F = 4, m_F = 4 \rightarrow F' = 4, m'_F = 4\rangle$ transition and pumps atoms back to the $|F = 3, m_F = 3\rangle$ state. When the "Gammap beam" is off, the "Side beam" scatters atoms to $|F = 4\rangle$ state and hides them from optical density measurement at the same time that this beam is measuring the optical density. This rate of scattering atoms to $|F = 4\rangle$ is proportional to the beam intensity and can be measured by detecting the optical density of atoms in $|F = 3, m_F = 3\rangle$ state. In this way, we scan the beam focus along the x axis, fit the curve of scattering rate, and find the position with the highest scattering rate. This is the position where the "Side beam" is focused onto the atomic ensemble. For fine alignment along the y axis, we scan the focus point along the y axis and measure the optical density. The position with highest optical density is where the "Side beam" focuses on the densest part of atomic ensemble in the cavity mode. The data of measured optical density with respect to the "Side beam" focus position along the y axis is shown in Fig. 3-8. The Gaussian fitting gives a combined beam-cloud size of 13 μm in a trap depth of 27 MHz.

3.4 Frequency Locking Scheme

We use twelve laser beams in our system to prepare the atomic ensemble, lock the cavity, and provide both cavity and free-space photons, as listed in Tab. 3.2.1. All the beams at 852.3 nm need to be frequency stabilized to an uncertainty better than the linewidth of the excited states of $\left|6P_{3/2}\right\rangle$ (Γ =5.2 MHz), as they all need to interact with atoms. This is achieved by first locking the "Ref beam" to an atomic transition by saturation absorption spectroscopy with a cesium vapor cell, and then, locking all the other laser beams directly, or indirectly via modulation sidebands generated by Electro-optic modulators (EOM) or acousto-optic modulators(AOM), through comparing their frequencies to that of the "Ref beam".

As "Gammap beam" that provides EIT coupling beam is supposed to generate transparency window for free-space photons (provided by the "Side beam") through EIT, the "Gammap beam" and "Side beam" needs to be phase locked to each other within a stabilization better than the decoherence rate of two stable ground states $\gamma/2\pi \sim 10$ kHz. We generate ∼9.2 GHz sidebands for "Gammap beam" using an broadband EOM (EOSPACE PM-0k5-20-PFU-PFU-850), and filter out the carrier and other sidebands with an Etalon. The 1^{st} order blue sideband alone gets transmitted through the Etalon and becomes the "Side beam". A synthesizer locked to a Rubidium clock (stabilization and uncertainty better than 10^{-8}) drives the EOM and guarantees relative frequency stabilization between the "Gammap beam" and the "Side beam" better than 1 kHz.

3.4.1 Locking the Cavity

The cavity frequency needs to be stabilized to better than $\Gamma/2\pi$ =5.2 MHz with respect to atomic transition, and to be stabilized to better than $\kappa/2\pi = 0.14$ kHz with respect to the "Etac beam" providing cavity photons. This is the most difficult part among all our frequency locking schemes. We accomplish this in the following way.

First, because we are looking for interactions between photons at the single-photon

level, directly locking of the cavity to the "Etac beam" is not allowed, since this requires many photons to go through the cavity. Holding the lock and extinguishing the locking light during the experimental sequence is not allowed either, as our high-finesse cavity is not rigid enough and its length couples to mechanical oscillations that drive the cavity frequency out of the frequency lock's capture range within 0.5 ms. To bypass these difficulties, we choose to use a stable and complicated solution consisting of a transfer cavity and a transfer laser, which enables the cavity to be locked to a frequency across a very large range, while transferring the frequency stability. We choose this transfer frequency to be at 817 nm, where the frequency is close enough so that cavity finesse remains high and the frequency is far enough that atoms will not be affected much by the locking beam. Furthermore, the wavelength difference allows for efficient filtering using interference filters, such that the "Transfer beam" transmitted through the cavity does not disturb the counting of transmitted cavity photons.

Second, the cavity linewidth $\kappa = 2\pi \times 0.14$ MHz is significantly smaller than the linewidth of DFB lasers at $\sim 2\pi \times 1$ MHz. To frequency stabilize lasers onto the cavities, we use optical feedback to pre-narrow each of the "817 laser" and "Eta laser" down to an intrinsic subkilohertz linewidth [52]. These optical feedbacks are achieved by long external cavities with optical length of 1.5 meter, implemented with an optical fiber and a mirror mounted on a piezoelectric transducer (PZT).

Lastly, we use Pound-Drever-Hall (PDH) technique to stabilize frequency of the cavity to the "Transfer beam". In order to keep frequency of a cavity of finesse $\mathcal{F}$ within the capture range of PDH signal, this cavity must have its length fluctuations suppressed to less than $\frac{\lambda}{\mathcal{F}}$. Since the cavity couples to a mechanical oscillation resonant at 2 kHz in the mounting structure, the cavity oscillates with an amplitude of ~ 0.1 nm ($2\pi \times 2$ MHz) in the free-running mode at this frequency, excited by mechanical pulse of anti-Helmholtz coils when their currents increase to load and compress MOT. As a result, for the locking loop that stabilizes the frequency of the cavity to the "Transfer beam", the open loop gain at frequency of 2 kHz has to be larger than $\frac{2\ MHz}{0.14\ MHz} = 14$ to keep the cavity in lock. And the open loop gain at frequency of

2 kHz has to be larger than $\frac{2\ \text{MHz}}{0.02\ \text{MHz}} = 100$ if the relative linewidth less than 20 kHz is required. The feedback loop bandwidth is limited by PZT resonance at ∼30 kHz if the error signal feeds back to cavity length. We increase the feedback bandwidth to 2 MHz by adding a fast feedback loop feeding back to the "Transfer beam" frequency, via an AOM. This extra frequencies change added by AOM is multiplied by a factor of $\sim \frac{23}{24}$ which is close to $\frac{\lambda_{817}}{\lambda_{852}}$, and add it to the frequency of the "Etac beam" via an EOM modulating the "Eta laser", to maintain the high relative stability of the frequencies of the cavity and the "Etac beam" in a feed-forward scheme.

To conclude, we pre-narrow and lock both "Eta laser" and "817 laser" to the transfer cavity, lock the length of transfer cavity to the beat note of "Eta laser" and "Ref beam", lock the cavity length to the "817 beam" with feedforward to both "817 beam" and "Etac beam". As a result, the cavity frequency is stabilized to the "Etac beam" frequency within 20 kHz, both cavity and "Etac beam" frequency are stabilized to the atomic transition within 2 MHz, and all the detunings are controlled independently. Details of the locking scheme are illustrated in [49].

3.4.2 Locking the Trap Laser

Trapping more atoms in the optical dipole trap requires a high power (>2 mW) "Lattice beam" incident onto the cavity. The cavity-enhanced optical dipole trap requires high laser frequency stability, as frequency noise of the incident trap light would convert into intensity noise in the cavity, and the intra-cavity intensity noise at twice of the axial (or radial) trap frequency can cause parametric heating [53]. So we need a "Lattice beam" with both high power and narrow linewidth. We use a DFB laser that is pre-narrowed by the optical feedback from a 0.7-meter-long external cavity as the seed laser, injection lock a high-power diode laser (slave laser) to this seed laser, and lock the frequency of the seed laser to the cavity frequency. This frequency locking is achieved by electronic feedback to both seed laser current and seed laser external cavity length, based on an PDH signal from the reflection of the slave laser off the cavity.

With the optimized frequency locking of "Lattice beam", we are able to trap atoms

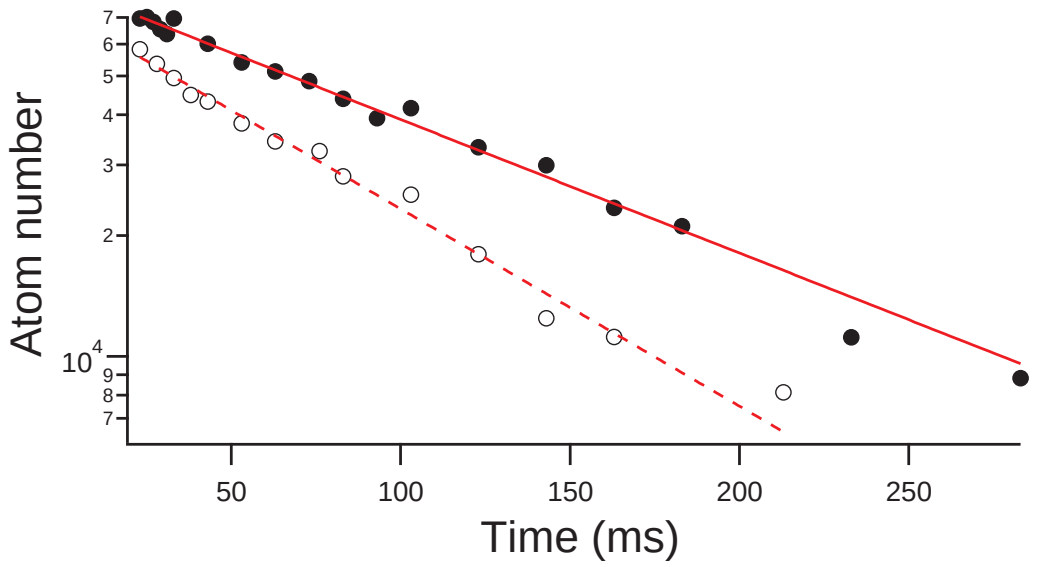

Figure 3-9: Lifetime of atoms in $\left|6S_{1/2}, F=3\right\rangle$ state (black dots) and $\left|6S_{1/2}, F=4\right\rangle$ state (black circle) in the optical dipole trap at a typical trap depth. The lifetime is measured to be 130 ms for atoms in $|F=3\rangle$ and 88 ms for atoms in $|F=4\rangle$.

in the state $\left|6S_{1/2}, F=3\right\rangle$ for 130 ms and the state in $\left|6S_{1/2}, F=4\right\rangle$ for 88 ms, as shown in Fig. 3-9.

3.5 System Test

3.5.1 Free-space Mode

To calibrate interactions between free-space photons and atomic ensemble, we turn off photons that are incident onto the cavity and tune the cavity frequency away from $|c\rangle \rightarrow |e\rangle$ transition to turn off the cavity-atom interactions (Fig. 3-4). Then we measure the transmission spectra of free-space photons through the atomic ensemble versus coupling beam Rabi frequency Ω_{cp}, while fixing the coupling beam detuning Δ_{cp} close to zero (Fig. 3-10). By fitting each of the measured EIT spectra using Eqn. 2.8, we extract the Rabi frequencies Ω_{cp}, the decay rate Γ of the excited state $|d\rangle$, and the dephasing rate γ of the transition $|f\rangle \leftrightarrow |c\rangle$. The extracted coupling beam Rabi frequency is fitted with respect to the measured coupling beam power, from which we can control the exact coupling beam Rabi frequency by monitoring

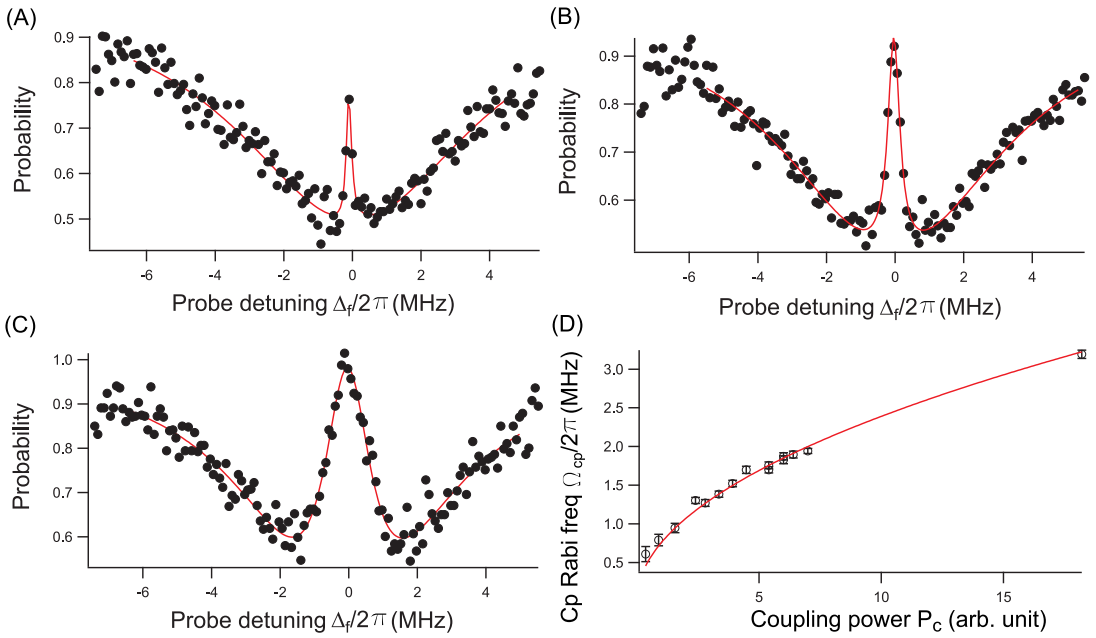

Figure 3-10: (A to C) Examples of EIT spectra for different coupling beam Rabi frequencies with fitted (a) $\Omega_{cp}/2\pi$=0.95(0.06) MHz, $\Gamma = 2\pi \times 7.2(0.5)$ MHz, $\gamma = 2\pi \times 80(60)$ kHz, (b) $\Omega_{cp}/2\pi$=1.70(0.03) MHz, $\Gamma = 2\pi \times 6.9(0.4)$ MHz, $\gamma = 2\pi \times 50(20)$ kHz, (c) $\Omega_{cp}/2\pi = 3.19(0.05)$ MHz, $\Gamma = 2\pi \times 6.7(0.4)$ MHz, $\gamma = 2\pi \times 60(80)$ kHz. The transmission probabilities (black dots) are measured versus probe-atom detuning Δ_f by photon-counting detector D_f. (D) Coupling beam Rabi frequencies extracted from fits to measured EIT spectra versus measured coupling beam power in arbitrary units. The extracted coupling beam Rabi frequency is expected to scale as $\Omega_{cp}/2\pi = A \times \sqrt{P_c}$, and we find good agreement with a square root fit with fitted $A = 0.756(0.005)$.

the beam power and controlling the AOM drive power for the coupling beam. The fitted decay rate Γ is found to be $2\pi \times 6.4$ MHz, which agrees with the combination of atomic linewidth $2\pi \times 5.2$ MHz and "Gamma laser" linewidth of $2\pi \times 1$ MHz. The fitted dephasing rates γ are averaged to be $2\pi \times 70$ kHz.

The dephasing rate γ is mostly due to Doppler broadening in our system, as free-space mode and the coupling beam are spatially orthogonal to each other. Having measured the dephasing rate and calibrated the coupling beam Rabi frequency, we optimize the coupling beam intensity for each of the following experiments in Chapters 4-6 to tradeoff between free-space photon transmission probability and interaction time of free-space and cavity photons.

3.5.2 Cavity Mode

To test cavity-atom interactions, we have demonstrated efficient detection of a single atom trapped in the cavity mode by monitoring the cavity photon transmission. We apply a magnetic field to define the quantization axis along the z axis, and send σ_+-polarized photons onto the cavity. The cavity photons couple resonantly to the $\left|6S_{1/2}, F=4, m_F=4\right\rangle \rightarrow \left|6P_{3/2}, F'=5, m'_F=5\right\rangle$ transition with a Clebsch-Gordon coefficient of one, which maximizes the effective cooperativity to 8.6. An atomic ensemble is loaded into the optical dipole trap and prepared in the $\left|6S_{1/2}, F=3, m_F=3\right\rangle$ state. Then, we shine a *lin*-polarizing weak coherent beam onto the atomic ensemble in the free-space mode, resonant with the $\left|6S_{1/2}, F=3, m_F=3\right\rangle \rightarrow \left|6P_{3/2}, F'=4, m'_F=4\right\rangle$ transition, which scatters one of the atoms in the atomic ensemble into the state $\left|6S_{1/2}, F=4, m_F=4\right\rangle$ with small probability. We tune both the cavity and the cavity photons resonant to the cycling transition of $\left|6S_{1/2}, F=4, m_F=4\right\rangle \rightarrow \left|6P_{3/2}, F'=5, m'_F=5\right\rangle$, apply incident cavity photons for 20 μs, and measure the total transmitted cavity photon number with a photon counter D_t. Then we initiate all the atoms into $\left|6S_{1/2}, F=3, m_F=3\right\rangle$ state again and repeat the process. In this way, we measure the histogram of transmitted cavity photon numbers as shown in Fig. 3-11.

Each of the two peaks in the figure is a Poisson distribution due to detection photon shot noise. In the absence of atoms in state $|c\rangle$, all the cavity photons are transmitted. In the presence of one atom, the cavity photon transmission is suppressed by a factor of $\frac{1}{(1+\eta)^2}$. In the pesence of N_c atoms, the cavity photon transmission is suppressed by a factor of $\frac{1}{(1+N_c\eta)^2}$. This suppressing factor is decreased by spatial distribution of the atoms that are not situated at an antinode or not on the axis of the cavity mode. Thus by choosing a proper photon number in between the two peaks and setting it as a threshold, we can distinguish between no atom and one or more atoms in the cavity, by detecting the transmitted cavity photon numbers.

To better distinguish between no atom and one or more atoms using this method, we need to make sure that atoms are not saturated by the cavity photons. When

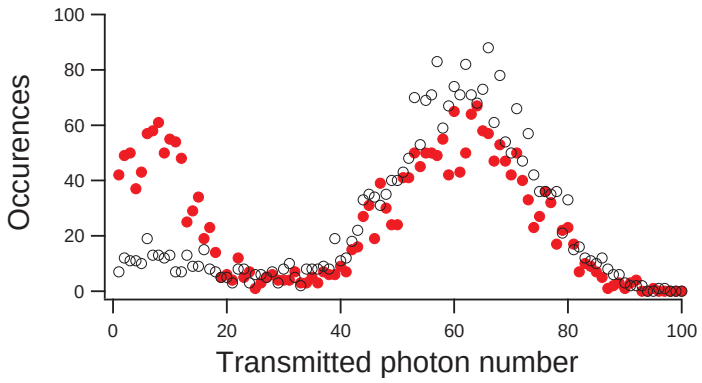

Figure 3-11: Single atom detection using high-cooperativity cavity. Histogram of detected transmitted cavity photon number into 20 μs bins with (red solid circle) and without (black open circle) incidence of weak coherent light in free-space mode. With light in free-space mode, the red solid circle data is the weighted sum of two Poisson distributions, indicating the atom number of 0 and 1. By choosing a proper photon number in between the two peaks and set it as a threshold, we can determine whether there is none or one atom in the cavity in state $|c\rangle$ by detecting transmitted cavity photon number above or below this threshold.

the atoms are saturated by cavity photons, the cavity transmission is suppressed by a factor $1/\left(1+\frac{N_c\eta}{1+s_{N_c}}\right)$, determined by both the number of atoms N_c and the saturation parameter s_{N_c} for that atom number. In this limit, by choosing the incident cavity photon rate, we distinguish between 0, 1, 2 and >2 intracavity atoms, with the histogram shown in Fig. 3-12.

These measurement verify that our system is shot-noise limited, showing that the control of laser and cavity frequencies, the laser power, and the atom loading process are sufficiently stable for the following experiments.

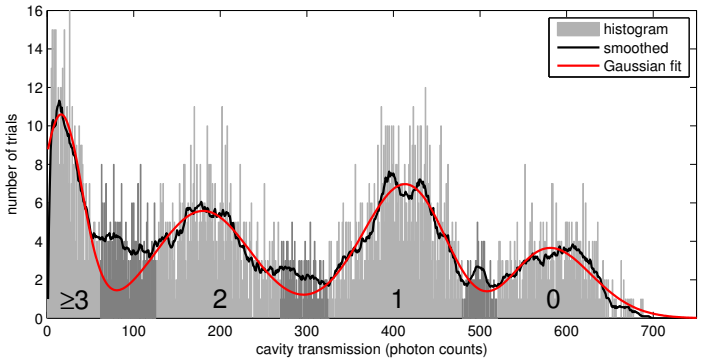

Figure 3-12: Atom number detection of a few atoms. Histogram of detected transmitted cavity photon number into 50 μs bins (black dots). The fitting curve (red curve) is the weighted sum of Poisson distributions for different atom numbers, indicating the atom number of 0, 1, 2 and more than 2, as atoms are excited by a coherent light in the free-space mode.

Chapter 4

Photon Switch and Transistor Gated by Individual Photons

4.1 Overview

Light is one of the most important things in our lives. We need light to illuminate paths, we need light to warm up our body, and we need light to enlighten the hope in our mind. Light is so important that people have even invented candles and electric bulbs to shine in the evenings.

One important question about light is how we should characterize light. Starting from Newton, Fresnel, Maxwell and many other scientists investigated the natural properties of light. One way to characterize light is by energy [3]. For a 35W LED light bulb, the energy radiated during each second is 35 Joules, which contains $\sim 10^{20}$ photons. By analyzing the energy, we get information of the wavelength, intensity and the frequency spectrum. The most widely-used detectors of light are our eyes. On each day, our eyes receive large numbers of photons, and each photon just carries a tiny amount of energy. As the energy carried by each photon is so low, we are wondering whether one photon could change anything.

Before answering this question, I would like to mention electronic transistors [54]. After electrodynamics was established, people started to use electrons to transport and process information. The transistor is one of the most important elements in

electronic devices. Logic gates, integrated circuits and CPUs are all composed of transistors. When the first transistor came out, it was necessary to drive a vacuum tube with a large current. As a result, huge numbers of electrons are needed to process information via vacuum tubes. At that time, it was hard to believe that information could be transported and processed using only a few electrons. As technology developed, transistors became smaller, and currents or the electron numbers that carry the same amount of information became smaller. Today's smartphone is thousands of times faster and much smaller than the first computer which occupied several rooms. In 2012, researchers from MIT invented a transistor that is gated by only one electron [55]. These technologies have made our computers faster and smaller.

The answer to the previous question is yes. One photon can change things. One photon can be used to carry information and drive an optical transistor to process optical information [31, 56]. And it might become the fundamental element of a quantum computer and an optical network in the future.

Using photons to carry information has already been investigated for more than a decade with many important results. One photon can be used to deliver a secure message from one location to another by quantum key distribution [57,58]. It can also be used to connect different ends to form an optical network by DLCZ scheme [41]. Later, one can transfer the information carried by photons into atoms and retrieve this information from atoms [36, 40, 59]. However, these techniques are not enough to construct an optical computation network. We need a transistor which can work in the optical domain and allow light beam to control one other.

Recently, people have researched and realized such optical transistors. A few experiments have been demonstrated in different systems [31, 60–62]. They all used more than 1000 gate photons to control the states of transistors, because each photon carries small amount of energy. Is it possible to reduce the gate photon number to one? Yes! One of the project of my PhD work was to demonstrate an optical transistor gated by one stored photon [56].

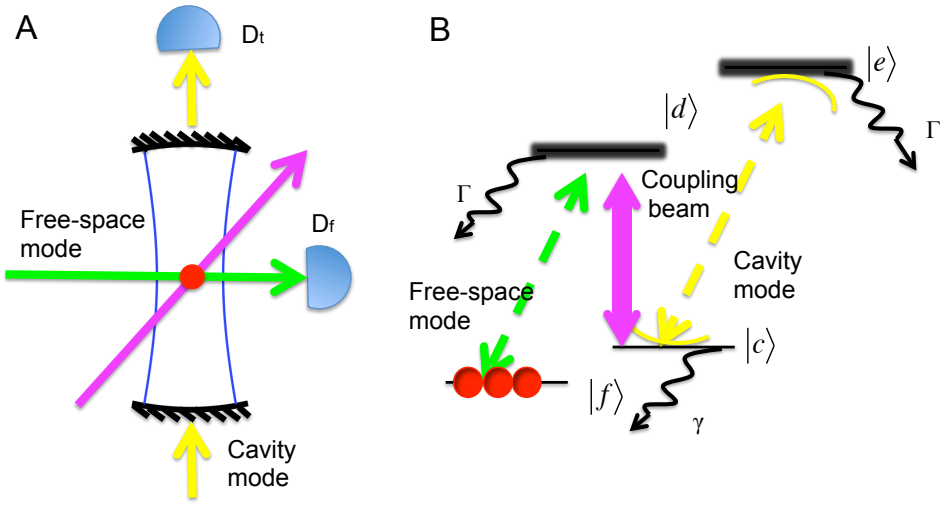

Figure 4-1: Experimental (A) scheme and (B) atomic level structure for the all-optical transistor. The cesium atoms are cooled and trapped in the optical high-finesse cavity. We send in a coupling beam from the side of the cavity to couple the transition $|c\rangle \leftrightarrow |d\rangle$. Free-space photons are coupling the $|f\rangle \leftrightarrow |d\rangle$ transition, while the cavity mode couples the $|c\rangle \leftrightarrow |e\rangle$ transition. Here, states $|f\rangle$, $|c\rangle$ and $|d\rangle$ form an EIT system. The atomic states in Cesium-133 are chosen as $|f\rangle = |6S_{1/2}, F = 3, m_F = 3\rangle$, $|d\rangle = |6P_{3/2}, F' = 3, m'_F = 3\rangle$, $|s\rangle = |6S_{1/2}, F = 4, m_F = 4\rangle$ and $|e\rangle = |6P_{3/2}, F' = 5, m'_F = 5\rangle$.

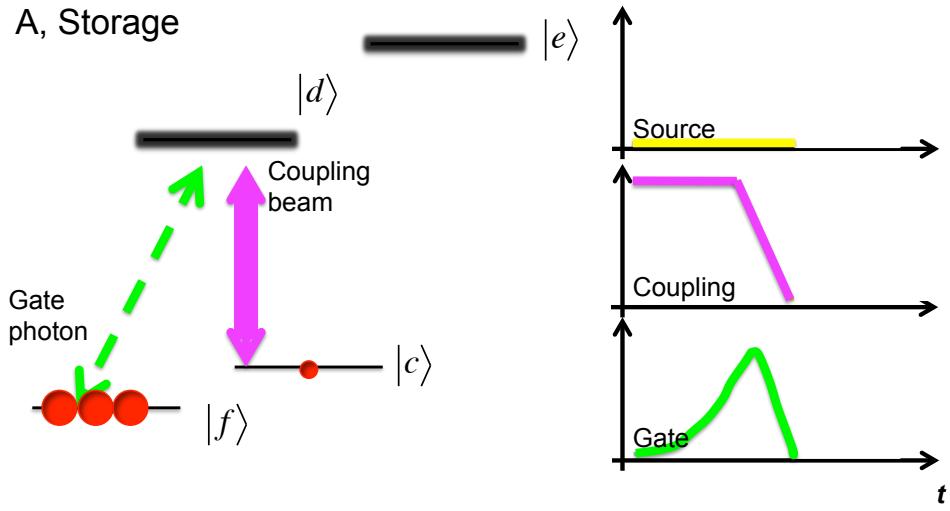

Figure 4-2: (a) Storage. We use EIT to transform a gate photon (in free-space photon) into an atomic excitation in state $|c\rangle$. If the incident gate photon number is one, it transfers exactly one atom into state $|c\rangle$. We ramp the gate pulse and the coupling beam adiabatically to make this process coherent. The atomic excitation in state $|c\rangle$ is a collective excitations shared by all the atoms addressed by the free-space mode, so that they can later be retrieved into the free-space photons in the original mode.

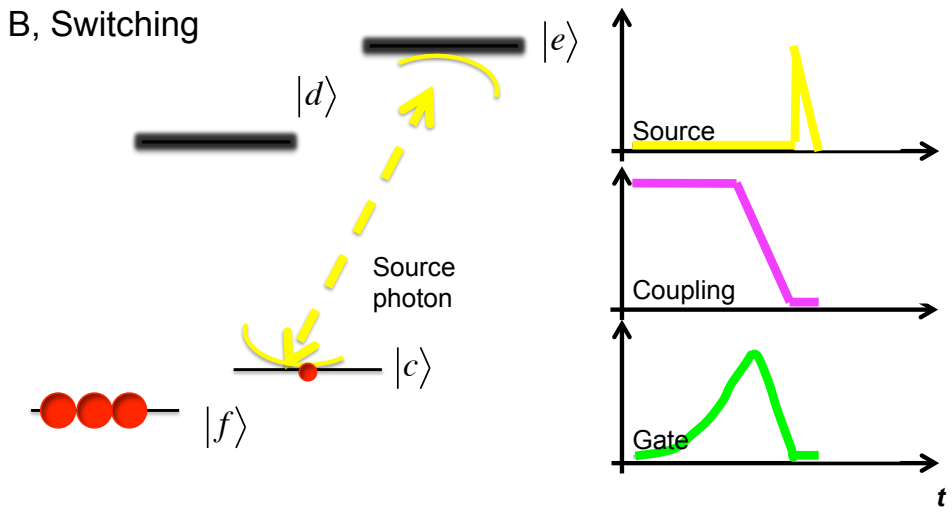

Figure 4-3: (b) Switching. After the storage process, we send source photons (in cavity mode) into the cavity. Both the cavity and the source photon pulse are exactly on resonance with the atomic transition $|c\rangle \leftrightarrow |e\rangle$. If there is no atomic excitation in $|c\rangle$, the source photons will simply be transmitted through the cavity. If there is one atomic excitation in $|c\rangle$, the source photons are reflected by the cavity. This way, the transmission of the source photons is switched by the stored gate photon number.

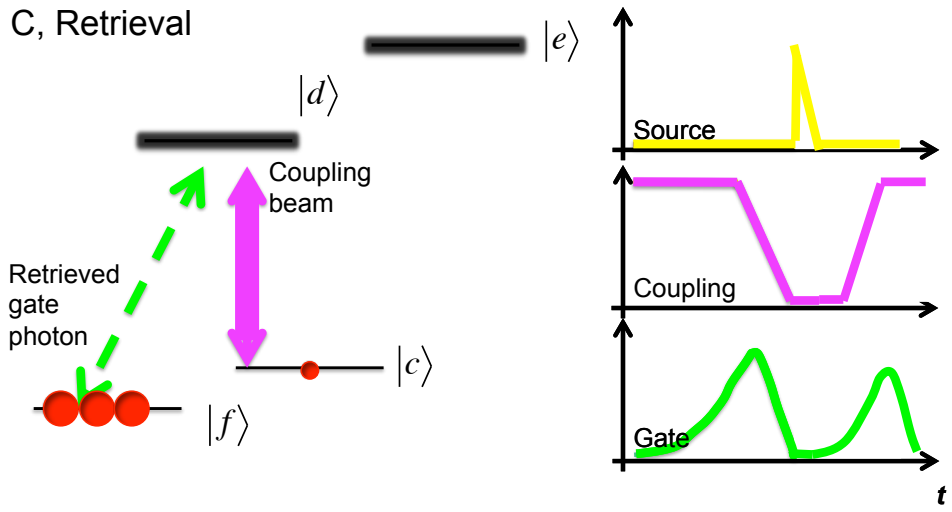

Figure 4-4: (c) Retrieval. After switching the source photons, we can retrieve the gate photon. If everything is ideal without any decoherence or scattering loss, we will get exactly the same retrieved wave packet as the gate photon pulse. In the real system, the decoherence and scattering process disturb the phase coherence of the collective atomic excitations and reduce the fidelity of our retrieval process.

4.2 Storage and Switch

In this experiment, we demonstrate a cavity QED version of an optical transistor [63] based on EIT in a four level system [33–35]. The experimental scheme and atomic level structure are shown in Figure 4-1. Here, the green dashed line labels the gate photon transition, and the yellow dashed line labels the source photons. Our goal is to use the gate photons to switch off the transmission of the source photons. Working in the limit of a very weak gate photon pulse, zero or one gate photon determines the transmission or reflection of the source photons.

Three processes are conducted in our experiment, storage, switching and retrieval. We control the gate photon pulse, the coupling laser beam and the source photon pulse individually in each process. The details of each process are illustrated in the captions of Fig. 4-2, Fig. 4-3 and Fig. 4-4. The first and the third processes rely on the EIT phenomenon. The second process depends on the cavity blocking. Using the general form of the atom-cavity interaction introduced in Sec. 2.4, I will describe the cavity blocking in detail as below.

Using the general form of the cavity transmission in Eqn. 2.25, we set $\Delta_c = \delta_c$ which indicates that the cavity frequency is on the atomic resonance. We expand and simplify the equation and get

$$E_{tr} = E_{in}\frac{1}{1+\frac{N_c\eta\Gamma^2}{\Gamma^2+4\delta_c^2}+2i\delta_c\left(-\frac{1}{\kappa}+\frac{N_c\eta\Gamma}{\Gamma^2+4\delta_c^2}\right)}. \tag{4.1}$$

When cavity photons are on resonance $\delta_c = 0$,

$$E_{tr} = E_{in}\frac{1}{1+N_c\eta}. \tag{4.2}$$

Our cavity-atoms interaction works in the strong-interaction regime with effective cooperativity $\eta = 4.3$. Thus the cavity transmission is strongly suppressed by one cavity atom where $N_c = 1$. The transmission spectra predicted by Eqn. 4.1 are shown in Fig. 4-5. One can easily distinguish the peaks denoting different cavity atom numbers $N_c = 0$ and $N_c = 1$ in the cavity photon transmission histogram in

Out[27]=

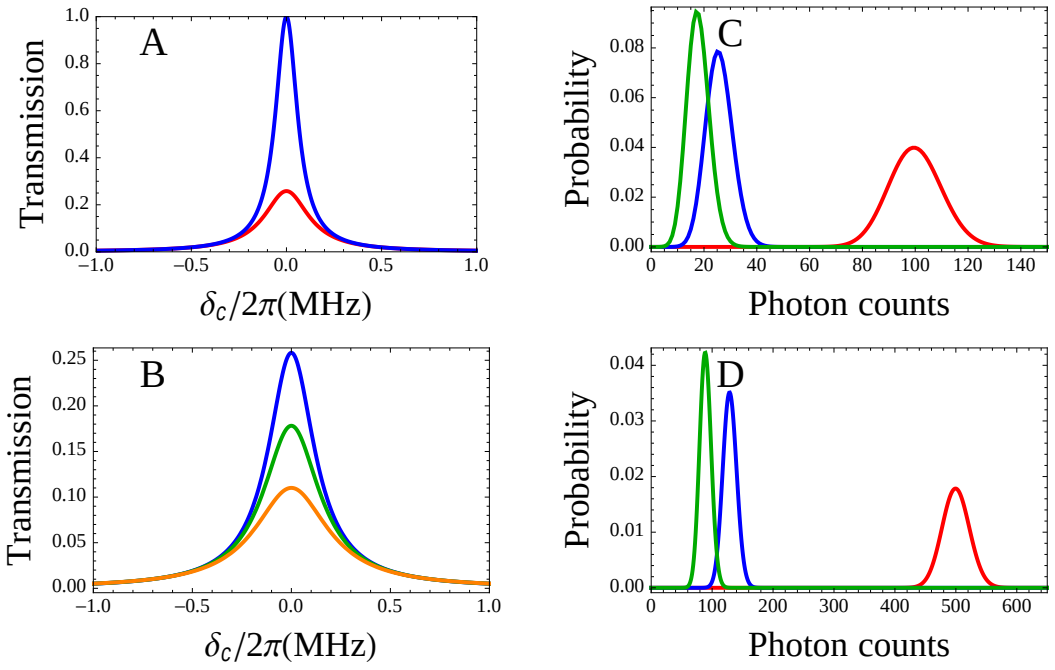

Figure 4-5: (A) Predicted transmission spectra for $N_c = 0$ (blue) and $N_c = 1$ (red). (B) Predicted transmission spectra for $N_c = 1$ (blue), $N_c = 2$ (green) and $N_c = 5$ (orange). Here we use the realistic parameters in our experiment, $\kappa = 2\pi \times 0.14$ MHz, $\Gamma = 2\pi \times 5.2$ MHz and $\eta = 4.3$ at antinode. (C) Predicted histogram of transmission for on resonant cavity photons. The incident cavity photon pulse is in coherent state which obeys the Poisson distribution $P(k) = e^{-\langle n_c \rangle} \frac{n_c^k}{k!}$, where $P(k)$ is the probability to detect exact k photons and $\langle n_c \rangle$ is the average photon number. For $\langle n_c \rangle$ =100 photons incident onto the cavity, the red, blue and green curves show the probabilities of detected transmission photon counts for $N_c = 0$, $N_c = 1$ and $N_c = 2$, respectively. In this graph, the two peaks indicating $N_c = 0$ and $N_c = 1$ have already been separated. (D) When we increase incident cavity photon number $\langle n_c \rangle$ to 500, the overlap between the peaks is even smaller.

Fig 4-5 (c) and (d). As a result, we can send in a pulse which contains an average of 100 photons and measure the transmitted cavity photons. If the transmitted photon count is above a threshold, for example, a threshold of 60 for an average incident photon number of 100, we know the cavity pulse is transmitted and the cavity atom number is $N_c = 0$. Otherwise, we can claim the cavity pulse is reflected and cavity atom number $N_c = 1$.

In our experiment, we send in a gate photon pulse in weak coherent state. We use the average stored gate photon number $\langle n_g \rangle$ to characterize the gate photon pulse. Ideally, each gate photon is stored as one collective atomic excitation and the effective cavity atom number $N_c = n_g$. So the transmission spectrum is a weighted average of different N_c spectra. We send a photon pulse in coherent state with an average of 22 photons onto the cavity within a time duration of 24 μs. The measured photon number is $M_s = \frac{\tilde{T}}{\tilde{T}+\tilde{L}} \int dt m_c(t)\kappa$ for on cavity resonance. Here, $m_c(t)$ is the intracavity photon number at time t, $\tilde{T}$ is the transmission of each of the cavity mirrors, $\tilde{L}$ is the reflection loss of each of the cavity mirrors, and $\frac{\tilde{T}}{\tilde{T}+\tilde{L}} = 0.66$ in our cavity. So for $n_g = 0$, we expect to detect an average of 15 photons at cavity transmission. For $n_g \neq 0$, we need to include the inhomogeneous cavity field coupling of the atoms to predict the cavity transmission. As we use 936.7 nm laser to trap the atoms in the cavity mode and use 852.3 nm laser (Cesium D2 transition) to probe the atoms, the transmission probability of cavity photons is corrected to

$$\langle T_{trans} \rangle = \frac{\int dz n(z) e^{-2z^2/w^2} T_{trans}(\eta \cos^2(kz))}{\int dz n(z) e^{-2z^2/w^2}}, \tag{4.3}$$

where

$$T_{trans}(\eta) = \left| \frac{1}{1 + \frac{n_g \eta \Gamma^2}{\Gamma^2 + 4\delta_c^2} + 2i\delta_c \left(-\frac{1}{\kappa} + \frac{n_g \eta \Gamma}{\Gamma^2 + 4\delta_c^2} \right)} \right|^2 . \tag{4.4}$$

The experimentally detected cavity transmission spectra at different average stored gate photon number $\langle n_g \rangle$ are shown in Fig. 4-6. The on resonant cavity transmission for each $\langle n_g \rangle$ is not blocked as much as those in Fig. 4-5. This is because we used a gate photon pulse in a coherent state which mixes all the Fock state transmis-

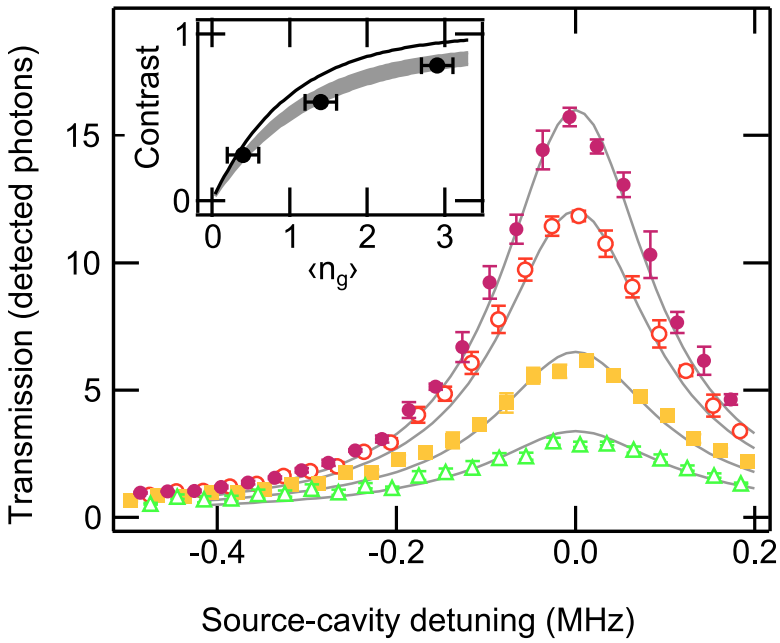

Figure 4-6: Cavity transmission with weak coherent gate photon pulses. Here, we fix the average incident cavity photon number and tune the cavity photon frequency over a 1 MHz range. We measure the average transmission spectra of the cavity photons applied for 24 μs for mean stored gate photon numbers $\langle n_g \rangle = 0$, 0.4, 1.4 and 2.9 (top to bottom). The solid lines are the theoretical curves. (Inset) The transmission probability on cavity resonance (switching contrast) versus $\langle n_g \rangle$. The gray area indicates the theoretical prediction. The solid black line corresponds to the maximum average switching contrast that can be observed with coherent states of gate photons.

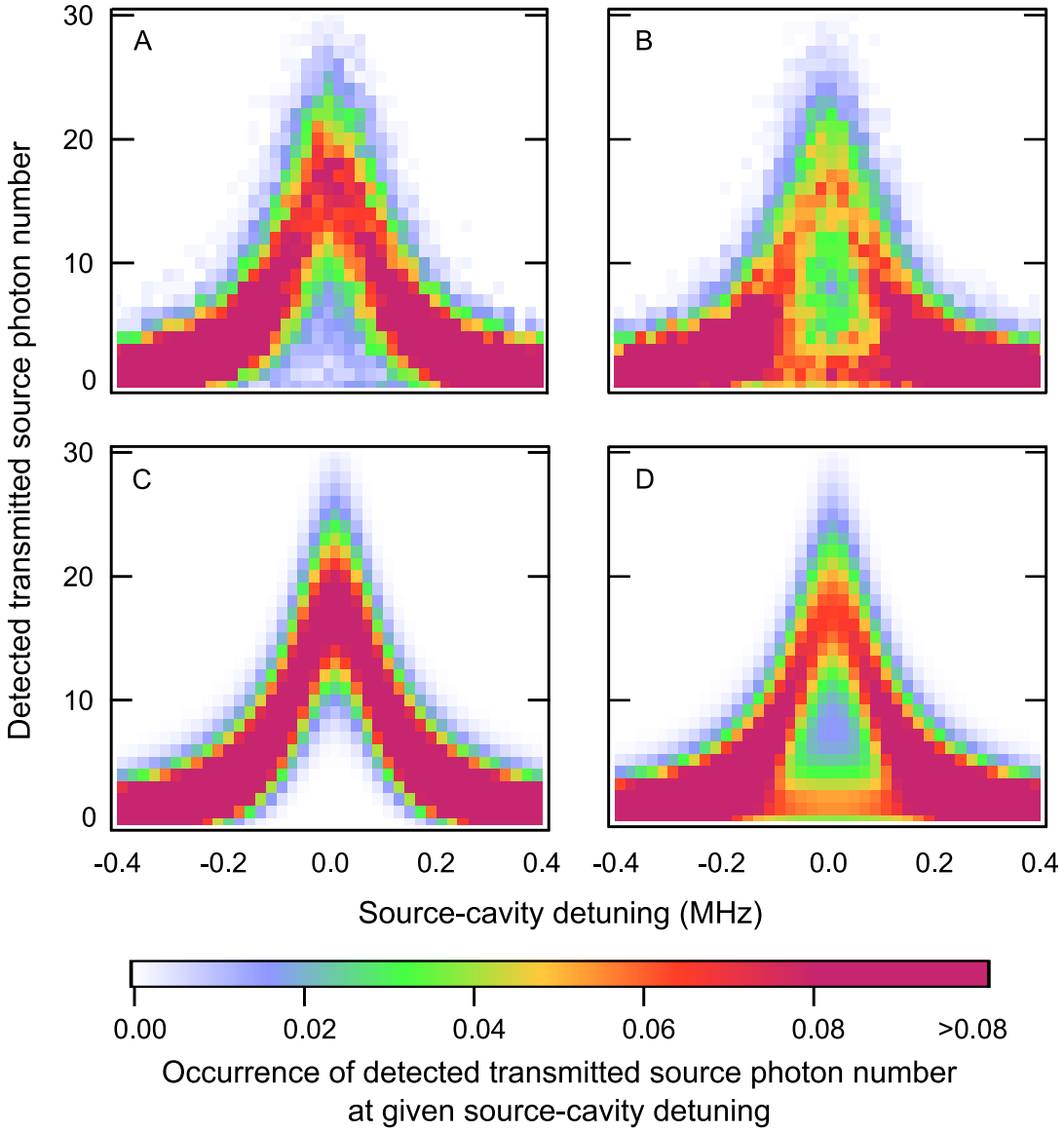

Figure 4-7: Histogram of cavity transmission spectra, occurrence of detected transmitted cavity photon (source photon) number at given photon-cavity (source-cavity) detuning. (A) Cavity transmission for $\langle n_g \rangle = 0$ gate photons and (B) for $\langle n_g \rangle = 0.5$. The horizontal axis indicates the detuning of the source beam from the cavity resonance. The vertical axis is the source photon number. We use the color to indicate the occurrence probability of one particular detuning. (C) and (D) are the theoretical calculation histograms for (A) and (B). In the plot, we find a clear separation between $n_g = 0$ and $n_g \geq 1$ peak near the cavity resonance. The extinction factor for one gate photon is 11 ± 1.

sion spectra in Figure 4-5, including a non-negligible $n_g = 0$ component. To supply stronger evidence, we detect the histogram of the cavity transmission spectra (Fig. 4-7). According to the theoretical curves shown in Fig. 4-5 (c) and (d), we expect two peaks in the histogram spectra which is indeed observed experimentally. These two peaks are well separated between the $n_g = 0$ and $n_g \geq 0$ cases.

4.3 Correlation Function

In order to operate the device while also retrieving the stored gate photons, we reduce the source integration time to 1 μs which is less than the EIT lifetime of 2.1 μs. Working in this mode, after switching off the source photons, a gate photon can be retrieved into its original mode for further information processes. We measure the cross correlation function g_2 between the source and gate photons to prove that the photon transistor is functioning in the retrieval mode:

$$g_2 = \frac{\langle n_g n_s \rangle}{\langle n_g \rangle \langle n_s \rangle}. \tag{4.5}$$

The photon in the gate mode suppresses the transmission of source photons. So we expect the system to introduce anti-correlation between retrieved gate and source photons. The cross correlation function between the gate and source photons transmitted through the system is

$$g_2(\tau) = \frac{1}{(1 + \eta e^{-\tau/t_{EIT}})^2}, \tag{4.6}$$

where t_{EIT} is the lifetime of EIT. For $\tau = 0$, g_2 is exactly the same as the cavity transmission probability for gate photon number $n_g = 1$.

Experimentally, the cross correlation function is measured to be $\tilde{g}_2 = 0.29^{+0.09}_{-0.08}$. This $\tilde{g}_2$ includes the uncorrelated background noise. We correct this number and get the real g_2 between the source and the gate using the following method. What we

measured is

$$\tilde{g}_2 = \frac{\langle (n_g + b_g)(n_s + b_s) \rangle}{\langle n_g + b_g \rangle \langle n_s + b_s \rangle}, \tag{4.7}$$

where b_g and b_s are the background counts for the gate and the source. Since they are uncorrelated with the other counts, the equation can be expanded as

$$\tilde{g}_2 = \frac{g_2 + \langle b_g \rangle / \langle n_g \rangle + \langle b_s \rangle / \langle n_s \rangle + \langle b_g \rangle / \langle n_g \rangle \times \langle b_s \rangle / \langle n_s \rangle}{1 + \langle b_g \rangle / \langle n_g \rangle + \langle b_s \rangle / \langle n_s \rangle + \langle b_g \rangle / \langle n_g \rangle \times \langle b_s \rangle / \langle n_s \rangle}. \tag{4.8}$$

Defining $B = \langle b_g \rangle / \langle n_g \rangle + \langle b_s \rangle / \langle n_s \rangle + \langle b_g \rangle / \langle n_g \rangle \times \langle b_s \rangle / \langle n_s \rangle$, we get

$$g_2 = (1 + B)\tilde{g}_2 - B. \tag{4.9}$$

Using this correction, we find out the corrected value for the cross correlation to be

$$g_2 = 0.17^{+0.08}_{-0.06}.$$

This result is consistent with the transmission $T = 0.16 \pm 0.01$ from the theoretical prediction including the effect of inhomogeneous coupling.

4.4 Retrieval and Transistor Gain

One important parameter to quantify the quality of the transistor is the transistor gain. We define the gain for our transistor as the source photon number that a single stored gate photon can switch off. In Fig. 4-8, the histogram of the source photon transmission counts shows a double-peaked feature for gate photons in a weak coherent state. Using this histogram, we measure the average transmitted source photon number $\langle M_s \rangle|_{n_g=0}$ for no gate photon and $\langle M_s \rangle|_{n_g \geq 1}$ for one or higher gate photons. The optical gain per stored gate photon is defined as $G = \langle M_s \rangle|_{n_g=0} - \langle M_s \rangle|_{n_g \geq 1}$, which is directly measurable from the source photon transmission histogram.

In Fig. 4-8 (B), the gain saturation occurring around 1000 source photons is due to optical pumping of the atomic excitation in state $|c\rangle$ into the other magnetic sublevels with weaker cavity coupling. Consequently, one stored gate photon can block more

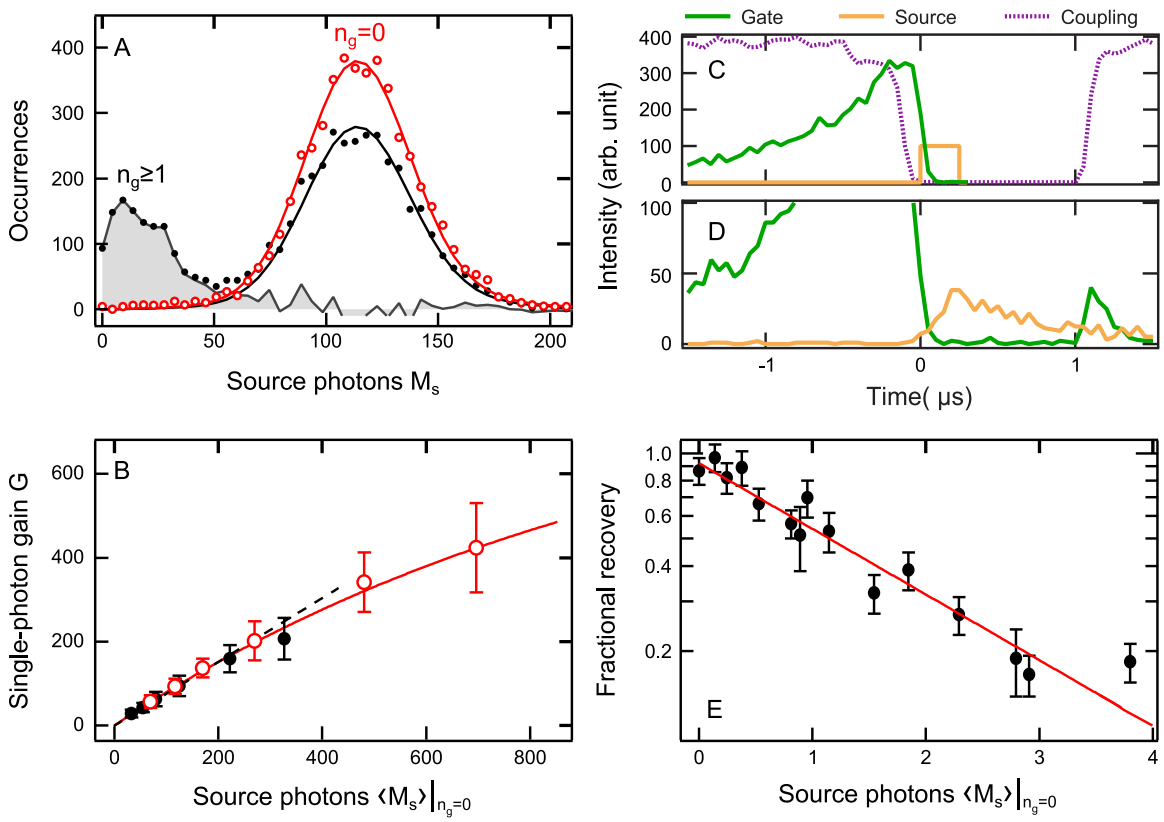

Figure 4-8: Measurement of transistor gain. (A) Histogram of the transmitted source photon M_s in a 50-μs window. The graph shows M_s for no applied gate photon (n_g=0, open red circles) with a Poissonian fit and for a coherent state with $\langle n_g \rangle = 0.4$ stored gate photons (solid black circles). The gray area indicates the contribution from events with $n_g \geq 1$, with average value denoted by $\langle M_s \rangle|_{n_g \geq 1}$. (B) Transistor gain $G = \langle M_s \rangle|_{n_g=0} - \langle M_s \rangle|_{n_g \geq 1}$ as a function of source strength $\langle M_s \rangle|_{n_g=0}$ for integration time of 25 μs (solid black circles) and with an exponential fit to show gain saturation (red line). (C) and (D) Timing sequence for retrieval operation with (C) input pulses and (D) output pulses. The actual gate, coupling, and source beam waveforms are shown, while their relative powers are not to scale. First, the coupling beam is adiabatically ramped down at $t = 0$ to store a gate photon in the atomic medium. Then, a source pulse is sent onto the cavity, and its transmission is measured. Subsequently, the coupling beam is adiabatically ramped up in order to retrieve and detect the gate photon. (E) Measurement of transistor gain in retrieval mode. The average fractional retrieval efficiency of the gate photon after 1 μs is plotted versus $\langle M_s \rangle|_{n_g=0}$ with an exponential fit.

than 600 source photons, of which 400 are available outside the cavity.

This gain of a few hundred is the incoherent gain. When a source photon gets scattered by the atomic excitation into free space modes (modes other than the cavity mode), it projects the collective EIT excitation into a specific atomic excitation and destroys the coherence of EIT. Then, the stored gate photon cannot be retrieved anymore. In order to retrieve the gate photon after the switching process, we need to reduce the incident source photon number and limit the switching time to 1 μs.

A source photon scattered into free space reveals the location of the EIT polaritons and collapses the collective excitation. Luckily, this scattering probability is strongly suppressed by the cavity in the strong-coupling (high-cooperativity) regime. The physical gain of our transistor operated at $1/e$ retrieval reduction is $G_r = 2.2 \pm 0.2$, and the available gain outside the cavity is 1.4 ± 0.1 (lower by a factor of 0.66 due to out coupling efficiency).

The measurement data are plotted in Fig. 4-8. The combined storage and retrieval efficiency in the absence of source photons after a storage time of 1 μs is (3.0±0.1)%, which can be improved by increasing optical density in the gate mode and decreasing the decoherence between $|f\rangle$ and $|c\rangle$ states. The fitted source photon number that results in $1/e$ gate photon retrieval reduction is $M_{s0} = 1.9 \pm 0.1$ outside of the cavity. This source photon number in the retrieval mode is $M_{s0} = 2.8 \pm 0.2$ in the ideal case where the cavity out coupling losses are negligible, which is in good agreement with the theoretical value 2.8 ± 0.1.

This demonstrates a gain exceeding unity in transistor operation in which the gate photon can be retrieved for further use.

4.5 Conclusion

We combine EIT and cavity blocking effects, and demonstrate an optical transistor. The maximal gain of the transistor is up to 400 driven by a single stored gate photon. Working in the coherent regime (and retrieving the gate photon later), the gain is 2.2. Because the cavity-blocking mechanism does not rely on the collective effect in

EIT, the incoherent gain is robust against the environment decoherence and can be directly applied to an all-optical transistor.

This experiment is a test bed that provides an inspiration for the optical transistor design. We can increase the cavity cooperativity to achieve a transistor with higher coherent and incoherent gain. This system can also be integrated into solid-state system such as a photonic crystal to enable scalable photon transistors at the single photon level. The coupling efficiency can be improved from 0.66 to 0.97 using state-of-the-art mirrors [4, 5, 7].

The present work is opening a new window for optical information processing with strong deterministic interactions between initially uncorrelated, distinguishable photons. The gain $G > 1$ in operation with gate photon retrieval may enable not only hitherto unexplored all-optical quantum circuits with feedback and gain, but also the nondestructive detection of the gate photon (see Chap. 6), a feat that has so far only been accomplished for microwave photons confined in a cavity. The correlation between one gate photon and multiple source photons produced by the effective photon-photon interaction can be used to create two-mode entangled states of many photons. Lastly, cavities with higher cooperativity (see Chap. B) may enable high-fidelity deterministic photonic quantum gates.

Chapter 5

Cross Modulation of Two Laser Beams at the Individual-Photon Level

5.1 Overview

For two light beams crossing each other in the vacuum, each beam simply passes through the other without any perturbation. The frequency, amplitude and phase of one beam are not changed by the presence of the other beam. At the fundamental level, we find out that there are no direct photon-photon interactions in vacuum. The photon is the carrier of the electromagnetic force [64, 65]. All the photon interaction terms include

$$\psi^{\dagger}(\vec{r})\vec{A}(\vec{r})\psi(\vec{r}),$$

where ψ is the wave function for a charged particle such as electron or proton and $\vec{A}$ is the vector potential for the photon. To let two photons interact with each other, we need to consider at least the third order perturbation theory in the form of

$$\psi^{\dagger}(\vec{r}_1)\vec{A}(\vec{r}_1)\psi(\vec{r}_1)\psi^{\dagger}(\vec{r}_2)\vec{A}(\vec{r}_2)\psi(\vec{r}_2)\psi^{\dagger}(\vec{r}_3)\vec{A}(\vec{r}_3)\psi(\vec{r}_3).$$

This shows that a medium or matter is required to generate photon-photon interaction.

Now, let's review Maxwell's equations and electric polarization relation:

$$\nabla \times \vec{H} = \vec{J} + \frac{\partial \vec{D}}{\partial t}, \tag{5.1}$$

$$\vec{D} = \epsilon_0 \vec{E} + \vec{P} = \epsilon \vec{E}. \tag{5.2}$$

For most of the medium, ϵ is independent of the field intensity. When ϵ is constant, all the Maxwell's equations are linear equations and no photon-photon interactions are found. Following this argument, we must employ a nonlinear medium which satisfy $\vec{P} = \chi_1 \vec{E} + \chi_2 \vec{E}^2 + ...$ to enable photon-photon interactions. Meanwhile, the electric field has to be enhanced in some way to observe the nonlinear effect on top of the linear effect.

Based on this, creating deterministic photon-photon interactions has become a long-standing goal in optical science. In standard bulk materials, nonlinear effects such as second harmonic generation and parametric down conversion has been found. However, it is very hard to observe nonlinear effects with very weak electric fields or at the level of individual photons using bulk materials.

One approach to observe the nonlinear effect at the individual-photon level is by enhancing the electric field inside the matters [30, 34, 56, 66–69]. This can be done using a cavity, as discussed in the previous chapters. The optical cavity can enhance the electromagnetic field by a factor of up to one million. Nonlinear effects have been observed at individual photons level in experiments with an optical cavity [56, 67].

In this experiment, we use a similar experimental setup as the optical transistor in Chapter 4, replacing the gate photon pulses by a continuous light in a weak coherent state [56]. We demonstrate that two continuous light beams at different frequencies can modulate each other at the level of individual photons.

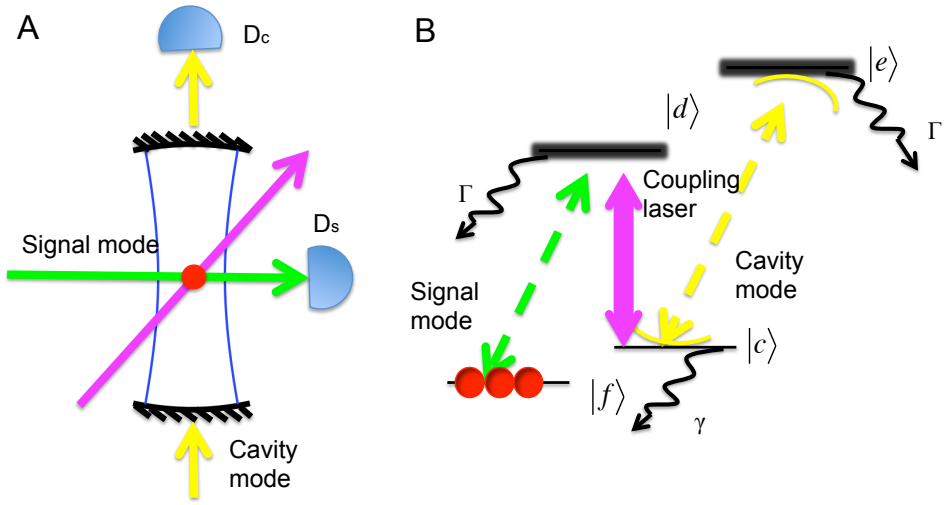

Figure 5-1: Experimental setup and atomic level scheme for cross modulation of two laser beams (in signal mode and cavity mode) at individual photons level. The signal mode and the cavity mode are continuous light beams in weak coherent states. We detect the transmission of each beam through the system, measuring the cross modulation between them. The coupling beam and atoms mediate the nonlinear interactions between the two beams.

5.2 Cavity Blocking

We first characterize how signal photons induce blocking for the cavity photon transmission. When there are no signal photons passing by, cavity photons transmit through system with full probability (mirror losses introduce a coupling efficiency of 0.66 both in and out of the cavity). As signal photons slowed down in the atomic ensemble as polaritons, the atomic components of these polaritons partially blocks the cavity photon transmission. We set the cavity photon transmission without signal photon to one and normalize all the other transmissions to it. In Fig. 5-2, we measured the maximal cavity transmission for each average signal photon number $\langle n_s \rangle = R_s\Gamma/\Omega^2$, the average signal photon number per EIT lifetime. Here R_s is the incident signal rate, Γ/Ω^2 is the EIT lifetime. The average number of atomic excitation components in state $|c\rangle$ is $\langle N_c \rangle = R_s(1-e^{-\mathrm{OD}})\Gamma/\Omega^2$. And the cavity photon transmission probability depends on this atomic component number $\langle N_c \rangle$ following Eqn. 2.25 and spatial field average. In Fig. 5-2, the data show good agreement with the predicted transmission.

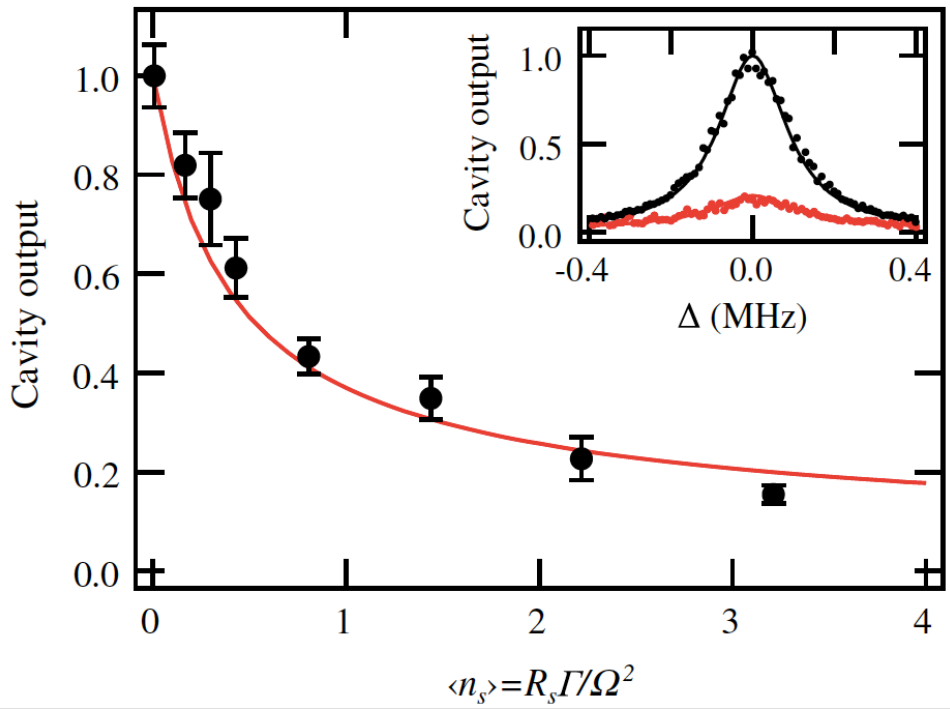

Figure 5-2: For each average signal photon number $\langle n_s \rangle$, we measure the transmission spectra of cavity photons and fit the transmission probability on cavity resonance at each of the $\langle n_s \rangle$. We plot the cavity transmission probability versus average signal photon number per EIT lifetime $\langle n_s \rangle = R_s \Gamma / \Omega^2$. The measurement was performed with $\Omega^2/\Gamma = 1.4(1)\mu\text{s}^{-1}$ and $\langle n_c \rangle|_{N_c=0} = 2.7$ intracavity photons. The red line is the theoretical prediction. Inset: examples of the cavity photon transmission spectra with (red) and without (black) signal photons. All error bars are one standard deviation.

5.3 EIT Decoherence Introduced by the Cavity Photons

While signal photons block the transmission of cavity photons, cavity photons also decrease the transmission and coherence of the signal photons. We need to consider the decoherence mechanisms in EIT carefully here to reveal the details of signal photons' propagation. The cavity photons couple the $|c\rangle$ and $|e\rangle$ states and introduce scattering for the atomic component in state $|c\rangle$ of the traveling polaritons. The coherent lifetime of EIT and transmission of signal photons decrease due to decoherence introduced by such cavity photon scattering. Therefore, both signal and cavity photons are trying to block each other.

As we know, the transmission of signal photons resonant on EIT peak without cavity photons is

$$T_s = \exp\left[-\mathrm{OD}/\left(1+\frac{\Omega^2}{\Gamma\gamma}\right)\right], \tag{5.3}$$

where γ is the decoherence rate between the two ground states $|f\rangle$ and $|c\rangle$. Without cavity photons, γ is mainly due to the thermal Doppler broadening, since our signal mode and coupling beam are perpendicular to each other. The spectrum of the Doppler broadening is a Gaussian profile with FWHM of $2\gamma_d$.

With cavity photons, the state $|c\rangle$ is coupled to $|e\rangle$. Working in the dressed-states picture, it is easy to find out the scattering rate γ_c of state $|c\rangle$ to be

$$\gamma_c = 4n_c\frac{g^2}{\Gamma} = n_c\eta\kappa, \tag{5.4}$$

where n_c is the intracavity photon number. When the lifetime of EIT is much smaller than the cavity lifetime, the atomic components in state $|c\rangle$ see the average effect of the cavity photons. So we use the average intracavity photon number to replace n_c here. We also count in the cavity blocking introduced by signal photons in the weak

coherent state, so n_c is corrected to

$$n_c = \frac{\langle n_c \rangle|_{n_s=0}}{\left[1 + \frac{\eta}{1+\Omega^2/(\kappa\Gamma)}\right]^2}$$

in the limit of OD > 1. Here $\frac{1}{1+\Omega^2/(\kappa\Gamma)}$ is the average atomic excitation number the cavity photons see when a signal photon are traveling in the atomic ensemble, assuming that the signal beam is in weak coherent state.

We calibrate $\langle n_c \rangle|_{N_c=0}$ in our system by measuring the photon rate R_c transmitted through the cavity without EIT polaritons component in $|c\rangle$. Knowing the cavity decay rate κ and the output coupling efficiency $T/(T+L)$,

$$\langle n_c \rangle|_{n_s=0} = \frac{2R_c}{\kappa}\frac{T+L}{T}. \tag{5.5}$$

At each different average intracavity photon number $\langle n_c \rangle|_{n_s=0}$, the EIT spectrum is measured and γ is determined from the fit to the EIT spectrum. From an approximation to the width of the Voigt profile, accurate to better than 1%, we expect $\gamma = 0.535\gamma_c + \sqrt{\gamma_d^2 + 0.217\gamma_c^2}$, where γ_c is the decoherence due to cavity photon scattering, and γ_d is decoherence due to the Doppler effect. In Figure 5-3, the data agree with our fit and indicate $\gamma_d = 2\pi \times 110(10)$kHz for the Doppler broadening and $\gamma_c = n_c \times 2\pi \times 70(25)$kHz. It is consistent with the theoretical calculation $\gamma_c = n_c \times 2\pi \times 71(8)$kHz.

By measuring EIT spectra at different cavity photons, we show that the signal photon transmission depends strongly on the intracavity photon number $\langle n_c \rangle|_{n_s=0}$.

5.4 Cross Correlation Function

In the photon transistor experiment, we have measured g_2 correlation function at time $\tau = 0$. And we find out that the gate photons and source photons transmitted through the system are anti-correlated with g_2 at 0.17.

For this experiment, we should also expect an anti-correlation between the cavity

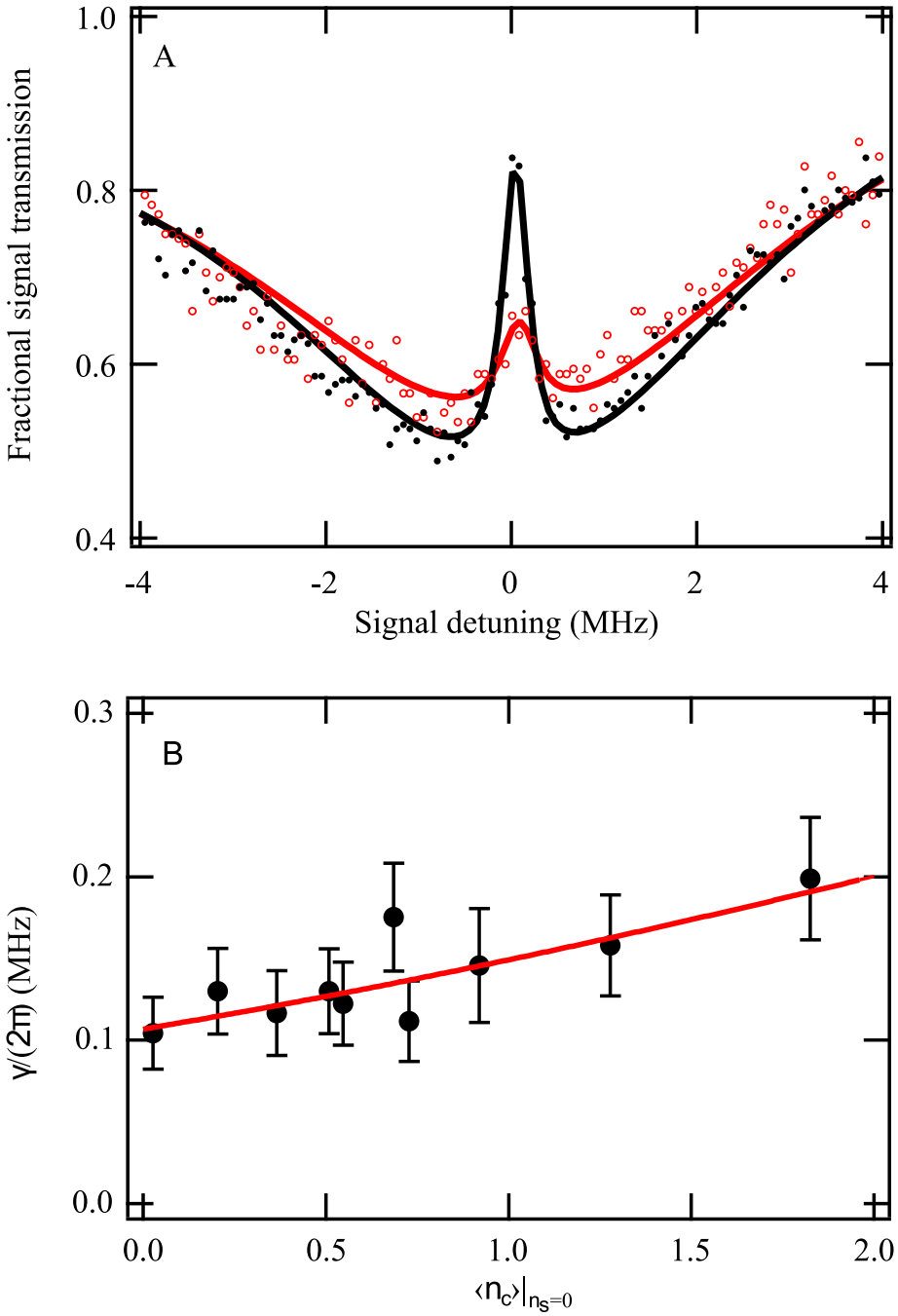

Figure 5-3: (A) An example of the EIT spectra we measure. Black and red curves correspond to $\langle n_c \rangle|_{n_s=0} = 0$ and 11.5. (B) After we get the decoherence rate γ, we plot it versus $\langle n_c \rangle|_{n_s=0}$. Here, we use $\Omega^2/\Gamma = 1.4(1)\ \mu s^{-1}$. The red solid line is the fit according to $\gamma = 0.535\gamma_c + \sqrt{0.217\gamma_c^2 + \gamma_d^2}$. The fit gives us $\gamma_c/(2\pi n_c) = 70(25)$ kHz which is consistent with the theoretical prediction. All error bars are one standard deviation.

mode and the signal mode. However due to the continuous nature of the signal mode, it should be less anti-correlated comparing to the transistor experiment. We use the same definition for g_2

$$g_2(\tau) = \frac{\langle n_c(0) n_s(\tau)\rangle}{\langle n_c(0)\rangle \langle n_s(\tau)\rangle}. \tag{5.6}$$

Here $\tau = t_s - t_c$ is the time separation. When $\tau > 0$, we are measuring the signal-mode-retarding correlation. When $\tau < 0$, we are measuring the signal-mode-advancing correlation. The theoretical calculation shows that $g_2(\tau)$ is given by

$$g_2(\tau) = \left[1 - (1 - e^{-\mathrm{OD}/(2\xi)}) \frac{\eta}{1+\eta} e^{-\kappa_{>/<}|\tau|/2}\right]^2. \tag{5.7}$$

Here, we notice something interesting. The retarding and advancing correlation have different rate constants. For $\tau < 0$, $\kappa_< = \kappa$ is the cavity linewidth. The cavity mode is dominating the correlation function. For $\tau > 0$, $\kappa_> = \Omega^2/\Gamma + \gamma_d$ is the EIT linewidth including decoherence from the Doppler broadening γ_d. There is a correction factor in g_2 formula

$$\xi = \frac{\kappa_>}{\kappa_> - \gamma} \left[1 + \frac{\kappa_>}{\kappa_<(1+\eta)}\right]. \tag{5.8}$$

The first multiplicative factor arises from imperfect EIT which reduces the cross modulation by decreasing the lifetime of the polariton. The second multiplicative factor accounts for the overlap in the cavity photon lifetime and the polariton lifetime. When the lifetime of the polariton is comparable to or shorter than the cavity photon lifetime, the photons interaction time and the cross modulation efficiency are reduced.

In the limit of large optical depth $\mathrm{OD}/\xi \gg \ln\eta$, each incoming signal photon is converted into a dark state polariton. In this case, the cavity transmission is modified by $(1+\eta)^{-2}$, which is also the minimum value of the correlation function $g_2(0)$. This is why we get 0.17 in the transistor experiment. In the other limit $\mathrm{OD}/\xi \ll \ln\eta$, the collective atomic excitations in $|c\rangle$ completely lose their phase information due to the strong cavity-atom coupling. Then EIT effect is strongly suppressed and $g_2(0) \approx e^{-\mathrm{OD}}$ is simply the transmission for the signal photon passing through the medium without coupling laser.

The following arguments could help us understand this cross modulation effect: the detection of a cavity photon at time $t = 0$ implies that the EIT transmission must have been reduced for times $t < 0$ on a time scale of the order of the cavity lifetime $1/\kappa$ and will approach its uncorrelated steady-state value $g_2(\infty) = 1$ for times $t > 0$ with a time constant determined by the polariton lifetime, or equivalently, the EIT linewidth $\kappa_> = \Omega^2/\Gamma + \gamma_d$. A similar argument can be made if we assume the signal photon to be detected at $t = 0$.

In Figure 5-4, we first plot the correlation function measured at different coupling laser powers. In all the three plots, they show that photons in the two modes are anti-correlated at $\tau = 0$. They extinguish each other when they arrive at the atomic medium at the same time. We use Eqn. 5.7 to fit the data. Especially in Figure 5-4(c), it is obvious that the rate constants are asymmetric around $\tau = 0$. Fitting these data points, we get the following parameters: (a) $\{g_2(0), \kappa_</\mu\text{s}^{-1}, \kappa_>/\mu\text{s}^{-1}\} = \{0.91(1), 1.6(2), 1.4(2)\}$, (b) $\{g_2(0), \kappa_</\mu\text{s}^{-1}, \kappa_>/\mu\text{s}^{-1}\} = \{0.89(1), 1.5(2), 2.4(3)\}$ and (c) $\{g_2(0), \kappa_</\mu\text{s}^{-1}, \kappa_>/\mu\text{s}^{-1}\} = \{0.90(1), 1.6(1), 3.9(3)\}$. The negative-time rate constant $\kappa_< = 1.6(1)\mu\text{s}^{-1}$ is independent of the coupling laser powers. However, it is 80% larger than the cavity linewidth. We believe it is due to occasional presence of absorbing atoms in the state $|c\rangle$ under imperfect optical pumping. Noting that at this time, we do not have three repetitive cycles of spatial selection in atoms preparation, and have a total atom number of $N = 2 \times 10^4$. One atom out of $N = 2 \times 10^4$ is sufficient to increase the cavity linewidth by a factor of $1 + \eta$. The positive-time rate constant is linearly depending on Ω^2/Γ. We fit $\kappa_>$ to $a\Omega^2/\Gamma + b$ and get $a = 0.7(1)$, $b = 1.2(2)\mu\text{s}^{-1}$.

5.5 Conclusion

By measuring the correlation function between the signal mode and the cavity mode, we find $g_2(0) \approx 0.89$. It means one photon in one beam extinguish another photon in the perpendicular direction by a probability of 11%. It shows deterministic photon-photon interaction between two perpendicular beams.

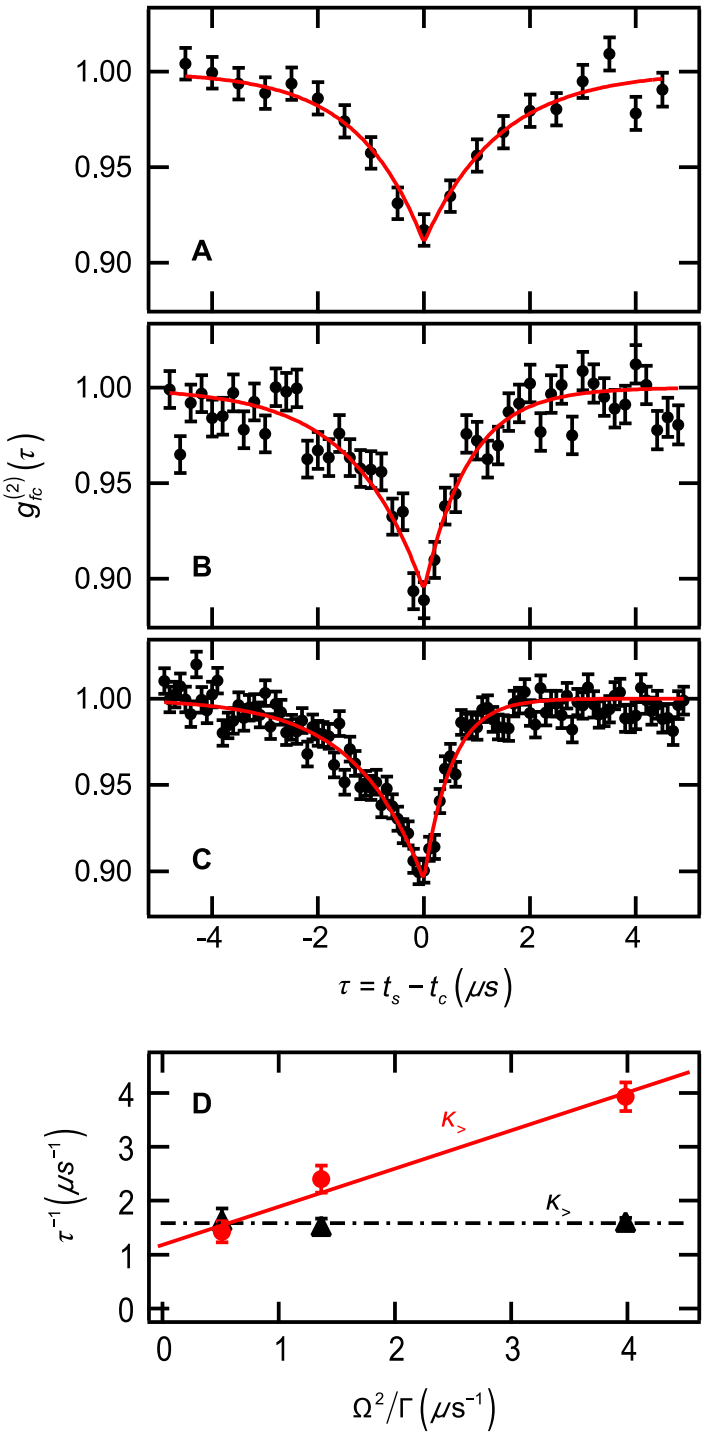

Figure 5-4: (A), (B) and (C) The correlation function $g_2(\tau)$ versus time τ for different coupling laser powers: Ω^2/Γ=0.5, 1.4 and 4.0 μs^{-1}. (D) Fitted rate constants $\kappa_{>/<}$ versus the EIT linewidth Ω^2/Γ. The measurements were performed at input coherent state of $\langle n_c \rangle = 0.2$ and $\langle n_s \rangle = 0.2$.

This result can be improved by a few technical upgrades. We have improved our system with a higher optical depth of 1.5 now, while this result was achieved with optical depth of 0.9. In principle, the atoms can be cooled down even further and reach Bose-Einstein condensation with much higher atomic density. In this case, the optical depth will be dramatically increased. We can also reorient the coupling beam to use a Doppler-free configuration for EIT. The third potential upgrade is using mirrors with smaller radius of curvature to build a micro-optical cavity. In this case, the cooperativity η can be up to 20 with negligible cavity in and out coupling loss [70]. By using these upgrades, the expected correlation function will be $g_2(0) = 0.09$ and the modulation efficiency will be 91%.

Chapter 6

Towards Real Time Non-destructive Detection of an Optical Photon

6.1 Overview

Measurement is the most mysterious part in quantum mechanics. Measurement projects a quantum state into different eigenstates with certain probabilities. As a result, measurements always disturb original quantum states unless the system is already in an eigenstate. What is even worse, some measurements completely destroy quantum states.

As an example of the latter, one detects the power of a laser beam using a photodiode by measuring the photocurrent out of the device. After this measurement, the detected photons cannot be recovered as all the photons are converted into electron-hole pairs. Possible quantum states such as the photons' polarization, correlation or spatial mode are destroyed. Since the measurement using a photodiode completely destroys the measured photons, no photons remain to measure these other interesting properties.

In quantum mechanics, non-destructive measurement is allowed. After a non-

destructive measurement, the quantum system still remains. As in the photon detection case, one can detect photon number in a photon pulse without absorbing photons. After this detection measurement, the polarization property of these photons is untouched. There is, however, back-action of the measurement on the phase of the light beam, which is randomized.

Quantum non-destructive detection is very useful. It can be used to measure the parity, to verify the CHSH inequality or to prepare spin squeezed states. Since most of the work described in this thesis has potential applications in quantum information, I will discuss in detail an application of non-destructive detection in quantum key distribution (QKD), which is one of the most important technologies in quantum information [71–73].

QKD requires the sender Alice to send single photons each time to the receiver Bob. Each photon's polarization is randomly selected from 0, 45, 90, 135 degree linear polarization. If the eavesdropper, Eve, captures the photons and performs any measurement on them, the photon polarizations would change. When Bob receives the photons, he will notice a higher error rate of photon polarization and figure out the existence of Eve.

QKD is perfectly secure when there is a perfect single photon source. However, such photon source does not exist yet. Scientists are working on improving single photon sources, but the correlation function g_2 of these photon sources does not yet reach to exact zero. Even for a good single photon source with low $g_2 = 0.04$ which is a pretty strong evidence proving the quantum nature of this photon source [66], there is still a probability of 4% that multi-photons states exist. Then, there is a security loophole.

Eve can perform a non-destructive detection to measure the photon number of each pulse transported from Alice to Bob. If there is only one photon in the pulse, Eve blocks it and throws it away. If there are many photons, Eve uses a beamsplitter to obtain at least one photon from this pulse. Then, Eve sends the rest of the pulse to Bob through a lossless channel. Eve's signal blocking looks like signal loss in the communication channel from Alice to Bob. Currently, commercial fibers work with

attenuation losses as low as 0.2 dB/km for a weak pulse, with which the signal loss is significant over a distance of 100 km. Someone with a high fidelity fiber and non-destructive detections can easily eavesdrop. As a result, QKD becomes unsafe and there is no way to keep the key private anymore.

As illustrated above, non-destructive detection of the photon number is the key to hack the QKD process. On the other hand, if Alice has this technology instead, she can make sure that all the pulses she sends out are single photon pulses, to prevent the eavesdroping. The non-destructive detection is a double-edged sword. It is proposed to hack the security of QKD, while it helps to enhance the security level of quantum communication.

A simple modification of optics in the cavity photon detection path changes our experimental system from a cross modulation medium into a nondestructive photon detector.

6.2 Theory

We use cavity photons to detect the presence of a photon in the free-space mode in real time. Instead of measuring the transmission of the cavity photons as in cross modulation experiment (Chap. 5), we measure the polarization-analyzed cavity reflection signal. As shown in Fig. 6-1, lin-polarization ($\sigma_+ + \sigma_-$) photons are sent onto the cavity with quantization axis along the free-space mode, and the reflection of these photons by the cavity in the orthogonal polarization ($\sigma_+ - \sigma_-$) is detected by a photon counter D_r. The free-space photon is resonant on $|f\rangle \leftrightarrow |d\rangle$ transition, while the σ_+ component of cavity photons couples the $|c\rangle \leftrightarrow |e\rangle$ transition, and the σ_- component of cavity photons does not couple any atomic transitions. When there is no free-space photon passing by, no cavity photon will be detected by photon counter D_r. When a free-space photon passes through the atomic ensemble as a dark-state polariton, its atomic excitation component in $|c\rangle$ state will change the reflection for the σ_+-polarization component of cavity photons while keeping the σ_--polarized component untouched. As a result, the photon counter D_r detects reflected cavity

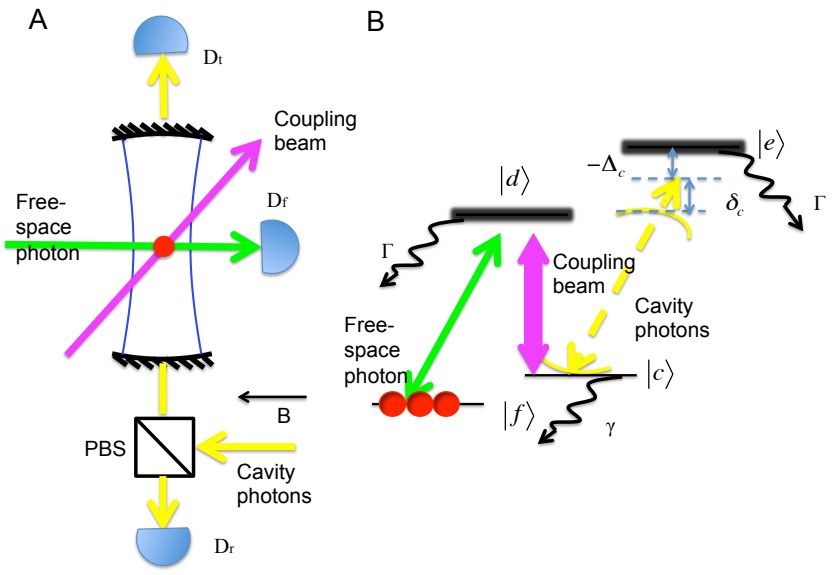

Figure 6-1: (A) Setup and (B) atomic level scheme for real-time non-destructive detection of optical photons. Free-space photons are slowed down in atomic ensemble as dark-state polaritons while their atomic excitation component is detected via a change of the reflected cavity photons' polarization. PBS denotes a polarizing beam splitter which generates the cavity photons incident onto the cavity to be $\sigma_+ + \sigma_-$-polarized, and filters $\sigma_+ - \sigma_-$-polarized photons for photon counter D_r to detect. The σ_+-polarization component of cavity photons is coupling to the atomic transition $|c\rangle \leftrightarrow |e\rangle$ while the σ_--polarization component of cavity photons does not couple any atomic transition. This creates a real-time signal on photon counter D_r when a free-space photon is transmitted through the atomic ensemble.

photons and reveals that a free-space photon is passing by in real time. After this measurement, the free-space photon is transmitted through the atomic ensemble in its original mode.

We will first look at the simplest case, where the cavity detunings $\Delta_c = \delta_c = 0$ and the input fields in both cavity and free-space modes are in weak coherent states. Working in the Hamiltonian frame described in Chap. 2 and [43], we obtain the probability of detecting a photon in photon counter D_r when one free-space photon is transmitted through the atomic ensemble, assuming only one cavity photon is incident onto the cavity:

$$
\begin{aligned}
P_{det} &= \frac{\langle n_{df} n_{dr} \rangle}{\langle n_{df} \rangle \langle n_{cin} \rangle} \\
&= \frac{1}{2} \frac{\left\langle \left(\varepsilon - \frac{\kappa}{2} b^\dagger(0)\right) a^\dagger(0) a(0) \left(\varepsilon - \frac{\kappa}{2} b(0)\right) \right\rangle}{\langle a(0)^\dagger a(0) \rangle \langle \varepsilon^2 \rangle} \\
&= \frac{1}{2} \frac{\langle \chi_J | \left(\varepsilon - \frac{\kappa}{2} b^\dagger(0)\right) \left(\varepsilon - \frac{\kappa}{2} b(0)\right) | \chi_J \rangle}{\langle \chi_{ss} | \varepsilon^2 | \chi_{ss} \rangle} \\
&= \frac{1}{2} \left(\frac{\eta}{1+\eta}\right)^2 \left(1 - e^{-\frac{\mathcal{N}}{2\zeta}}\right)^2,
\end{aligned}
\tag{6.1}
$$

where $\zeta = \left(1 + \frac{\Gamma\gamma}{\Omega^2}\right)\left(1 + \frac{\frac{\Omega^2}{\Gamma} + \gamma}{\kappa(1+\eta)}\right)$ as defined in Chap. 2.2.

To increase the detection efficiency, we send more cavity photons onto the cavity, with a trade off in increasing the destruction probability of the free-space photon. In this multi-cavity-photon condition, we intuitively understand and quantitatively model the system by splitting the interactions in the system into two mechanisms, electromagnetically induced transparency in the free-space mode, and atom-cavity interactions in the cavity mode.

The detection efficiency of the real time non-destructive detection of a free-space photon is described by the probability of cavity photons detected by the photon counter D_r when a free-space photon is sent into the atomic ensemble. It is dependent on the incident photon rate onto the cavity R_{cin} and the coupling beam Rabi frequency Ω_{cp}. The free-space photon travels as a dark-state polariton with atomic excitation component in $|c\rangle$ with a probability of $1 - e^{-\mathcal{N}}$ for an average time of $\tau_{fs} = \Gamma/\Omega_{cp}^2$. This excitation component in state $|c\rangle$ changes the reflection probability of each σ_+-polarization cavity photon sent into the cavity within this time duration. The reflection probability is changed from zero to $P_r = \frac{(n_a\eta)^2}{(1+n_a\eta)^2}$, where the atomic excitation number $n_a = \left(1 - e^{-\mathcal{N}}\right) \times \frac{1}{1+\frac{\Omega_{cp}^2}{\Gamma\kappa}}$. The factor of $\frac{1}{1+\frac{\Omega_{cp}^2}{\Gamma\kappa}}$ comes from the overlapping probability of cavity photon and free-space photon in the nonlinear medium in time. As a result, the detection efficiency of the free-space photon is $1 - \left(1 - \frac{1}{2}P_r\right)^{R_{cin}\tau_{fs}}$.

Each cavity photon reduces the transmission of free-space photon by destroying

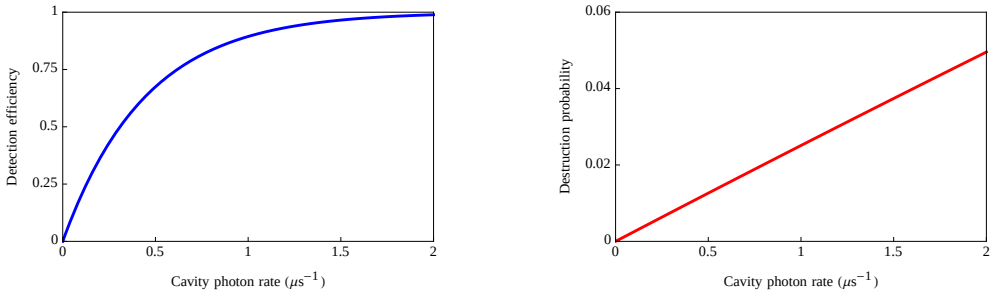

Figure 6-2: (Left) Detection efficiency and (Right) destruction probability of real time non-destructive detection of free-space photon versus cavity photon incident rate, using $\Gamma = 2\pi \times 5.2$ MHz, $\kappa = 2\pi \times 0.14$ MHz, $\eta = 200$, $\Omega_{cp} = 2\pi \times 0.5$ MHz, and $\mathcal{N} = 2$.

the coherence of the dark-state polariton whenever this cavity photon is scattered into one of the free space modes rather than the cavity mode. The destruction probability introduced by each cavity photon is $P_{de} = \frac{2n_a\eta}{(1+n_a\eta)^2}$. The total destruction probability is $1-(1-P_{de})^{R_{cin}\tau_{fs}}$.

If we improve our cavity cooperativity to 200 (method described in Appendix B), the non-destructive detection can be achieved with an efficiency of 99% and destruction probability of 5%. Note that we can also choose to tune the cavity detuning off of the atomic resonance to work with a more linear detection signal while using cavity phase shift to generate detection signal. The ratio between P_r and P_{de} is fixed for different photon-atom detuning Δ_c when the photon cavity detuning δ_c is optimized.

6.3 Preliminary Result

As a first step to test our theory, we measured the detection signal (detection probability at photon counter D_r when one photon incident into the cavity) at several atomic excitation numbers n_a for different coupling beam Rabi frequencies. This measurement shows that, the ratio between detected cavity photons and incident cavity photon depending on the atomic excitation number n_a not the coupling beam Rabi frequency. The detection efficiency is quite low (5%) for 20% destruction probability, mostly due to the large decoherent rate between states $|f\rangle$ and $|c\rangle$ due to Doppler shift. By changing the experimental setup so that the coupling beam di-

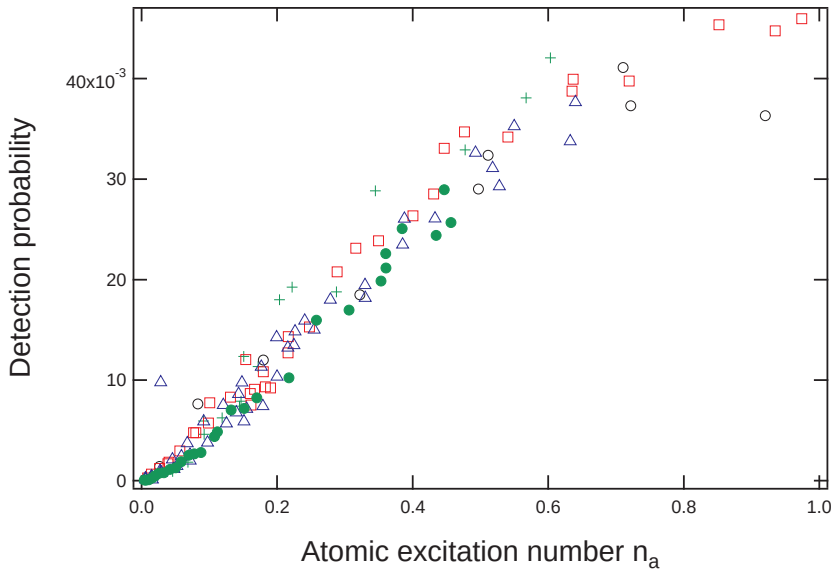

Figure 6-3: Detection probability at photon counter D_r when one photon is sent into the cavity for different atomic excitation numbers n_a and for different coupling beam Rabi frequencies. The Rabi frequencies are $2\pi \times 2$ MHz (black open circle), $2\pi \times 3.2$ MHz (red open square), $2\pi \times 4.1$ MHz (blue open triangle), $2\pi \times 4.9$ MHz (green solid circle).

rection takes advantage of the Lamb-Dicke confinement of the standing wave optical dipole trap, this problem would be fixed.

6.4 Measuring the Beatnote of the Atom-Cavity Coupling

As illustrated above, the detection signal is a function of the effective cooperativity η. It is a good tool to measure the atom-field coupling strength at different locations on z axis. In fact, it does show the incommensurate nature of the 937 nm (atoms in optical dipole trap) and 852 nm (cavity photon) wavelength standing waves. Each data point in Fig. 6-4 shows a darkport signal detected by photon counter D_r, which is a spatial averaged signal over the Gaussian distribution with waist of 2 μm defined by the free-space mode. These data show a sinusoidally periodic coupling strength, which agrees with the nature of the atom-field coupling along the cavity axis. The expected beatnote between the standing waves of the optical dipole trap at 936.7 nm

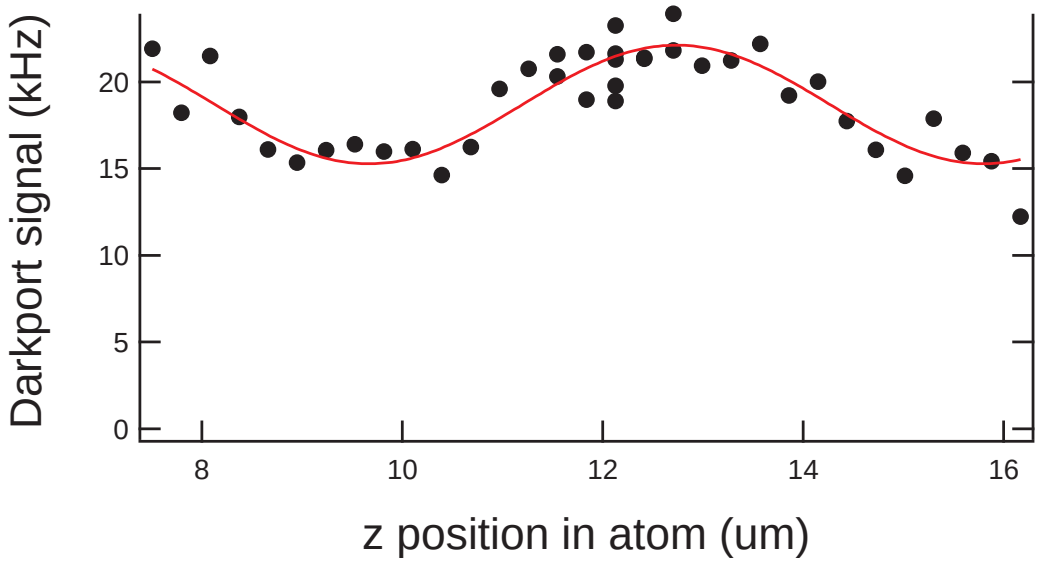

Figure 6-4: Darkport signal versus scanning of the position of the free-space mode at atomic ensemble along cavity axis. These data are fitted by a sinusoidal curve with a period of 6.1 μm.

and the cavity mode at 852.3 nm has a period of 4.7 μm. The difference between the measured and expected period is likely due to the error bar of z position in atom as this position is roughly estimated from the geometrics of optical path assuming the free-space beam is collimated [50, Fig. 6.6]. A more accurate z position in atom can be calibrated using absorption image of the atomic ensemble by heating out the atoms addressed by the free-space beam.

Chapter 7

Vacuum-Induced Transparency

7.1 Overview

Vacuum is interesting. According to the Merriam-Webster dictionary [74], vacuum is defined as an empty space in which there is no air or other gas. Thus it seems that the vacuum is just empty and probably boring. However in the view of physicists, this is not true. In this chapter, I will show that the vacuum electromagnetic mode can be engineered to induce a strong photon-atom interaction by using two high reflection mirrors. The phenomenon of vacuum induced transparency (VIT) is experimentally demonstrated and shows that vacuum is not empty and can interact with atoms.

Before discussing the details of this experiment, I will show some similar properties between the vacuum and a coherent state $|\alpha\rangle$ coming from the laser. The coherent state is defined as $\hat{a}|\alpha\rangle = \alpha|\alpha\rangle$. When $\alpha = 0$, the state $|\alpha = 0\rangle$ is vacuum. This is not a coincidence since the coherent state is only a shifted state of vacuum in phase space, as shown in their Wigner quasi-probability distribution function $W(x, p)$ where $\hat{x} = (\hat{a} + \hat{a}^\dagger)/\sqrt{2}$ and $\hat{p} = (\hat{a} - \hat{a}^\dagger)/(i\sqrt{2})$. For the coherent state $|\alpha\rangle$,

$$W_\alpha(x, p) = \frac{1}{\pi} \exp\{-[x - Re(\alpha)]^2 - [p - Im(\alpha)]^2\}. \tag{7.1}$$

For the vacuum state, we have

$$W_0(x,p) = \frac{1}{\pi}\exp(-x^2-p^2). \tag{7.2}$$

Both of them have $\Delta x^2 = 1/2$ and $\Delta p^2 = 1/2$ which indicate the electromagnetic fluctuation in both states are the same.

Therefore we define a new set of coordinates $\hat{b} = \hat{a} - \alpha$ and $\hat{b}^\dagger = \hat{a}^\dagger - \alpha^*$. In this situation, the original coherent state $|\alpha\rangle$ becomes the new vacuum state which satisfies $\hat{b}|\alpha\rangle = 0$ and the original vacuum state $|0\rangle$ becomes the new coherent state $\hat{b}|0\rangle = -\alpha|0\rangle$. So it is obvious that the coherent state is only a shifted vacuum in phase space. This is a strong indication that vacuum has some similar properties with a laser pulse in the coherent coupling regime.

Now we can describe the details of photon-atom interaction. Let's start with a three-level atomic system.

$$H = E_f|f\rangle\langle f| + E_d|d\rangle\langle d| + E_c|c\rangle\langle c| + \frac{\hbar}{2}\left(\Omega_p e^{i\omega_p t}|f\rangle\langle d| + \Omega_c e^{i\omega_c t}|c\rangle\langle d| + h.c.\right) \tag{7.3}$$

Here we use the rotating wave approximation which is valid when the detuning is only a few MHz or GHz compared to the optical frequency of hundreds of THz. In the interaction picture, the interaction Hamiltonian is

$$H_I(\Delta_p,\Delta_c) = \frac{\hbar}{2}\left(\Omega_p e^{i\Delta_p t}|f\rangle\langle d| + \Omega_c e^{i\Delta_c t}|c\rangle\langle d| + h.c.\right). \tag{7.4}$$

Here $\Delta_p = \omega_p - (E_d - E_f)$ and $\Delta_c = \omega_c - (E_d - E_c)$. When $\Delta_p = \Delta_c = 0$, $H_I = \frac{\hbar}{2}\left(\Omega_p|f\rangle\langle d| + \Omega_c|c\rangle\langle d| + h.c.\right)$ and there is a dark state $|D\rangle$ in the system which satisfies

$$|D\rangle = \frac{\Omega_c|f\rangle - \Omega_p|c\rangle}{\sqrt{\Omega_c^2+\Omega_p^2}}, \tag{7.5}$$

$$H_I|D\rangle = 0. \tag{7.6}$$

If the atom is in state $|D\rangle$ initially, it remains in this state. And there is no population

in the excited state $|d\rangle$ which has a much higher decay rate compared to the ground states $|f\rangle$ and $|c\rangle$. We can understand this from the following physics picture: both the probe light Ω_p and the coupling light Ω_c are resonant with the absorptive medium. The excitations from both beams display strong destructive interference with each other, and the excited state population remains zero all the time. Since the medium is not excited, the photons will not be scattered or absorbed. Then the probe light is transmitted through the medium without any absorption and the transmission is 100% for the ideal system. This is what happens in the EIT system.

In the discussion above, we used two c-numbers to represent the probe light and coupling light. In order to see the effect of vacuum, we need to quantize these fields. The Hamiltonian is rewritten as

$$H_I = \frac{\hbar}{2}\left(2g_p\hat{a}_p^\dagger|f\rangle\langle d| + 2g_c\hat{a}_c^\dagger|c\rangle\langle d| + h.c.\right), \tag{7.7}$$

where $2g_p(2g_c)$ is the single-photon Rabi frequency for probe light (coupling light). Let's assume the light as a Fock state $|m\rangle_p \otimes |n\rangle_c$ for now. The unnormalized dark state in the Fock state representation

$$|D_{mn}\rangle = g_c\sqrt{n}|f\rangle|m\rangle_p|n-1\rangle_c - g_p\sqrt{m}|c\rangle|m-1\rangle_p|n\rangle_c. \tag{7.8}$$

Any supposition of $\{|D_n\rangle\}$ is the dark state of the Hamiltonian in Eqn 7.7. So we combine $|D_{mn}\rangle$ with different coefficients to reproduce the semi-classical result,

$$|D\rangle = A\sum_{mn}\frac{\alpha^m}{\sqrt{m!}}\frac{\beta^n}{\sqrt{n!}}|D_{mn}\rangle = A\left(g_c\beta|f\rangle - g_p\alpha|c\rangle\right)|\alpha\rangle_p|\beta\rangle_c. \tag{7.9}$$

Here, $A = 1/\sqrt{g_c^2\beta^2 + g_p^2\alpha^2}$. In the semi-classical approximation, $\Omega_p = 2g_p\alpha$ and $\Omega_c = 2g_c\beta$. Therefore by using Ω_p and Ω_c, we will get exactly the same expression for the dark state

$$\frac{1}{\sqrt{\Omega_c^2 + \Omega_p^2}}(\Omega_c|f\rangle - \Omega_p|c\rangle)|\alpha\rangle_p|\beta\rangle_c.$$

The only difference is here we describe the light fields in quantum states.

In our experiment, we send in the probe light as a coherent state and use the vacuum cavity mode as the coupling light. So we treat the probe light as a classical field and the coupling light as a quantum field. We replace g_p with $\frac{\Omega_p}{2\alpha}$ and put the probe light state's quantum state aside in the following derivation. Before starting the experiment, the cavity field is in the vacuum state. When we send in the probe light, there is a small probability of excitations in the cavity mode because of the three-level-coupling. Therefore, we write the coupling light as $|\beta\rangle = |0\rangle + \beta|1\rangle$. Combining all these treatments, we rewrite the dark state and keep terms to the first order of β

$$|D\rangle = g_c\beta|f\rangle|0\rangle_c - \frac{\beta\Omega_p}{2}|c\rangle|1\rangle_c - \frac{\Omega_p}{2}|c\rangle|0\rangle_c = \beta\left(g_c|f\rangle|0\rangle_c - \frac{\Omega_p}{2}|c\rangle|1\rangle_c\right) - \frac{\Omega_p}{2}|c\rangle|0\rangle_c \tag{7.10}$$

Here, both terms $\beta\left(g_c|f\rangle|0\rangle_c - \frac{\Omega_p}{2}|c\rangle|1\rangle_c\right)$ and $\frac{\Omega_p}{2}|c\rangle|0\rangle_c$ are the dark states. The second term means we prepare all the atoms in a different initial state $|c\rangle$ which is shielded from the probe light. Of course in this case, the atoms do not absorb any light but it is a trivial case. So we can ignore the second term and focus on the first term. This approximation is also consistent with our state preparation which initializes all the atoms in $|f\rangle$.

Until now, every step of the discussion has been in the ideal case. Under these conditions, the dark states and EIT effect always exist when we replace two classical fields by two quantum fields or vacuum fields. EIT is a robust and universal phenomenon in the three-level systems.

7.2 The VIT Scheme

The previous section proved the validity and universality of our VIT experiment. In order to observe the VIT effect, we can perform a measurement of the probe light transmission and group velocity delay in our real system. So I need to include some decay terms in the evolution and let the system build a steady state which also depends on the decay mechanism. The general N_a-atom Hamiltonian for our system

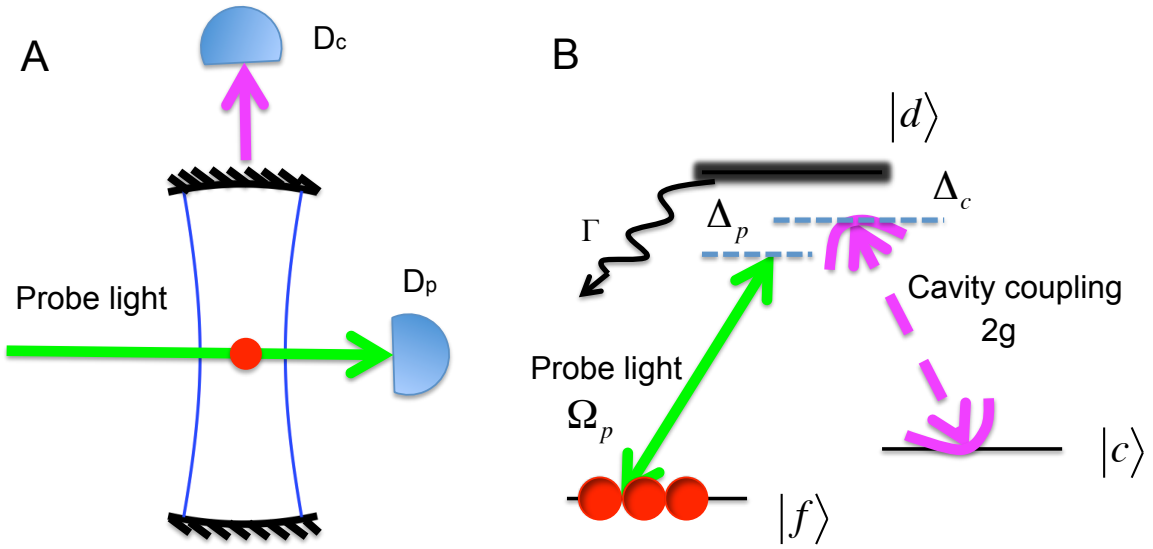

Figure 7-1: The VIT scheme. (A) The configuration of the system. The atoms are trapped inside a high-finesse cavity. A probe beam from side is addressing the atoms. There are two detectors D_p and D_c which measure the probe light and the cavity light. (B) The atomic level scheme of VIT. All atoms are initialized in the $|f\rangle$ state. Probe light couples the atomic transition $|d\rangle \leftrightarrow |f\rangle$. The cavity mode couples the transition $|d\rangle \leftrightarrow |c\rangle$. When there is a photon coming from the probe beam, it coherently transfers one atom from $|f\rangle$ to $|c\rangle$, forming a dark state.

is

$$\begin{aligned} H_I/\hbar &= \sum_{i=1}^{N_a}\left(-\Delta_p + i\frac{\Gamma}{2}\right)|d\rangle_i\langle d|_i + \left(\Delta_c - \Delta_p + i\frac{\kappa}{2}\right)\hat{a}_c^\dagger\hat{a}_c \\ &+ \left[\sum_{i=1}^{N_a}\left(g_c\hat{a}_c^\dagger|c\rangle_i\langle d|_i + \frac{\Omega_p}{2}|f\rangle_i\langle d|_i\right) + h.c.\right]. \end{aligned} \tag{7.11}$$

Γ is the spontaneous decay rate of the excited state, κ is the cavity line width and Δ_p (Δ_c) is the detuning of the probe light (coupling light). If we restrict our initial state to $\prod_{i=1}^{N_a}(\otimes|f\rangle_i)\otimes|0\rangle_c$, we can simplify the Hamiltonian by projecting it into the lowest excitation manifold.

$$\begin{aligned} H/\hbar &= \left(-\Delta_p + i\frac{\Gamma}{2}\right)|E\rangle\langle E| + \left(\Delta_c - \Delta_p + i\frac{\kappa}{2}\right)|1\rangle_c\langle 1|_c \\ &+ \left(g_c|C\rangle\langle E|\otimes|0\rangle_c\langle 1|_c + \sqrt{N_a}\frac{\Omega_p}{2}|F\rangle\langle E| + h.c.\right) \end{aligned} \tag{7.12}$$

And $|E\rangle$, $|C\rangle$ and $|F\rangle$ are defined as

$$|E\rangle = \frac{1}{\sqrt{N_a}} \sum_{i=1}^{N_a} \left[\prod_{j \neq i} (\otimes |f\rangle_j) \otimes |d\rangle_i \right], \tag{7.13}$$

$$|C\rangle = \frac{1}{\sqrt{N_a}} \sum_{i=1}^{N_a} \left[\prod_{j \neq i} (\otimes |f\rangle_j) \otimes |c\rangle_i \right], \tag{7.14}$$

$$|F\rangle = \prod_{i=1}^{N_a} \otimes |f\rangle_i. \tag{7.15}$$

7.2.1 Transmission

The key factor to evaluate the dispersive relation of our system is the susceptibility. The susceptibility is

$$\chi = \chi' + i\chi'', \tag{7.16}$$

where the real part χ' determines the refractive index n for the medium and the imaginary part χ'' determines the transmission T.

$$n = 1 + \frac{\chi'}{2}, \tag{7.17}$$

$$T = e^{-\chi'' kL}. \tag{7.18}$$

Here, k is the wave vector in the vacuum and L is the length of the medium. It is easy to relate χ with the coherence term ρ_{df} in the steady state.

$$\chi = 2\frac{\sqrt{N_a}}{V} \frac{\mu^2 \rho_{df}}{\Omega_p \hbar \epsilon_0}. \tag{7.19}$$

Here μ is the dipole moment and ϵ_0 is the vacuum permittivity.

We calculate the steady state from the Hamiltonian in Eqn 7.12 and get

$$\rho_{df} = \frac{\sqrt{N_a}\Omega_p(\Delta_p - \Delta_c + i\kappa/2)}{2\left[g^2 - (\Delta_p + i\Gamma/2)(\Delta_p - \Delta_c + i\kappa/2)\right]}. \tag{7.20}$$

So

$$\chi = \frac{N_a}{V} \frac{\mu^2}{\hbar \epsilon_0} \frac{\Delta_p - \Delta_c + i\kappa/2}{g^2 - (\Delta_p + i\Gamma/2)(\Delta_p - \Delta_c + i\kappa/2)}. \tag{7.21}$$

As we use the cavity cooperativity $\eta = 4g^2/(\kappa\Gamma)$ to characterize the cavity, it is straightforward to replace g^2 by $\eta\kappa\Gamma/4$. We also use the optical depth $\mathrm{OD} = \frac{N_a}{V}\frac{6\pi}{k^2}L$ and excited state decay rate $\Gamma = \frac{k^3\mu^2}{3\pi\epsilon_0\hbar}$ in the expression.

$$\chi = \frac{\mathrm{OD}}{kL}\frac{\Gamma}{2}\frac{\Delta_p - \Delta_c + i\kappa/2}{\eta\kappa\Gamma/4 - (\Delta_p + i\Gamma/2)(\Delta_p - \Delta_c + i\kappa/2)}. \tag{7.22}$$

In the experiment, we put the cavity coupling on resonance $\Delta_c = 0$ and scan the frequency of the probe light. We plot the transmission and the refractive index depending on the probe light detuning in Fig 7-2. A transmission window is shown in the center of the plot when the probe light is resonant with the atomic transition. It is similar to the conventional EIT scheme; the maximal transmission window is reached when both light fields are on resonance.

We may discuss the scaling of the transmission properties with η in VIT system little further. If $\Delta_p = \Delta_c = 0$, the transmission reaches the maximum.

$$T_{VIT} = e^{-\frac{\mathrm{OD}}{1+\eta}} \tag{7.23}$$

In the absence of VIT, the transmission is given by

$$T = e^{-\mathrm{OD}}. \tag{7.24}$$

Because of the exponential dependence, the VIT transmission is enhanced by a large factor compared to normal transmission of the two-level system. The difference can also be explained by the atom-cavity interaction theory. There are three ways for the probe photons to go. The first path is the forward scattering Γ_{fw}. The second path is scattering to all the free space modes Γ_{fs} and the third path is scattering into the cavity mode Γ_{cav}. If we define Γ_0 as the scattering rate in the absence of the

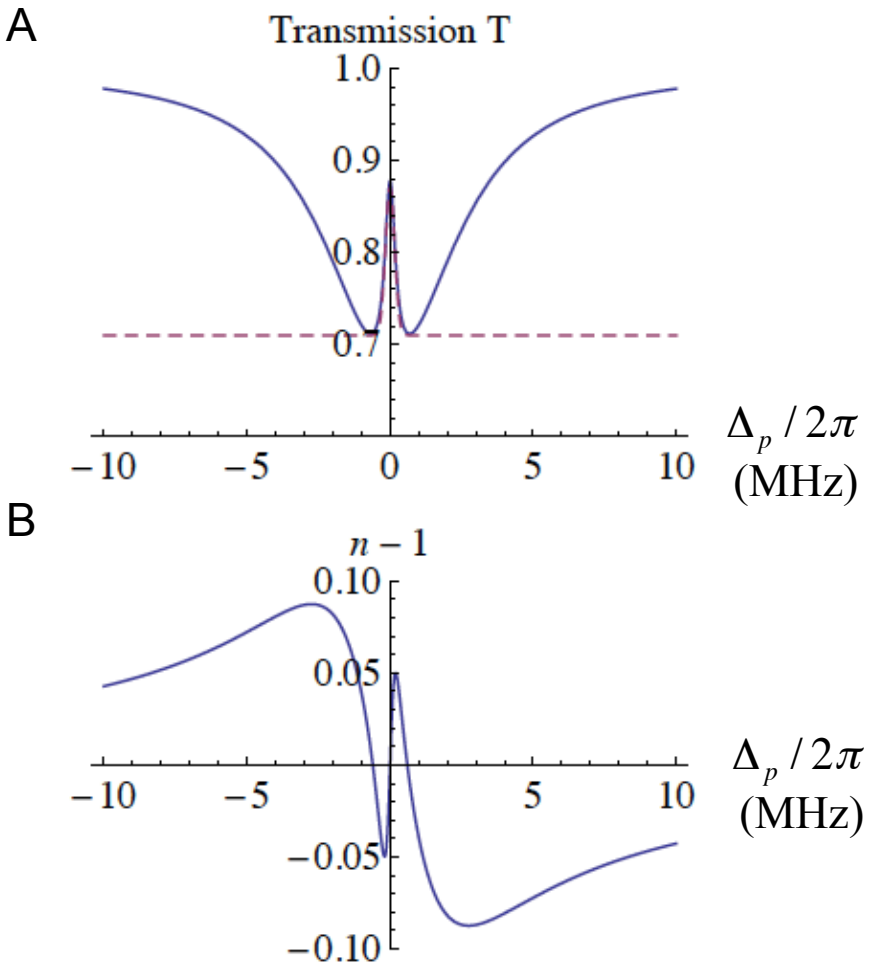

Figure 7-2: The theoretical calculation for the transmission and the reflection index. Here we use the realistic experimental parameters. OD=0.35, $\Gamma = 2\pi \times 5.2$MHz, $\kappa = 2\pi \times 170$kHz, L=20μm, $\lambda = 852$nm, η=1.7. The dashed line in (a) is the Gaussian fit $A\exp\left[-\left(2\Delta_p/\Delta_{VIT}\right)^2\right] + B$, where $\Delta_{VIT} = (1+\eta)\kappa$. A, B are the fitting amplitude and offset respectively.

cavity,

$$\Gamma_{fw} = \frac{\eta}{1+\eta}\Gamma_0, \tag{7.25}$$

$$\Gamma_{fs} = \frac{1}{(1+\eta)^2}\Gamma_0, \tag{7.26}$$

$$\Gamma_{cav} = \frac{\eta}{(1+\eta)^2}\Gamma_0. \tag{7.27}$$

The first term Γ_{fw} gets transmitted through the atomic ensemble because it is the same mode as the original beam. And the last two terms involve the loss in the probe beam. Comparing to Γ_0, the probe photon loss rate in VIT is

$$\Gamma_{fs} + \Gamma_{cav} = \frac{1}{1+\eta}\Gamma_0. \tag{7.28}$$

This shows that the photon loss rate in VIT is suppressed by a factor $1/(1+\eta)$. This is why the VIT transmission is enhanced by a factor $1/(1+\eta)$ in the exponent.

Another interesting thing to discuss is the width of the VIT window. We get the width by solving for the frequencies at $\frac{dn}{d\Delta_p} = 0$. In the limit $\eta \gg \kappa/\Gamma$, we find the width

$$\Delta_{VIT} = (1+\eta)\kappa. \tag{7.29}$$

We also check this width by fitting the transmission peak with a Gaussian $\exp\left(-\Delta_p^2/\delta^2\right)$ as shown in Fig. 7-2 with a dashed line. In this case, we get

$$\delta = \pm(1+\eta)\frac{\kappa}{2}, \tag{7.30}$$

which is consistent with the analytical solution.

This analysis gives a reasonable width for small OD and it is valid for our experiment (OD near 0.4). For a much larger OD ($\gg 1$), the absorption dip will saturate, and the width of the transparency window will be corrected by a factor of $1/\sqrt{\text{OD}}$:

$$\Delta_{VIT} = \frac{(1+\eta)\kappa}{\sqrt{\text{OD}}}. \tag{7.31}$$

7.2.2 Group Delay

In this section, we will discuss the group velocity in the VIT system. The phase velocity v_p and the group velocity v_g are defined as

$$v_p = \frac{\omega}{k_{med}}, \tag{7.32}$$

$$v_g = \frac{d\omega}{dk_{med}}, \tag{7.33}$$

where $k_{med} = nk$ is the wave vector in the medium and . As $v_p = c/n$,

$$v_g = \frac{d\omega}{dk} = \frac{d\omega}{d(n\omega/c)} = \frac{c}{n + \omega\frac{dn}{d\omega}} \tag{7.34}$$

When both couplings are resonant

$$\begin{aligned} \omega\frac{dn}{d\omega}\Big|_{\Delta_p=\Delta_c=0} &= \omega\frac{d\chi'}{2d\Delta_p}\Big|_{\Delta_p=\Delta_c=0} \\ &= c\frac{\mathrm{OD}}{L}\frac{\eta\Gamma-\kappa}{\kappa\Gamma(1+\eta)^2}. \end{aligned} \tag{7.35}$$

In Fig 7-2, the slope of refractive index is very sharp which means

$$\omega\frac{dn}{d\omega} \gg n|_{\Delta_p=\Delta_c=0} = 1. \tag{7.36}$$

Therefore the group velocity is much less than the speed of light in vacuum:

$$v_g = \frac{L}{\mathrm{OD}}\frac{\kappa\Gamma(1+\eta)^2}{\eta\Gamma-\kappa}. \tag{7.37}$$

The time delay from the group velocity is

$$\tau_g = \frac{L}{v_g} - \frac{L}{c} = \mathrm{OD}\frac{\eta\Gamma-\kappa}{\kappa\Gamma(1+\eta)^2} \tag{7.38}$$

passing through a medium of length L. The delay can be explained as the storage of photons in VIT. Each photon propagates in the VIT medium as a polariton, which is a superposition of a traveling photon and a collective atomic excitation. Each polariton

is passing to the next small but macroscopic volume of atomic ensemble. So the time for the photons to travel through the medium is proportional to the optical density of the atomic ensemble which indicates the number of atoms along the propagation direction.

Then we can ask another question, namely, under what conditions the entire photon pulse would fit into the atomic ensemble and would be delayed. This is also an important criterion if we want to slow down the photons by VIT.

In order to slow down the entire photon pulse, the pulse must fit into the sharp slope frequency region in Fig 7-2. The frequency window allowed for the incoming probe pulse is

$$F(\Delta_p) \propto \exp\left[-2\Delta_p^2/\Delta_{VIT}^2\right]. \tag{7.39}$$

By performing Fourier transformation, we obtain a time scale in real time domain

$$\tilde{F}(t) \propto \exp\left[-\frac{t_p^2}{2T_{min}^2}\right], \tag{7.40}$$

where the shortest allowed pulse duration

$$T_{min} = \frac{2}{\Delta_{VIT}} = \frac{2}{(1+\eta)\kappa}. \tag{7.41}$$

For our current setup, the shortest pulse we could delay is $T_{min} = 0.70\mu$s. Comparing with the delay time τ_g, the maximum fractional delay is

$$\frac{\tau_g}{T_{min}} = \frac{\mathrm{OD}}{2}\frac{\eta}{1+\eta}. \tag{7.42}$$

Unfortunately, the ratio is always smaller than 1 when we have a small OD < 1 regardless of the cavity cooperativity η.

In order to delay and separate the pulse into different Fock states, we need a higher OD. In the limit of OD $\gg 1$, the fractional delay is corrected to

$$\frac{\tau_g}{T_{min}} = \frac{\sqrt{\mathrm{OD}}}{2}\frac{\eta}{1+\eta}. \tag{7.43}$$

7.3 Nonlinearity at the Few Photons Level

In our experiment, we use the state $|6S_{1/2}, F = 3, m_F = 3\rangle$ of cesium atoms as $|f\rangle$, $|6P_{3/2}, F' = 4, m'_F = 4\rangle$ as $|d\rangle$ and $|6S_{1/2}, F = 4, m_F = 4\rangle$ as $|c\rangle$. First, we measure the probe transmission without the cavity coupling. We lock the cavity mode far off the atomic transitions. A typical transmission spectrum $f(\Delta_p) = \exp\left[-\frac{\mathrm{OD}}{1+(2\Delta_p/\Gamma)^2}\right]$ is observed in Figure 7-3(a). The black points are the experimental data and the red solid line is the transmission spectrum fit. The fit gives us an optical density OD = 0.401 and excited state decay rate $\Gamma = 2\pi \times 5.46$MHz. The measured Γ is consistent with the spontaneous decay rate of excited state in Cesium atoms. We also measure the probability of emission into the cavity (lower curves) with the blue solid line fit.

7.3.1 Vacuum Induced Transparency Window

Now we turn the cavity coupling frequency near the $|d\rangle \leftrightarrow |c\rangle$ transition ($\Delta_c < \Gamma$) and observe the VIT window at different cavity-atom detuning Δ_c. In Figure 7-3(b)-(d), we lock the cavity at different detuning of (b) $\Delta_c = 2\pi \times 0.5$MHz, (c) $\Delta_c = -2\pi \times 2.2$MHz and (d) $\Delta_c = 2\pi \times 2.8$MHz. The transmission rate is normalized to the incident photons. And the data are consistent with the theoretical prediction in Chap 7.2. The blue solid lines are predicted by Eqn 7.27.

There is always a small peak on the lower frequency side of the main peak in VIT spectra. This small peak comes from another VIT coupling $|F = 4, m_F = 3\rangle$ and $|F' = 4, m'_F = 4\rangle$ which 0.6 MHz away from the main peak which agrees with the independently measurement of the magnetic field 1.6 G. From the CG coefficients, we expect the peak to be four times weaker than the main VIT peak which is consistent with our measurement.

7.3.2 Non-linearity at a Few Photon Level

When we use cavity-enhanced vacuum or a few photons to couple $|d\rangle \leftrightarrow |e\rangle$ transition, the probe light transmission properties strongly depend on the photon number in

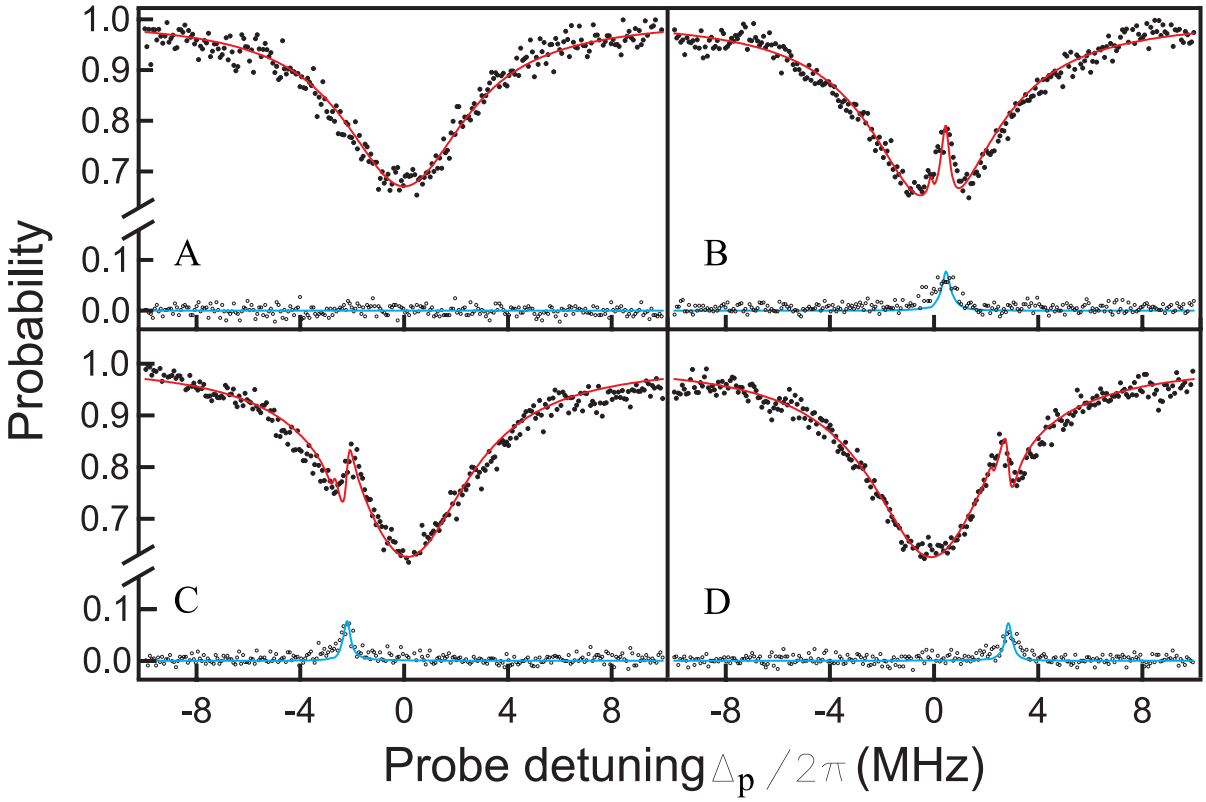

Figure 7-3: (A) Atomic absorption spectrum without the cavity coupling. (b)-(d) VIT transmission spectra for different atom-cavity detuning Δ_c: (B) $\Delta_c = 2\pi \times 0.5$MHz, (C) $\Delta_c = -2\pi \times 2.2$MHz, (D) $\Delta_c = 2\pi \times 2.8$MHz. The transmission probability (upper curves) and the probability of emission into the cavity (lower curves) are measured simultaneously versus Δ_p by two detectors D_p and D_c. Near the two-photon resonance $\Delta_p = \Delta_c$, the atomic absorption is suppressed by the VIT Λ shape coupling, and a small fraction of the incoming photon will be detected in the cavity mode. The peak frequency of the cavity emission is determined by the two-photon resonance.

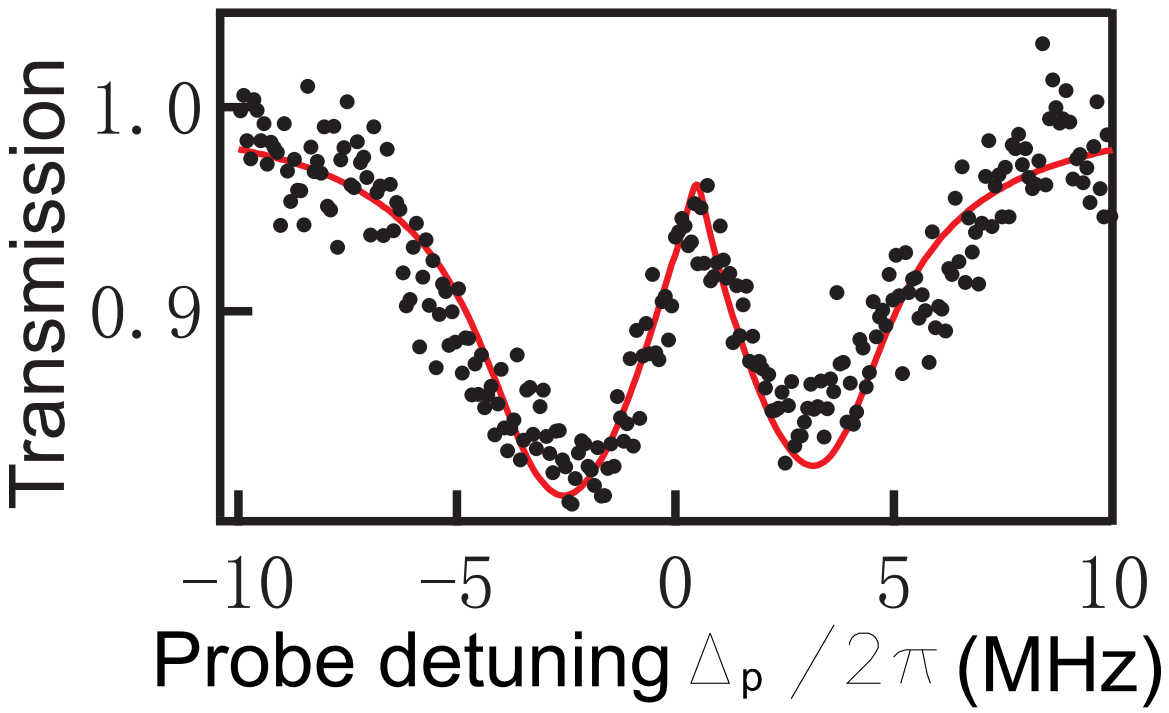

Figure 7-4: The transmission spectrum for $n_c = 22$. We fit the data with red curve according to the transmission $T = \exp(-\chi'' kL)$. The effective cooperative $\tilde{\eta}$ is obtained by fitting the data.

the coupling leg. In order to see this effect, we send coherent light with a fixed average photon number into the cavity each time and measure the transmission of the probe beam. In Figure 7-4, we show a typical transmission spectrum for 22 intracavity photons $\langle n_c \rangle$. We fit the red solid curve to the data and obtain the effective cooperativity for different $\langle n_c \rangle$.

From the definition of the cooperativity $\eta = 4g^2/\kappa\Gamma$, we expect the effective cooperativity to depend linearly on the intracavity photon number n_c.

$$\tilde{\eta} = \eta_0(1 + \langle n_c \rangle) \tag{7.44}$$

So we plot the measured effective cooperativity versus $\langle n_c \rangle$ in Figure 7-5. The data is consistent with the theoretical expectation.

We also measure the group velocity delay in our VIT system. The detunings are set to zero ($\Delta_p = \Delta_c = 0$) to allow maximal transmission within VIT window. A 25.2 ns delay is observed for a Gaussian pulse with width of 2.4 μs. Although the

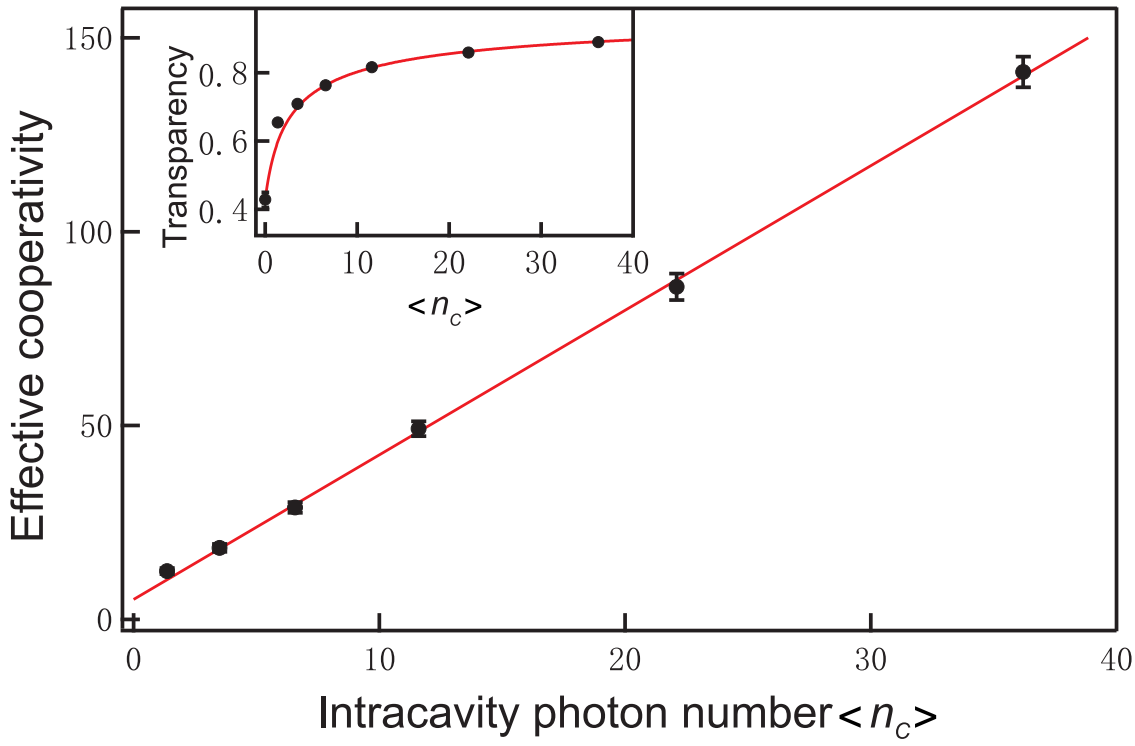

Figure 7-5: The effective cooperativity versus the intracavity photon number $\langle n_c \rangle$. We fit the data points with $\eta = An_c + B$ and we get $A = 3.7(1)$ and $B = 5(1)$. The theory predicts $A/B = 1$ for the ideal case. The inset shows the peak transparency versus average intracavity photon number.

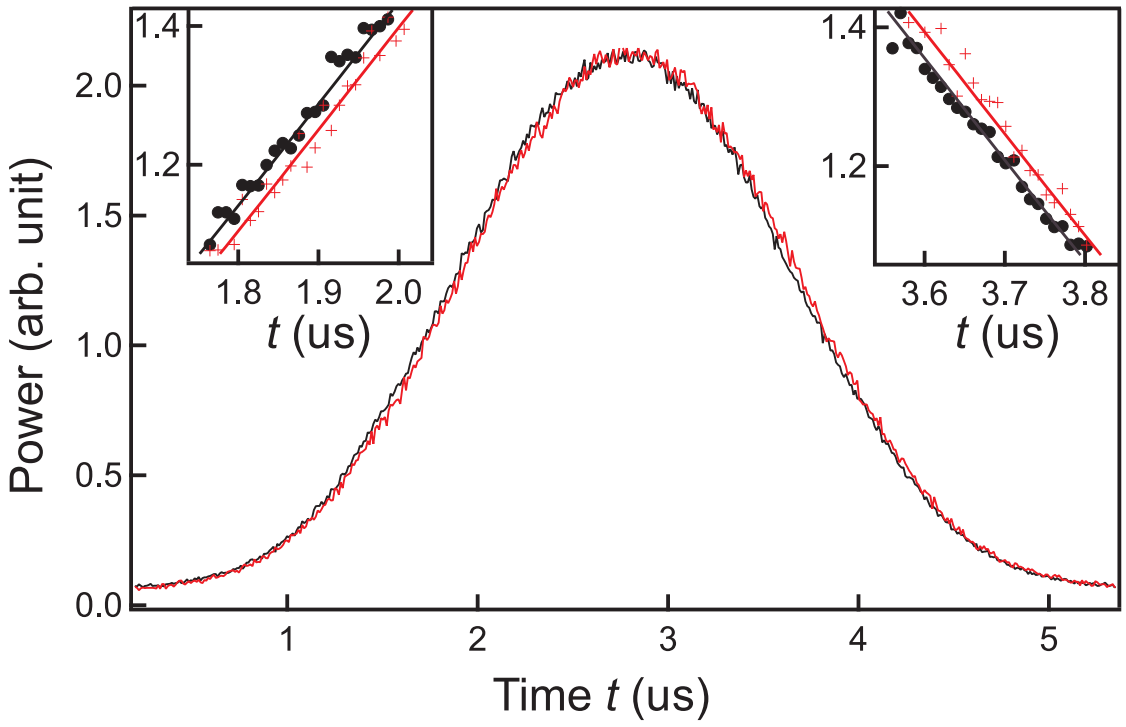

Figure 7-6: Vacuum-induced group delay of a probe pulse. Detected probe pulse with (red) and without (black) atoms. The pulse is a Gaussian shape of $\exp(-t^2/2\tau^2)$ with $\tau = 1.2\ \mu$s. The probe light and the coupling cavity are on resonance. The inset shows the zoom in parts of the curves. A delay time of 25 ± 2 ns is measured. Because of the atomic absorption, the delayed pulse in this figure has been rescaled by a factor of 1.6 for easier visualization.

delay time is tiny, it is significant noting that our sample size is as small as 22 μm. A group velocity of 1760m/s is achieved in the VIT system, much smaller than the speed of light in vacuum. In principle, we could collect more atoms and cool them down to a lower temperature that makes the sample much denser that result in higher OD. This way, we could slow down the group velocity even more and reach the Fock-state filter region [75].

7.4 Conclusion

In this experiment, we demonstrate that the vacuum can strongly distort the atom-light dispersive relation. The EIT effect is valid even at a few photons or zero photons level which indicates it to be a fundamental quantum property. We also observe the

nonlinear effect at a few-photon level. This experiment has opened a new path to engineer the vacuum effect.

Chapter 8

Towards Stronger Photon-Photon Interactions

We studied photon-photon interaction and strong non-linear effects at the single photon level in this thesis. A high-cooperativity optical cavity and the EIT mechanism has mediated and enhanced the photon-photon interaction. A single-photon transistor is demonstrated based on the cavity blocking effect, which is one of the fundamental properties of the cavity. Potentially other devices could be designed based on the cavity's properties.

We have also studied the cross-modulation effect in this system for two beams in weak coherent states. An anti-cross-correlation has been observed. One photon in one beam can extinct another photon in the perpendicular direction with a probability of 11% which reveals a quantum nature of the light.

The central technology of these two experiments is the electromagnetic induced transparency (EIT) in the optical cavity. EIT combined with a cavity is a powerful tool for us to study photon-atom or photon-photon interactions. Because of that, we have also focused on the properties of EIT itself.

When we replace the coupling beam in EIT with a quantized vacuum field, a transparency peak shows up. It reveals the quantum properties of both EIT and vacuum. On the other hand, VIT also proves the strong non-linearity at the single photon level.

These experiments can always be improved by upgrading the technology. In our system, we are first limited by the optical depth in the atomic ensembles. The optical depth can be enhanced by obtaining a colder ensemble and using a stronger trapping laser. If we cool the atoms to quantum degeneracy, the optical depth will increase dramatically. Meanwhile, A Bose-Einstein condensation can also increase the coherence time between the different ground states and suppress the Doppler broadening. By increasing the coherence time between two ground states in EIT, a longer EIT lifetime and more robust transparency windows are achieved which enables stronger photon-photon interaction.

Presently, we are changing the scheme of EIT coupling beam to suppress Doppler broadening and increase the lifetime of EIT. The coupling beam, probe beam and cavity axes will be aligned in the same plane. Along the cavity axis, the Doppler shift is suppressed by the lattice confinement working in the Lamb-Dicke regime. For the direction perpendicular to the cavity axis, the coupling beam and the probe beam sense the same velocity of the atoms and the Doppler shifts are reduced.

The next potential improvement is to increase the cavity cooperativity. One way is to increase the reflectivity of the cavity mirrors as the fabrication of high reflection coating is getting better. People can control the reflection very precisely in the coating process. However, scattering loss in the mirrors becomes dominant in the limit of ultra-high reflection regime which is limited by the surface roughness of the mirror substrates. The ratio of transmission over transmission plus reflection loss is much smaller unity in this limit. Then the output coupling of the cavity gets low and results in a lower total quantum efficiency that limits our measurement process.

Another approach to obtain higher cooperativity is changing the spatial design of the cavity. The first approach is replacing the confocal cavity by a concentric cavity. For the concentric cavity, there is no limit for the mode waist and the cooperativity can reach any higher number. However, this is an extremely unstable system. Any longitudinal perturbation will change the waist dramatically and any small angle twisting of the mirror will destroy the alignment of the cavity. This stability issue prevents us from reaching higher cooperativity in the concentric-cavity geometry.

A better approach is to keep the confocal design to maintain the maximal stability of the cavity system and using micro mirrors instead. The key point here is fabricating mirrors with smaller spatial radius of curvature while keeping a reasonable surface roughness. If we reduce the curvature from 1 cm to 200 μm, the cooperativity will be enhanced by a factor of 50. The enhancement here is significant. A few groups have successfully used the micro cavity system in their experiments. In Appendix B, I will introduce our preliminary results to implement a micro cavity system.

To maintain the benefit of long cavity for good atom loading, we will use a confocal asymmetric cavity design. In this design, we use one micro mirror and one normal size mirror to build the cavity. Because of the asymmetric design, the cavity mode waist is kept small and the space between two mirrors is kept large. The large space can help us load more atoms into the cavity. Another advantage of the asymmetric design is that we can couple the light more easily from the larger mirror side and collect the transmission in the micro mirror side.

In conclusion, we have observed several significant non-linear effects and strong photon-photon interactions at the single-photon level. We expect more interesting phenomena in our current system, as well as in our future system with a higher cooperativity and optical depth.

Appendix A

Parameters Measurements

This appendix supplements details of analysis used in the main text.

A.1 Optical Dipole Trap Scattering Probability

The optical dipole trap is a one-dimensional linearly-polarized intra-cavity lattice operated at 936 nm, whose optical field intensity and trap depth is amplified by the cavity finesse. Typically, we work with a trap depth where we measured the trap light power coupling out of the cavity to be 2.0 mW. Then the running wave power inside cavity will be amplified by a factor of $\mathcal{F}_{936}/\pi$, and the trap depth U_{936} at antinode turns out to be [76]

$$\begin{aligned} U_{936} &= \frac{1}{2}\frac{I}{I_s}\frac{\Gamma^2}{\Delta} \\ &= \frac{1}{2}\frac{2.0\text{ mW}\frac{368}{\pi}}{\frac{\pi}{2}(37.2\ \mu\text{m})^2}\times \\ &\left(\frac{1}{1.65\text{ mW/cm}^2}\frac{(2\pi\ 5.22\text{ MHz})^2}{2\pi\left(\frac{3\times10^8\text{ m/s}}{852\text{ nm}}-\frac{3\times10^8\text{ m/s}}{936\text{ nm}}\right)}+\frac{1}{2.50\text{ mW/cm}^2}\frac{(2\pi\ 4.56\text{ MHz})^2}{2\pi\left(\frac{3\times10^8\text{ m/s}}{895\text{ nm}}-\frac{3\times10^8\text{ m/s}}{936\text{ nm}}\right)}\right) \\ &= 2\pi\ 5.9\text{ MHz}, \end{aligned} \tag{A.1}$$

where I is the intra-cavity intensity at antinode, I_s is the saturation intensity, Γ is the natural line width of the excited states, Δ is the detuning of trap light frequency and atomic transition frequency, and the effects of Cesium D_1 and D_2 transitions are simply summed up.

The far detuned dipole trap light can excite a Cesium atom at a scattering rate of Γ_{sc},

$$\begin{aligned}\Gamma_{sc} &= \frac{I}{I_s}\left(\frac{\Gamma/2}{\Delta}\right)^2\frac{\Gamma}{2} \\ &= \frac{1}{2}\frac{2.0\ \text{mW}\frac{368}{\pi}}{\frac{\pi}{2}(37.2\ \mu\text{m})^2}\times \\ &\left(\frac{1}{1.65\ \text{mW/cm}^2}\frac{2\pi\ (5.22\ \text{MHz})^3}{\left(\frac{3\times10^8\ \text{m/s}}{852\ \text{nm}}-\frac{3\times10^8\ \text{m/s}}{936\ \text{nm}}\right)^2}+\frac{1}{2.50\ \text{mW/cm}^2}\frac{2\pi\ (4.56\ \text{MHz})^3}{\left(\frac{3\times10^8\ \text{m/s}}{895\ \text{nm}}-\frac{3\times10^8\ \text{m/s}}{936\ \text{nm}}\right)^2}\right) \\ &= 9\ \text{s}^{-1}.\end{aligned} \tag{A.2}$$

A.2 Atom-Induced Cavity Shift

Atoms in the cavity induces cavity resonance shift. The cavity shift can be used to measure the total atom number. N atoms are initiated in $|6S_{1/2}, F=3, m_F=3\rangle$ state, and "Gammap beam" on $\left|6S_{1/2}, F=4, m_F=4\right\rangle \leftrightarrow \left|6P_{3/2}, F'=4, m'_F=4\right\rangle$ transition keeps pumping atoms back to $|6S_{1/2}, F=3, m_F=3\rangle$ state. The cavity resonance frequency is $\Delta_l = 100$ MHz blue detuned from $\left|6S_{1/2}, F=4, m_F=4\right\rangle \leftrightarrow \left|6P_{3/2}, F'=5, m'_F=5\right\rangle$ transition to avoid cavity blocking and shift from atoms scattered in $\left|6S_{1/2}, F=4, m_F=4\right\rangle$ state. A lin-polarized cavity beam probes the cavity to measure frequency of cavity transmission peak. The atom-induced cavity shift Δ_s

is determined by cavity cooperativity η:

$$\begin{aligned}\Delta_s &= N\eta\kappa\Gamma\left(\sum\frac{CG_i^2}{\delta_i}\right)\\ &= N\frac{8.6}{2}\times 0.14\ MHz\times 5.2\ MHz\frac{1}{2}\\ &\left(\frac{5/14}{(9193-603)\ MHz-\Delta_l}+\frac{3/32}{(9193-452)\ MHz-\Delta_l}+\frac{5/14+5/672}{(9193-251)\ MHz-\Delta_l}\right),\end{aligned} \tag{A.3}$$

where CG_i is the Clebsch-Gordon coefficients for each coupling transitions, $\eta=\frac{8.6}{2}$ is the cavity cooperativity spatially averaged over antinode and node, the factor of $\frac{1}{2}$ is due to the polarization of the cavity beam, which has half σ_+ and half σ_- component. As a result, measured cavity shift of $\Delta_s = 3$ MHz indicates a total atom number of 10^5.

Appendix B

Micro Mirror Fabrication Using CO_2 Laser

CO_2 laser light is an appropriate tool for making concave profiles (micro mirror) on fused silica substrates [70]. Strong absorption of the CO_2 laser light at 10.6 μm enables controlled melting and evaporation on the surface (up to a few μm depth) of the fused silica substrates using easily achievable light intensities. The evaporation removes material on the surface and forms a concave shaped surface as laser beam intensity is Gaussian. The melting polishes the surface as the surface tension in the melted layer smoothens out the roughness. Fused silica is a good material for micro mirror substrates, not only because it is thermally isotropic and exceptionally good at resisting thermal shock, but also because of its high melting point (compared to ordinary glass) that lead to a concave profile for the micro mirrors by enabling material removal via evaporation to go beyond surface tension of melting material.

Here are the fabrication processes and parameters for making micro mirror profile. We use an RF powered CO_2 laser (Coherent Inc. GEM-30) with a measured average power of 35 Watts. The laser beam with a waist of 2.79 mm is focused down to the waist of 0.06 mm using a ZeSe lens with focus length of 50.8 mm (Edmund optics #47-072). The beam size hitting on the front surface of the substrates is controlled by changing the substrate's position relative to the beam's focal point with a translation stage. A visible laser beam overlapping with the CO_2 laser beam facilitates aligning

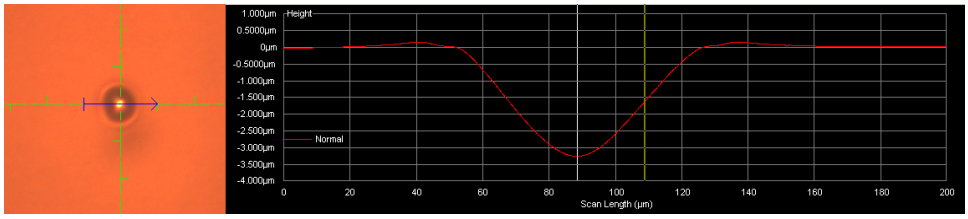

Figure B-1: Surface profile of a fabricated fused silica substrate. This profile is made with pulse duration of 0.07 ms and beam size of 65 μm. (Left) Camera photo of this profile. (Right) Cut through the center of the profile shows a Gaussian profile. Its central part can be fitted to a circle where the radius of curvature is measured.

substrates almost perpendicularly to the beam with a tiny angle to avoid optical feedback into CO_2 laser. A homemade electronic box controls the duration of the CO_2 laser pulse. We use 2 mm thick uncoated fused silica glass plates (Edmund optics #48-201) as substrates. After cleaning the substrates with chemical processes, we send single CO_2 laser pulses onto them to evaporate mirror profiles, adjusting the mirror positions on the substrates using translation stages.

With a combination of pulse length from 0.06 ms to 0.4 ms and beam size from 65 μm to 146 μm, we have fabricated micro mirror profiles with radius of curvature from 50 μm to 1000 μm, measured with surface profilometer (Tencor P-16). An example of the fabricated profile is shown in Fig. B-1.

The surface roughness of the micro mirror profile is evaluated by optical loss measurements at a wavelength of 852 nm. The substrates with micro mirror profiles are coated with high-reflection coatings at 852 nm on the micro mirror side and anti-reflection coatings on the other side (by ATfilm). A planar mirror with the same coatings is used to build cavities with each micro mirror. By measuring transmission of mirrors and transmission and reflection spectroscopy of each cavities [77], the loss of the micro mirrors is ~ 10 ppm. The cavities formed by one micro mirror and one planar mirror show geometric cooperativity η up to 250 as measured in Tab. B, which shows potentially ultra-strong cavity-atom interactions.

ROC	Cav Finesse	Mirror trans	Mirror loss	Cooperativity
133 μm	3.4×10^4	88 ppm	10 ppm	242.7
198 μm	4.0×10^4	75 ppm	5 ppm	191.8
380 μm	3.2×10^4	91 ppm	12 ppm	74.9
461 μm	2.9×10^4	102 ppm	10 ppm	57.7

Table B.1: List of micro-mirrors' parameters measured by Xudong Yu. Here, ROC denotes radius of curvature, Cav denotes cavity, and trans denotes transmission. For each of the micro mirrors, a cavity is built with the micro mirror and a high-reflection coated planar mirror with transmission of 93 ppm.

Bibliography

[1] I. Newtown. *Opticks*. London, 1704.

[2] Wikipedia. Huygens-fresnel principle. http://en.wikipedia.org/wiki/Huygens-Fresnel_principle.

[3] A. Einstein. Über einen die erzeugung und verwandlung des lichtes betreffenden heuristischen gesichtspunkt. *Annalen der Physik*, 17:132–148, 1905.

[4] K. M. Birnbaum, A. Boca, R. Miller, A. D. Boozer, T. E. Northup, and H. J. Kimble. Photon blockade in an optical cavity with one trapped atom. *Nature*, 436(7047):87–90, 2005.

[5] Ferdinand Brennecke, Tobias Donner, Stephan Ritter, Thomas Bourdel, Michael Kohl, and Tilman Esslinger. Cavity qed with a bose-einstein condensate. *Nature*, 450(7167):268–271, 2007.

[6] Yves Colombe, Tilo Steinmetz, Guilhem Dubois, Felix Linke, David Hunger, and Jakob Reichel. Strong atom-field coupling for bose-einstein condensates in an optical cavity on a chip. *Nature*, 450(7167):272–276, 2007.

[7] A. Kubanek, A. Ourjoumtsev, I. Schuster, M. Koch, P. W. H. Pinkse, K. Murr, and G. Rempe. Two-photon gateway in one-atom cavity quantum electrodynamics. *Phys. Rev. Lett.*, 101:203602, 2008.

[8] Haruka Tanji-Suzuki, Wenlan Chen, Renate Landig, Jonathan Simon, and Vladan Vuletić. Vacuum-induced transparency. *Science*, 333(6047):1266–1269, 2011.

[9] Daniel W. C. Brooks, Thierry Botter, Sydney Schreppler, Thomas P. Purdy, Nathan Brahms, and Dan M. Stamper-Kurn. Non-classical light generated by quantum-noise-driven cavity optomechanics. *Nature*, 488(7412):476–480, 2012.

[10] P. Michler, A. Kiraz, C. Becher, W. V. Schoenfeld, P. M. Petroff, Lidong Zhang, E. Hu, and A. Imamoglu. A quantum dot single-photon turnstile device. *Science*, 290(5500):2282–2285, 2000.

[11] David Press, Stephan Götzinger, Stephan Reitzenstein, Carolin Hofmann, Andreas Löffler, Martin Kamp, Alfred Forchel, and Yoshihisa Yamamoto. Photon

antibunching from a single quantum-dot-microcavity system in the strong coupling regime. *Phys. Rev. Lett.*, 98:117402, 2007.

[12] Ilya Fushman, Dirk Englund, Andrei Faraon, Nick Stoltz, Pierre Petroff, and Jelena Vučković. Controlled phase shifts with a single quantum dot. *Science*, 320(5877):769–772, 2008.

[13] Thomas Volz, Andreas Reinhard, Martin Winger, Antonio Badolato, Kevin J. Hennessy, Evelyn L. Hu, and Atac Imamoglu. Ultrafast all-optical switching by single photons. *Nat Photon*, 6(9):605–609, 2012.

[14] Ranojoy Bose, Deepak Sridharan, Hyochul Kim, Glenn S. Solomon, and Edo Waks. Low-photon-number optical switching with a single quantum dot coupled to a photonic crystal cavity. *Phys. Rev. Lett.*, 108:227402, 2012.

[15] P. A. Franken, A. E. Hill, C. W. Peters, and G. Weinreich. Generation of optical harmonics. *Phys. Rev. Lett.*, 7:118–119, 1961.

[16] N. Bloembergen and P. S. Pershan. Light waves at the boundary of nonlinear media. *Phys. Rev.*, 128:606–622, 1962.

[17] Mike Melnichuk and Lowell T. Wood. Direct kerr electro-optic effect in noncentrosymmetric materials. *Phys. Rev. A*, 82:013821, 2010.

[18] R. L. Carman, R. Y. Chiao, and P. L. Kelley. Observation of degenerate stimulated four-photon interaction and four-wave parametric amplification. *Phys. Rev. Lett.*, 17:1281–1283, 1966.

[19] Rogers H. Stolen. Phase-matched-stimulated four-photon mixing in silica-fiber waveguides. *Quantum Electronics, IEEE Journal of*, 11(3):100–103, 1975.

[20] Yichen Shen, Dexin Ye, Ivan Celanovic, Steven G. Johnson, John D. Joannopoulos, and Marin Soljačić. Optical broadband angular selectivity. *Science*, 343(6178):1499–1501, 2014.

[21] Shuai Chen, Yu-Ao Chen, Thorsten Strassel, Zhen-Sheng Yuan, Bo Zhao, Jörg Schmiedmayer, and Jian-Wei Pan. Deterministic and storable single-photon source based on a quantum memory. *Phys. Rev. Lett.*, 97:173004, 2006.

[22] Matthias Keller, Birgit Lange, Kazuhiro Hayasaka, Wolfgang Lange, and Herbert Walther. Continuous generation of single photons with controlled waveform in an ion-trap cavity system. *Nature*, 431(7012):1075–1078, 2004.

[23] Axel Kuhn, Markus Hennrich, and Gerhard Rempe. Deterministic single-photon source for distributed quantum networking. *Phys. Rev. Lett.*, 89:067901, 2002.

[24] Christian Kurtsiefer, Sonja Mayer, Patrick Zarda, and Harald Weinfurter. Stable solid-state source of single photons. *Phys. Rev. Lett.*, 85:290–293, 2000.

[25] J. McKeever, A. Boca, A. D. Boozer, R. Miller, J. R. Buck, A. Kuzmich, and H. J. Kimble. Deterministic generation of single photons from one atom trapped in a cavity. *Science*, 303(5666):1992–1994, 2004.

[26] D. N. Matsukevich, T. Chanelière, S. D. Jenkins, S.-Y. Lan, T. A. B. Kennedy, and A. Kuzmich. Deterministic single photons via conditional quantum evolution. *Phys. Rev. Lett.*, 97:013601, 2006.

[27] Max Hofheinz, E. M. Weig, M. Ansmann, Radoslaw C. Bialczak, Erik Lucero, M. Neeley, A. D. O/'Connell, H. Wang, John M. Martinis, and A. N. Cleland. Generation of fock states in a superconducting quantum circuit. *Nature*, 454(7202):310–314, 2008.

[28] Ian D. Leroux, Monika H. Schleier-Smith, and Vladan Vuletić. Implementation of cavity squeezing of a collective atomic spin. *Phys. Rev. Lett.*, 104:073602, 2010.

[29] Monika H. Schleier-Smith, Ian D. Leroux, and Vladan Vuletić. States of an ensemble of two-level atoms with reduced quantum uncertainty. *Phys. Rev. Lett.*, 104:073604, 2010.

[30] Ofer Firstenberg, Thibault Peyronel, Qi-Yu Liang, Alexey V. Gorshkov, Mikhail D. Lukin, and Vladan Vuletic. Attractive photons in a quantum nonlinear medium. *Nature*, 502(7469):71–75, 2013.

[31] M. Bajcsy, S. Hofferberth, V. Balic, T. Peyronel, M. Hafezi, A. S. Zibrov, V. Vuletic, and M. D. Lukin. Efficient all-optical switching using slow light within a hollow fiber. *Phys. Rev. Lett.*, 102:203902, 2009.

[32] Hsiang-Yu Lo, Yen-Chun Chen, Po-Ching Su, Hao-Chung Chen, Jun-Xian Chen, Ying-Cheng Chen, Ite A. Yu, and Yong-Fan Chen. Electromagnetically-induced-transparency-based cross-phase-modulation at attojoule levels. *Phys. Rev. A*, 83:041804, 2011.

[33] H. Schmidt and A. Imamoglu. Giant kerr nonlinearities obtained by electromagnetically induced transparency. *Opt. Lett.*, 21(23):1936–1938, 1996.

[34] A. Imamoḡlu, H. Schmidt, G. Woods, and M. Deutsch. Strongly interacting photons in a nonlinear cavity. *Phys. Rev. Lett.*, 79:1467–1470, 1997.

[35] S. E. Harris and Y. Yamamoto. Photon switching by quantum interference. *Phys. Rev. Lett.*, 81:3611–3614, 1998.

[36] M. Fleischhauer and M. D. Lukin. Dark-state polaritons in electromagnetically induced transparency. *Phys. Rev. Lett.*, 84:5094–5097, 2000.

[37] Michael Fleischhauer, Atac Imamoglu, and Jonathan P. Marangos. Electromagnetically induced transparency: Optics in coherent media. *Rev. Mod. Phys.*, 77:633–673, 2005.

[38] Zachary Dutton Lene Vestergaard Hau, S. E. Harris and Cyrus H. Behroozi. Light speed reduction to 17 metres per second in an ultracold atomic gas. *Nature*, 397:594–598, 1998.

[39] D. Budker, D. F. Kimball, S. M. Rochester, and V. V. Yashchuk. Nonlinear magneto-optics and reduced group velocity of light in atomic vapor with slow ground state relaxation. *Phys. Rev. Lett.*, 83:1767–1770, 1999.

[40] D. F. Phillips, A. Fleischhauer, A. Mair, R. L. Walsworth, and M. D. Lukin. Storage of light in atomic vapor. *Phys. Rev. Lett.*, 86:783–786, 2001.

[41] L. M. Duan, M. D. Lukin, J. I. Cirac, and P. Zoller. Long-distance quantum communication with atomic ensembles and linear optics. *Nature*, 414(6862):413–418, 2001.

[42] Q. A. Turchette, C. J. Hood, W. Lange, H. Mabuchi, and H. J. Kimble. Measurement of conditional phase shifts for quantum logic. *Phys. Rev. Lett.*, 75:4710–4713, 1995.

[43] Kristin M. Beck, Wenlan Chen, Qian Lin, Michael Gullans, Mikhail D. Lukin, and Vladan Vuletić. Cross modulation of two laser beams at the individual-photon level. *Phys. Rev. Lett.*, 113:113603, 2014.

[44] S. E. Harris. Lasers without inversion: Interference of lifetime-broadened resonances. *Phys. Rev. Lett.*, 62:1033–1036, 1989.

[45] Stephen E. Harris. Electromagnetically induced transparency. *Physics Today*, 50:36–42, 1997.

[46] J. Laurat K. S. Choi, H. Deng and H. J. Kimble. Mapping photonic entanglement into and out of a quantum memory. *Nature*, 452:67–71, 2008.

[47] F. Massou M. Fleischhaue A. S. Zibrov M. D. Eisama, A. André and M. D. Lukin. Electromagnetically induced transparency with tunable single-photon pulses. *Nature*, 438:837–841, 2005.

[48] H. Tanji-Suzuki, I.D. Leroux, M.H. Schleier-Smith, M. Cetina, A. Grier, J. Simon, and V. Vuletic V. Interaction between atomic ensembles and optical resonators: Classical description. *Adv. At. Mol Opt.*, 60:201, 2011.

[49] Jonathan Simon. *Cavity QED with Atomic Ensembles*. PhD thesis, Harvard University, 2010.

[50] Haruka Tanji. *Few-Photon Nonlinearity with an Atomic Ensemble in an Optical Cavity*. PhD thesis, Harvard University, 2011.

[51] Yu-Nan Zheng, Xiao-Ji Zhou, Jing-Biao Chen, and Chen Xu-Zong. Magic wavelength for caesium transition line $6s_{1/2} - 6p_{3/2}$. *Chin. Phys. Lett.*, 23:1687–1690, 2006.

[52] Qian Lin, Mackenzie A. Van Camp, Hao Zhang, Branislav Jelenković, and Vladan Vuletić. Long-external-cavity distributed bragg reflector laser with subkilohertz intrinsic linewidth. *Opt. Lett.*, 37(11):1989–1991, 2012.

[53] T. A. Savard, K. M. O'Hara, and J. E. Thomas. Laser-noise-induced heating in far-off resonance optical traps. *Phys. Rev. A*, 56:R1095–R1098, 1997.

[54] Wikipedia. Transistor. http://en.wikipedia.org/wiki/Transistor.

[55] Enrico Prati, Marco De Michielis, Matteo Belli, Simone Cocco, Marco Fanciulli, Dharmraj Kotekar-Patil, Matthias Ruoff, Dieter P Kern, David A Wharam, Jan Verduijn, Giuseppe C Tettamanzi, Sven Rogge, Benoit Roche, Romain Wacquez, Xavier Jehl, Maud Vinet, and Marc Sanquer. Few electron limit of n-type metal oxide semiconductor single electron transistors. *Nanotechnology*, 23(21):215204, 2012.

[56] Wenlan Chen, Kristin M. Beck, Robert Bücker, Michael Gullans, Mikhail D. Lukin, Haruka Tanji-Suzuki, and Vladan Vuletić. All-optical switch and transistor gated by one stored photon. *Science*, 341(6147):768–770, 2013.

[57] C.H. Bennett and G. Brassard. Public key distribution and coin tossing. *In Proceedings of IEEE International Conference on Computers, Systems and Signal Processing*, 175:8, 1984.

[58] Wikipedia. Bb84. http://en.wikipedia.org/wiki/BB84.

[59] Chien Liu, Zachary Dutton, Cyrus H. Behroozi, and Lene Vestergaard Hau. Observation of coherent optical information storage in an atomic medium using halted light pulses. *Nature*, 409(6819):490–493, 2001.

[60] J. Hwang, M. Pototschnig, R. Lettow, G. Zumofen, A. Renn, S. Gotzinger, and V. Sandoghdar. A single-molecule optical transistor. *Nature*, 460(7251):76–80, 2009.

[61] Martin T. Hill, Harmen J. S. Dorren, Tjibbe de Vries, Xaveer J. M. Leijtens, Jan Hendrik den Besten, Barry Smalbrugge, Yok-Siang Oei, Hans Binsma, Giok-Djan Khoe, and Meint K. Smit. A fast low-power optical memory based on coupled micro-ring lasers. *Nature*, 432(7014):206–209, 2004.

[62] Marijn A. M. Versteegh, Peter J. S. van Capel, and Jaap I. Dijkhuis. Ultrafast all-optical gated amplifier based on ZnO nanowire lasing. *Applied Physics Letters*, 101(2):021101, 2012.

[63] Darrick E. Chang, Anders S. Sorensen, Eugene A. Demler, and Mikhail D. Lukin. A single-photon transistor using nanoscale surface plasmons. *Nat Phys*, 3(11):807–812, 2007.

[64] Michael E. Peskin and Dan V. Schroeder. *An introduction to quantum field theory*. Westview Press, 1995.

[65] Steven Weinberg. *The quantum theory of fields, Volume 1.* Cambridge University Press, 2005.

[66] Qi-Yu Liang Sebastian Hofferberth Alexey V. Gorshkov Thomas Pohl Mikhail D. Lukin Thibault Peyronel, Ofer Firstenberg and Vladan Vuletić. Quantum nonlinear optics with single photons enabled by strongly interacting atoms. *Nature*, 488:57–60, 2012.

[67] Andreas Reiserer, Stephan Ritter, and Gerhard Rempe. Nondestructive detection of an optical photon. *Science*, 342(6164):1349–1351, 2013.

[68] T. G. Tiecke, J. D. Thompson, N. P. de Leon, L. R. Liu, V. Vuletic, and M. D. Lukin. Nanophotonic quantum phase switch with a single atom. *Nature*, 508(7495):241–244, 2014.

[69] Y. O. Dudin and A. Kuzmich. Strongly interacting rydberg excitations of a cold atomic gas. *Science*, 336(6083):887–889, 2012.

[70] D. Hunger, C. Deutsch, R. J. Barbour, R. J. Warburton, and J. Reichel. Laser micro-fabrication of concave, low-roughness features in silica. *AIP Advances*, 2:012119, 2012.

[71] Gilles Brassard, Norbert Lütkenhaus, Tal Mor, and Barry C. Sanders. Limitations on practical quantum cryptography. *Phys. Rev. Lett.*, 85:1330–1333, 2000.

[72] Xiang-Bin Wang. Beating the photon-number-splitting attack in practical quantum cryptography. *Phys. Rev. Lett.*, 94:230503, 2005.

[73] Xiang-Bin Wang and Jia-Zhong Hu. Quantum key distribution with the decoy-state method. *Sci. Sin. Phys. Mech. Astron.*, 41:459–465, 2011.

[74] Merriam-Webster. *Merriam-Webster's Collegiate Dictionary.* Merriam Webster Inc, 2003.

[75] Gor Nikoghosyan and Michael Fleischhauer. Photon-number selective group delay in cavity induced transparency. *Phys. Rev. Lett.*, 105:013601, Jun 2010.

[76] Daniel A. Steck. *Cesium D Line Data.* Theoretical Division (T-8), MS B285, Los Alamos National Laboratory, Los Alamos, NM 87545, 2003. revision 1.6.

[77] Christina J. Hood, H. J. Kimble, and Jun Ye. Characterization of high-finesse mirrors: Loss, phase shifts, and mode structure in an optical cavity. *Phys. Rev. A*, 64:033804, 2001.